Characterization of 12-Oxo-phytodienoic Acid Signaling in Broad-spectrum Plant Defense Responses and Its Coordination with Growth Fitness

by

Ashna Adhikari

A thesis submitted to the Graduate Faculty of
Auburn University
in partial fulfillment of the
requirements for the Degree of
Master of Science

Auburn, Alabama
August 5, 2023

Keywords: plant defense response, cellular redox homeostasis, glutathionylation, posttranslational modification, OPDA signaling, peroxidase detoxification

Approved by

Dr. Sang-Wook Park, Associate professor of Plant Pathology
Dr. Kathy Lawerence, Professor of Plant Pathology
Dr. Aaron Rashotte, Professor of Biology Sciences

ABSTRACT

The jasmonate family of phytohormones plays central roles in plant development and stress acclimation. However, the architecture of their signaling circuits remains largely unknown. Here, we describe the versatile activity of jasmonate family binding protein, cyclophilin 20-3 (CYP20-3), positioned as a key regulator in controlling the interface between 12-oxo-phytodienoic acid (OPDA, defense) and light-dependent redox (growth) signaling. The latter, also known as the electron (e^-) transport chain (ETC) photosystem I (PSI), is a primary metabolism converting solar energy into biologically useful chemical energies, necessary for the production of overall biomass of plants and living organisms. When the PSI captures solar energy, it excites e^- that reduce thioredoxins (TRXs) via a ferredoxin (Fd) and a Fd-TRX reductase (FTR). TRXs, small oxidoreductases, then deliver e^- and activate target enzymes in the Calvin cycle that balances consumption in photosynthesis. The present study validated that TRXs can also reduce other Calvin cycle-unrelated proteins including CYP20-3 and photosynthetic ETC as an e^- donor of 2-cysteine (Cys) peroxiredoxin A (2CPA). Plastid 2CPA is a thiol-based peroxidase involved in protecting and optimizing photosynthesis. When arrived at the chloroplasts, 2CPA is activated by oxidation folding with GSH (also called, S-glutathionylation), which in turn reduces toxic byproducts (e.g., H_2O_2) in photosynthesis or activates Calvin cycle enzymes such as a fructose 1,6-bisphosphatase. In line with this scenario, OPDA-binding promotes the interaction of CYP20-3 with TRXs (esp., type-f2), illuminating the mode of OPDA/CYP20-3 signaling in transferring e^- from TRX-f2 to SAT1. This then stimulates plastid sulfur assimilations and subsequently GSH accumulations, which coordinates redox-resolved nucleus gene expressions in defense responses against biotic and abiotic stresses, while accelerating the S-glutathionylation (activation) of 2CPA that promotes photosynthetic energy productions, postulating that OPDA/CYP20-3 signaling optimizes growth, reproduction and survival of plants under constant environmental stresses. Traditionally, the cost of resistance (often referred to as growth and defense tradeoff) has been typically described as a teeter-totter model where for defense to increase, growth must decrease

and vice versa. This model well circumstantiates the responses of plants to the persistent and excess surge of environmental stresses. However, in nature, plants are more often situated to encounter a consistent array of temporal and modest levels of environmental changes, while concurrently trying to ensure normal growth and developmental processes, in order to maximize their yields and production. Hence, recent studies have begun to elaborate an alternative model, “growth and defense coordination”, wherein a balancing act between growth and defense can synergistically optimize plant fitness. In agreement, plant acclimations towards environmental changes and pressures causing oxidative stresses (e.g., tissue injury, excess light and temperature, and drought and salinity) accompany the accumulation of OPDA on a time sale of hours with concomitant accumulation of reduced, nonprotein thiols.

AKNOWLEDGEMENTS

I would like to extend my gratitude to my major advisor Dr. Sang-Wook Park for allowing me the opportunity to attain a master's degree at Auburn University and for all the guidance and knowledge he has given me during my time at the university. I would like to thank my co-advisor Dr. Kathy Lawrence and committee member Dr. Aaron Rashotte for their guidance in the area of plant pathology. I would also like to thank many of my colleagues who all have helped me in my experimental procedures. Finally, I would like to thank my family and friends for continual love and support throughout my graduate school. As hard as it was away from home and family, my friends and family have continued to push me to be the best I can be and always encourage me to keep a positive outlook on life. I especially dedicate this thesis to my Parents and my brother who always give me a strong back and love.

TABLE OF CONTENTS

LIST OF TABLES

LIST OF FIGURES

CHAPTER 1: INTRODUCTION AND REVIEW OF LITERATURE

12-oxo-phytodienoic acid (OPDA) is a primary precursor of (-)-jasmonic acid (JA), able to trigger autonomous signaling pathways that regulate a unique subset of jasmonate-responsive genes, activating and fine-tuning defense responses, as well as growth processes in plants. Recently, a number of studies has illuminated the physiol-molecular activities of OPDA signaling in plants, which interconnect the regulatory loop of photosynthesis, cellular redox homeostasis and transcriptional regulatory networks; together shedding new light on *i*) the underlying modes of cellular interfaces between growth and defense responses (e.g., fitness tradeoffs or balances), and *ii*) vital information in genetic engineering or molecular breeding approaches to upgrade plants' own survival capacities. However, our current knowledge regarding its mode of actions is still far from complete. This review will briefly revisit recent progresses on the roles and mechanisms of OPDA and information gaps within, which help understanding the phenotypic and environmental plasticity of plants.

1.1. Phyto-Oxylipins: Jasmonate Signaling in Plants. Oxylipins, the oxygenated derivative of fatty acids (FA), are critical signal molecules in diverse physiological processes in life including plants and animals (Marnett, 2008). In plants, oxylipins are involved in a layer of defense and ontogenetic pathways, while mammalian oxylipins (eicosanoids) control intricate regulatory mechanisms in immunity, functioning as messengers in the central nervous system and participating in the resolution process following tissue injury (Funk, 2001; Mosblech et al., 2010). Recent studies, moreover, have illuminated the medicinal values of phyto-oxylipins, presenting their anticancer, anti-inflammatory and antioxidative activities (Flescher, 2007; Dang et al., 2008; Take-Nakano et al., 2014). Noticeably, the molecular components and metabolic pathways, in which are involved oxylipin biogenesis and signaling, share common ancestry and evolutionary processes across Kingdoms (Marnett, 2008). Hence, uncovering the modes of actions associated with oxylipins will not only assist the development of agricultural strategies in advancing disease

resistance and stress adaptation, as well as yield and biomass increases in plants, but also the improvement of drug development through facilitating the rational design of more potent and safe anti-cancer (and anti-inflammation) drugs. However, our current knowledge regarding oxylipin signaling is still incomplete, despite decades of investigations (Funk, 2001; Mosblech et al., 2010).

Lately, molecular underpinnings have been investigated for OPDA signaling in plant defense responses. OPDA is a primary precursor of the jasmonate family of oxylipins which includes JA and its precursors and derivatives. Jasmonates are derived from trienoic-FA via the octadecanoid pathway in the chloroplasts. Lipase-mediated oxidation of trienoic-FA leads to the release of OPDA that travels to peroxisomes through ATP-binding transporters (e.g., COMATOSE, Theodoulou et al., 2005) and undergoes β-oxidations to form JA. JA can be further metabolized to several derivatives including JA-isoleucine (JA-Ile), JA-tryptophan (JA-Trp), methyl-JA and hydroxyl-JA. Signaling of these jasmonate molecules then control a large number of nucleus gene expressions, and mediate defense (adaptive) responses to various forms of biotic and abiotic stresses including microbial pathogens and insect herbivores, tissue injury and light damage. Jasmonate signaling also plays essential roles in reproduction and other developmental processes such as senescence, root growth and tuberization, fruit ripening, and tendril coiling (reviewed in Acosta and Farmer, 2010; Pieterse et al., 2012). These important, yet diverse activities of jasmonates must be tied to their versatility as major molecular and cellular modulators.

The most well characterized jasmonate-associated signaling pathway revolves around JA-Ile. Once it is produced, JA-Ile binds a F-box protein, CORONATINE INSENSITIVE 1 (COI1, a part of SCF ubiquitin E3 ligase). This complex then binds and ubiquitinates jasmonate ZIM-domain (JAZ) proteins which are negative transcription regulators of JA-responsive genes (JRGs). Thus, JAZ degradation by 26S proteasomes frees transcription factors (TFs) and allows subsequent gene expressions (Thines et al., 2007; Chini et al., 2007). Jasmonate signaling, however, must involve a much more complex network, given that a number of JRGs respond independently of COI1

(Devoto et al., 2005). For example, JA induction of *GRX480* and *AOC3* is mediated via a COI1-independent MYC2 regulatory pathway, whereas JA-activated MAP kinase cascades (e.g., *MPK1*, *MPK2*, *BIK1*) and *GST25* are regulated in a COI1- and/or MYC2-independent manner (Veronese et al., 2006; Ortiz-Masia et al., 2007; Stotz et al., 2013). MYCs are key TFs of JA-Ile/COI1 signaling, whose activities are suppressed by JAZ proteins during a resting condition (Staswick, 2008). In addition, OPDA is capable of triggering autonomous signaling pathways that regulate unique subsets of jasmonate-responsive genes, coordinated with and without the canonical JA pathway (Taki et al., 2005). OPDA signaling is presumed to be independent of COI1, as it is unable to bind the COI1/JAZ complex (Thines,et al., 2007). However, OPDA induction of *PHO1;H10* needs COI1 activity (Ribot et al., 2008), suggesting additional layers of complexity in jasmonate signaling. The other study also established a distinct role of JA-Trp conjugate, linking jasmonate with auxin signaling (Staswick, 2009) further supporting the notion that distinct messages sent out by specific jasmonate coordinate essential molecular and cellular processes.

1.2. Biosynthesis of OPDA and Its Derivatives. As alluded, jasmonates are synthesized in the chloroplasts from oxygenized FAs, linolenic acid (18:3) and hexadecatrienoic acid (16:3), that are stored mostly as the esterified monogalactosyl diacylgalycerol (MGDG). The first step, hydroperoxidation, is began by 13-lipoxygenases adding molecular oxygen to 18:3 and 16:3 and form 13(*S*)-hydroperoxy-octadecatrienoic acid and 11(*S*)-hydroperoxy-hexadecatrienoic acid, respectively. These compounds are then transformed via allene oxide synthase into (*13S*)12,13-epoxy-octadecatrienoic acid and (11*S*)10,11-epoxy-octadecatrienoic acid, which are in subsequent cyclized through allene oxide cyclase to yield *cis*-(+)-OPDA and dinor-OPDA; their natural *cis*/*trans* stereoisomers possess an α, β-unsaturated carbonyl group with reactive electrophilic properties. The formation of *cis*-(+)-OPDA and dinor-OPDA (collectively, OPDA) is known to be activated in response to various herbivories and microbial pathogens, as well as abiotic stresses such as extreme temperatures and tissue injury (Stintzi et al., 2001; Kourtchenko et al., 2007; Vu et al., 2012; Bosch et al., 2014; Monte et al., 2020). Some portions of OPDA induced are then

further derivatized to a glutathione (GSH) conjugate, or galactolipids by binding with MGDG and digalactosyl DG, later named 'arabidopsides' (Hisamatsu et al., 2003, 2005; Davioine et al., 2005, 2006; Andersson et al., 2006; Buseman et al., 2006). The biological role(s) of OPDA-GSH and arabidopsides are yet largely elusive, but has been hypothesized as the vacuolar delivery and storage forms, respectively, in maintaining the cellular level homeostasis of OPDA to avoid their potential toxicity and/or negative effects on physiol-molecular processes in plants (Böttcher and Pollmann, 2009; Ohkama-Ohtsu et al., 2011). Alternatively, recent studies have been suggesting that arabidopsides could interact with plant plasma membrane lipids such as glycosyl inositol phosphor ceramides, which thus lead them to locate and modify membrane organizations and such changes could signal defense mechanism activations (Genva et al., 2019).

1.3. OPDA Signaling in Plant Defense Responses. In plants, OPDA signaling plays intrinsic roles in activating and fine-tuning defense (adaptive) responses against an array of biotic and abiotic stresses, as well as growth processes (Böttcher and Pollmann, 2009; Dave and Graham, 2012; Maynard et al., 2018). Its distinctive activity in plant defense activations was first described by the pathoanalyses of a mutant Arabidopsis plant (*opr3*) arresting the conversion of OPDA to JA/JA-Ile (Stintzi et al., 2001). WT-like resistance of *opr3*, in contrast to enhanced susceptibility in other mutants disrupting trienoic- FA biosynthesis (*fad3*/*7*/*8*) and the octadecanoid pathway (*dde2* and *aos*), against fungal pathogens (*Alternaria brassicicola* and *Scerotinia sclerotiarum*) and an insect herbivory (*Bradysia impatiens*), underlined a critical activity of OPDA signaling in plant disease resistance in the absence of JA/JA-Ile (Stintzi et al., 2001; Zhang and Turner, 2008; Stotz et al., 2011). Following studies with genetically modified (GM) plants reducing or impairing JA productions (*OPR3-RNAi*, *SiOPR3*s, and *opr7opr8*) or enhancing OPDA accumulations (*OPR3ox*) further substantiate that OPDA signaling is essential for the full activation of basal defense responses in tomato, maize, and rice against microbial and/or pest attacks such as *Botrytis cinerea*, tobacco hornworm (*Manduca sexta* larvae), beet armyworm (*Spodoptera exigua* larvae), brown plant hopper (*Nilaparvata lugens*), green peach aphid (*Myxus persicae*), and corn leaf aphid

(*Rhopalosiphum maidis*) (Bosch et al., 2014a,b; Guo et al., 2014; Scalschi et al., 2015; Varsani et al., 2019; Grover et al., 2020b; Wang et al., 2020). Upon their infections, OPDA isinduced rapidly in the chloroplasts and triggers the retrograde signaling toward the nucleus, which coordinates large-scale changes in defense gene expressions (Taki et al., 2005). These then lead to (*i*) the spatiotemporal induction of protease inhibitors (PIs) such as miraculin-like proteins, which likely serve as antinutrients against insect attackers by reducing their digestibility of dietary proteins (Felton, 2005; López-Galiano et al., 2017), (*ii*) the actuation of other hormone and metabolite biosynthesis (Figure 1.1) in maximizing defense capacity and survival of plants, and (*iii*) the stimulation of callose deposition (Scalschi et al., 2015; Varsani et al., 2019), a multifaceted cell wall barrier developed at the sites of infection, preventing the cell-to-cell spread of microbes and limiting the feeding capacity and colonization of insects (Luna et al., 2010; De Storme and Geelen, 2014). OPDA signaling appeared to trigger abscisic acid (ABA) accumulations (Dave et al., 2016) that activate a NADPH oxidase subunit of RBOHF (Respiratory Burst Oxidase Homolog Protein F) leading to transient reactive oxygen species (ROS) productions (Sirichandra et al., 2009; Figure 1.1) and in consequence stimulating callose synthesis (Luna et al., 2010). However, OPDA signal alone did not elevate the expression levels of callose synthase gene such as *Tie-dyed2* in maize, suggesting rather the need of additional or alternative, yet unknown, defense and/or OPDA-inducible element(s), perhaps free thiols such as GSH and glucosinolates (Park et al., 2013; Zhou and Memelink, 2016; Varsani et al.,2019).

Indeed, it is still largely elusive how OPDA is perceived for signaling. Recently, in search of OPDA derivatives potentially binding SCF^{COI}, OPDA conjugated with Ile (OPDA-Ile) was identified in Arabidopsis (Floková et al., 2016) and described its ability to induce OPDA-responsive genes (ORGs) such as *GRX480* and *ZAT10* in JA/JA-Ile-deficient mutant (*opr3* and *jar1*) plants (Arnold et al., 2016). The latter suggests that OPDA-Ile is a bioactive signal and conveys JA/JA-Ile-independent, OPDA- dependent signaling pathway. OPDA-Ile is though only active under specific conditions as it was found exclusively in wounded leaves of flowering plants

(Floková et al., 2016). It would be interesting to delineate mechanisms underlying the perception of OPDA-Ile and its cross-networking with other OPDA signaling pathways (see "Summary: Mode of Action of OPDA Signaling").

Besides its roles in local defenses, a new study has proposed that OPDA is a long-distance signal for "induced systemic resistance" (ISR) (Wang et al., 2020), a state of heightened defense that is activated throughout the plant following an initial encounter with plant growth-promoting rhizobacteria/fungi (PGPR/F) (Pieterse et al., 2014). Their oxylipin profiling of xylem saps collected from ISR-induced maize leaves detected uniquely OPDA and KODA (α-ketol-octadecadienoic acid). In addition, the transfusion of OPDA and KODA into naïve plants ed to develop systemic resistance against an anamorphic fungus *Collectotrichum graminicola* in a dose-dependent manner (Wang et al., 2020), together proposing their role in conveying ISR signaling. A caveat is that OPDA appears to be stationary exhibiting little or no distal accumulation under pathogen attacks (Christensen et al., 2015). This speculates if an ISR receptor of OPDA is present in xylem. Alternatively, OPDA may be rapidly converted to and activate JA/JA-Ile signaling, upon arrival to systemic tissues, for priming systemic defense (Koo et al., 2009; Bosch et al., 2014a). In this context, an earlier grafting experiment using WT and JA/JA-deficient (*OPR3- RNAi*) plants showed that OPDA can substitute for JA/JA- Ile in the local induction of defense gene expressions, but the production of JA/JA-Ile is required for systemic responses (Bosch et al., 2014b). It will be intriguing to find out whether OPDA is "truly" moved from local to vascular to systemic tissues, and if OPDA can autonomously signal ISR priming or is converted to JA/JA-Ile for ISR development. In addition, we cannot still rule out a potential role of phloem in channeling a mobile signal of ISR development (Varsani et al., 2019). Perhaps, ISR may also involve multiple signals and transduction pathways as does in systemic acquired resistance (Klessig et al., 2018).

On the other hand, a recent report argued that only a biologically active jasmonate molecule is JA-Ile (Chini et al., 2018). Using a new mutant allele (*opr3-3*) completely lacking OPR3 reductase

activity, the study demonstrated the increased accumulation levels (~fifteen-folds) of non-reduced cyclopente none, 4,5-didehydrojasmoante, in *opr3* and its provisional reduction to JA by one of OPR3 isoforms, OPR2 reductase, together postulating that WT-like resistance of *opr3* is actuated not by OPDA signaling, rather by COI1- dependent JA-Ile signaling. However, the OPR3-independent pathway of JA biosynthesis appeared to contribute to the accumulation of dismal amounts of JA-Ile (<2.0 % [less than its basal levels] of WT) under stress conditions, while conferring tenable strength defense responses against pathogen infections, prompting speculation that *opr3-3* mutants may exert alternative, OPDA-associated defense pathways. In fact, *coi1* mutants feedback suppress JA biosynthesis so that lack stress-induced OPDA and JA accumulations (Chung et al., 2008; Park et al., 2013). Thus, *coi1*-like increased susceptibility shown in *coi1*/*opr3-3* against insect and fungal attacks (Chini et al., 2018) might be, not because WT-like resistance of *opr3- 3* requires COI1, due to auxiliary side effects led by double mutagenesis, perhaps lowering the level threshold of OPDA and JA-Ile signaling.

1.4. OPDA Signaling in Plant Growth and Developmental Processes. An earlier study of COMATOSE, a peroxisomal ATP-binding cassette transporter, and its mutant plants (*cts*) disrupted the transport of OPDA into the peroxisome, where JA biosynthesis occurs, illuminated a critical activity of OPDA signaling in coordinating seed germination and dormancy (Russell et al., 2000). The mutant *cts* seeds exhibited increased accumulation level of OPDA and low germination rates (Russell et al., 2000; Dave et al., 2011), while exogenous OPDA applications stimulated the repression of the germination of WT seeds (Dave et al., 2011). Such an inhibitory effect of OPDA signaling is perhaps mediated through its activation of ABA biosynthesis by upregulating the expression of an ABA biosynthesis gene (*ABA1* and *ABA-deficient 1*) and an inducer (*RGL2, Repressor of Gibberellic Acid-like 2*) of RING-H2 XERICO (ABA biosynthesis regulator) (Ko et al., 2006; Piskurewicz et al., 2008; Dave et al., 2016). OPDA and ABA both are then able to induce and/or stabilize the activity of GRL2 and ABI5 (ABA insensitive 5) bZIP TF, which in subsequence promotes the expression of *MET* (*Mother-of FT and TFL1*), an inhibitor of

seed germination or early seedling growth (Skubacz et al., 2016; Vaistij et al., 2018), so that it suppresses seed germinations (Dave et al., 2016; Barros-Galvão et al., 2019). Two hormones, however, displayed different mechanistic outcomes that ABA signal ruptures seed coats and endosperm tissues, whereas OPDA-treated seeds keep intact endosperm and seed coats (Dave et al., 2011), indicating that OPDA signal, besides coordinating ABA biosynthesis/signaling, can execute its autonomous, unique regulatory metabolic pathways in plant organismal development.

OPDA-responsive ABA accumulations also convey the inhibition of root growth and morphogenesis in plants (Mueller et al., 2008; Park et al., 2013; Sun et al., 2018; Vissenberg et al., 2020). ABA could suppress primary root growth and lateral root branching, mediated *via* balancing the cellular homeostasis of several growth components (Arc et al., 2013; Sun et al., 2018) that enhance the production of ROS, Ca^{2+}, and ethylene but reduce auxin levels (Wang et al., 2002; He et al., 2012; Jiao et al., 2013; Luo et al., 2014). These changes then stimulate the expression of *PLETHORA* TFs, rhizotatic regulators, and some cell cycle-related genes (e.g., *Cyclin- dependent Protein Kinase* and *Cell Cycle B-type Cyclins*), thus affecting DNA replication, cell division, and cell elongation in roots and inhibiting root growth (Wang et al., 2008, 2011; Yin et al., 2009; Xu et al., 2010; Hofhuis et al., 2013; Yao et al., 2013). However, the effects of OPDA signal on roots did also not entirely depend on ABA signaling. Our recent study indicated that OPDA signaling could act as a positive regulator in root growth and development (Figure 1.2). Disruption of OPDA signaling in Arabidopsis (*cyp20-3*, Park et al., 2013) engendered the impairment of root hair growth. It is though unclear if the opposite is correct; the increased accumulation level of OPDA under stress conditions could enhance root growth and branching; further studies are needed to reconstitute the complete, functional networks of OPDA signaling in plant growth and development.

1.5. A Mode of OPDA Signaling by Its Binding Protein, Cyclophilin 20-3. Previously, our search of jasmonate receptors uncovered that a small plastid protein, cyclophilin 20-3 (CYP20-3),

can physically interact with OPDA, and its T-DNA insertion mutant Arabidopsis (*cyp20-3*) attenuates the expression of ORGs (Park et al., 2013). The Arabidopsis genome encodes 29 CYP and CYP-like proteins, belonging to the family of, namely, immunophilins that possess binding abilities toward immunosuppressive drugs, cyclosporin A, and functions in broad ranges of cellular processes, including transcriptional regulation, organogenesis, photosynthetic and hormone signaling pathways, stress adaptation, and defense responses (Dos Santos and Park, 2019). CYP20-3 is the only isoform localized in the chloroplast stroma and acts as a dual-enzyme able to chaperone protein folding (peptidyl-prolyl *cis-trans* isomerase; PPlase) and transfers electrons (e^-) to peroxide substrates (reductase) in cysteine (Cys) biosynthesis (i.e., sulfur assimilation; Romano et al., 2004; Laxa et al., 2007; Dominguez-Solis et al., 2008; Park et al., 2013). In line with this scenario, OPDA, once accumulated under stress states, binds and stimulates CYP20-3 to form a complex with serine acetyltransferase1 (SAT1), which triggers the formation of a hetero-oligomeric Cys synthase complex (CSC) with *O*-acetylserine(thiol)lyase B (OASTL-B) (Figure 1.3., left side). CSC formation then leads to the production of Cys and subsequently thiol metabolites (e.g., GSH), which builds up cellular reduction potentials. The enhanced redox capacity in turn coordinates the expression of a subset of ORGs that activate and calibrate pathogen defense and stress adaptation processes. Thus, the KO of *CYP20-3* (*cyp20-3*) displays enhanced susceptibility against necrotrophic fungal (e.g., *A. brassicicola* and *B. cinerea*) and oomycete (*Pythium irregulare*) infections, as well as nematode (*Meloidogyne hapla*) infestations, compared with WT (Park et al., 2013; Gleason et al., 2016; Dos Santos and Park, 2019), together concurring with the conclusion that OPDA is an autonomous metabolic messenger, connecting stress cues to the readjustment of cellular redox homeostasis in actuating retro- directional signaling from the chloroplasts to the nucleus for regulating defense gene expressions.

1.6. Summary: Mode of Action of OPDA Signaling. As sessile organisms, plants cope with constant encounters with a wide range of biotic competitors and consumers, and abiotic constraints, through mobilizing a number of primary and secondary metabolites, and intricate

signaling networks that interconnect and orchestrate large-scale changes in transcriptome, proteome, and metabolome. As described in this review, the emerging evidence has espied that OPDA is a versatile signal molecule involved in a variety of metabolic pathways, coordinating plant growth and survival in optimal condition as well as under various forms of environmental stresses (Table 1.1.). In the recent decade, a large number of efforts have been devoted and begun to delineate the mechanistic modus operandi of OPDA signaling; thus far, three working models have been proposed. Once it is produced in the chloroplasts, OPDA is *i*) conjugated with galactolipids, GSH, and/or amino acids (e.g., Ile) before/after being released to the cytosol, in turn targets yet unknown effector/receptor proteins, and conveys ORG expressions (Böttcher and Pollmann, 2009; Ohkama-Ohtsu et al., 2011; Floková et al., 2016). Alternatively, OPDA itself can *ii*) serve as a reactive electrophile that targets and modifies thiol residues of, e.g., cysteine, histidine, and lysine in proteins (Mueller and Berger, 2009; Monte et al., 2020) triggering downstream signal transductions and metabolic cascades, or *iii*) covalently bind a CYP20-3 receptor and builds up a reduction capacity that modulates the cellular activity of oxidoreductase cascades in controlling retrograde signaling, rapidly adjusting nuclear gene expressions (Tada et al., 2008; Park et al., 2013; Cheong et al., 2017). It is, however, still unclear how these signaling mechanisms ultimately stimulate global, spatiotemporal gene expression dynamics with both distinctive and redundant transcriptional outputs. Our study suggests though that OPDA can target and fine-tune an interface between photosynthesis-derived ETC and sulfur assimilation processes in the chloroplasts (Cheong et al., 2017; Liu et al., 2020). This interplay enables plants to make an adaptive decision in allocating resources (e^{-}) between growth and defense responses (e.g., fitness trade-offs or balances) toward different ecological challenges such as pathogens, pests, tissue injury as well as light and oxidative stresses, in the end, ensuring optimal growth, reproduction, and survival of plants. Therefore, furthering our understanding of functional and biological activities of OPDA and associated molecular mechanisms (a) will not only provide new insights into a “broad-spectrum” defense responses and (b) can enrich plant breeding and engineering strategies for the selection of elite genetic traits that will maximize plant fitness, but also (c) will

address fundamental gaps in the immune activation of a mammalian system, and (d) help in improving drug developments through facilitating the rational design of more potent and safe reagents.

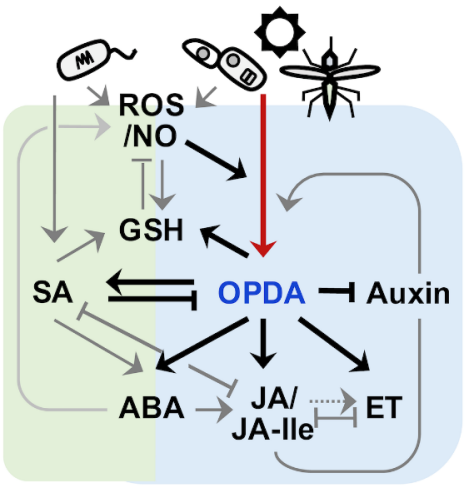

Figure 1.1. Schematic Crosstalk of OPDA with the Signaling Pathways of Other Phytohormones. OPDA and JA/JA-Ile (collectively, jasmonate) signaling activates defense responses to various forms of biotic and abiotic stresses including necrotrophe infection, insect attack, wonding and UV damage, whereas salicylic acid (SA) signaling confers disease resistance against mostly biotrophic pathogens. Once recognized 'non-self', plants rapidly produce ROS including nitric oxide (NO) (Huang et al., 2004; Wang et al., 2013) which in turn actuates jamonate biosynthesis (Palmieri, et al., 2008). OPDA signaling then stimulates, and coordinates with different defense signaling, e.g., JA/JA-Ile, SA, ABA, ethylene (ET) and GSH, pathways (Taki et al., 2005; Park et al., 2013; Dave et al., 2016; Varsani et al., 2019; Scalschi et al., 2020), while suppressing growth hormone (e.g., auxin) signaling (Take et al., 2005) to optimize plants' defense capability. On the other hand, JA/JA-Ile signaling can feedback induce own jasmonate biosynthesis (Taki et al., 2005), whereas SA signaling antogonizes both OPDA and JA/JA-Ile signaling (Leon-Reyes et al., 2010; Shim et al., 2013; Wei et al., 2014).

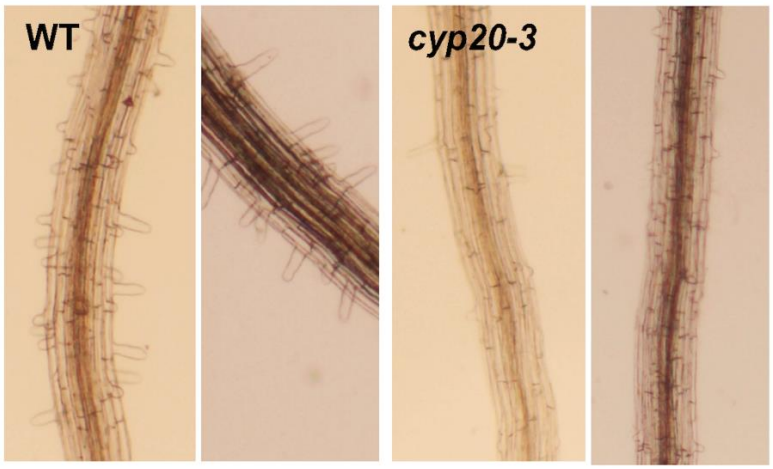

Figure 1.2. Important Roles of OPDA Signaling in Root Morphogenesis. OPDA signaling mutant Arabidopsis (*cyp20-3*) demonstrated the impairment of root hair growth.

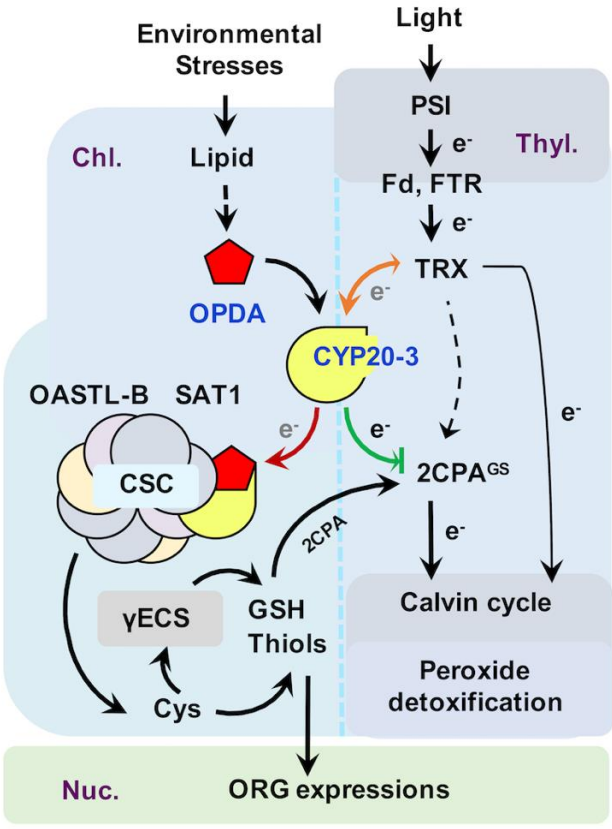

Figure 1.3. Proposed Model of CYP20-3 as a Regulatory Hub in the Interplay between Light and OPDA Signaling. In optimal conditions, CYP20-3 relays light signlaing in buffering cellular redox homeostasis, whereas, in stressed states, CYP20-3 interfaces light and OPDA signaling, which fine-tune plant fitness between growth (light-dependent detoxification and Calvin cycle) and defense response (redox-mediated retrograde signaling). Colored arrows indicate the enhanced interactions of CYP20-3 with TRXs (orange), SAT1 (red) and 2CPA (green) during stress (OPDA-signaling) defense responses. Hypothesized passage of electron (e^-) transfers are noted in grey.

Table 1.1. Biophysiological activities and functions of OPDA across diverse plant genres.

Crops	Defense Responses	Growth	References.
A. thaliana	Local defense against infections of fungal pathogens (*A. brassicacola* & *S. sclerotiarum*), insect (*B. impatiens*) and root-knot nematode (*M. hapla*). Enhanced resolution of tissue injury and tolerance to high light and heat stress.	Regulation of seed dormancy & germination, Inhibition of primary root growth	Stintzi, et al., 2001; Buseman, et al., 2006; Muller, et al., 2008; Park et al., 2013; Dave, et al., 2016; Gleason, et al., 2016; Balfagón, et al., 2019; Liu et al. 2020.
M. polymorpha	Enhanced protection against heat stress.		Monte, et al., 2020.
O. sativa	Local defense against insect (*N. Lugens* & *M. Persicae*) infections and increased tolerance toward salt stress.		Guo, et al., 2014; Hazman, et al., 2015.
P. trichocarpa	Local defense against spider mite (*T. urticae*) infestations and enhanced adaptation of tissue injury.		Zhao, et al., 2021.
S. bicolar	Enhance tolerance to aphids (*M. sacchari*).		Grover, et al., 2020.
S. lycopersicum	Local defense against fungal (*B. cinerea*) and insect (*M. sexta* larvae) infections.	Regulation of embryo development, and seed dormancy	Goetz, et al., 2012; Bosch, et al., 2014; Scalschi, et al., 2015.
S. melongena	Hexanoci acid-mediated systemic defense against insect (*L. decemlineata*) infestations.		López-Galiano, et al., 2017.
T. aestivum	Enhanced resistance to Hessian fly (Diptera: *Cecidomyiidae*) under heat stress		Cheng, et al., 2018.
Z. mays	Local defense against aphids (*R. maidis*) and *T. virens*-primed IST against parasites (*C. graminicola*).		Varsasni, et al., 2019; Wang, et al., 2020.

CHATER 2: INDUCTION OF GLUTATHIONE IN 12-OXO-PHYTODIENOIC ACID SIGNALING CO-REGULATES PHOTOSYNTHETIC EFFICIENCY AND DEFENSE ACTIVATIONS UNDER ENVIRONMENTAL STRESSES

2.1. ABSTRACT

12-oxophytodienoic acid (OPDA) is a primary precursor of jasmonic acid (JA), triggering signaling cascades that activate and fine-tune defense responses, as well as growth and development in plants. However, its mechanism of actions remains largely elusive. Here we describe a dual-function messenger of OPDA signaling, reduced glutathione (GSH), which cross-regulates photosynthesis machinery and stress-protection/adaptation: in concert, optimizing plant plasticity and survival potential. Under stress conditions, OPDA is rapidly induced in the chloroplasts and stimulates GSH accumulations, leading to protein S-glutathionylation in modulating the structure and function of redox-sensitive enzymes such as 2-cysteine (Cys) peroxiredoxin A (2CPA). GSH exchanges thiol-disulfides with the resolving Cys^{R}_{53}, while donating an electron (e^-, H^+) to the peroxidatic Cys^{P}_{175}, of 2CPA, which revives its reductase activity and in turn fosters peroxide detoxification in photosynthesis. Concurrently, GSH prompts retrograde signaling from plastids to nucleus in adjusting OPDA-responsive gene expressions, and actuating defenses responses against various ecological constraints such as salinity, excess oxidant and light, as well as mechanical wounding. We thus conclude that the OPDA pathway deploys GSH as a key, versatile signal that links various cellular and environmental cues to a multitude of plant physiological, e.g., growth, development, stress defense and acclimation, processes.

2.2. INTRODUCTION

Oxylipins, oxygenated derivatives of fatty acids, are essential signaling molecules in diverse physiological processes in plants and animals (Marnett, 2008). In plants, oxylipins operate a layer of defense (adaptation), growth and ontogenetic mechanisms, while mammalian oxylipins

(eicosanoids) control intricate regulatory mechanisms in immunity, functioning as messengers in the central nervous system and participating in resolution processes following tissue injury (Funk, 2001; Mosblech et al., 2010). Moreover, recent studies have illuminated the medicinal value of plant oxylipins, highlighting their anticancer and anti-inflammatory activities (Flesher, 2005, 2007; Taki-Nakano et al., 2014). Notably, molecular nodes and components, as well as metabolic pathways in which are involved oxylipin biogenesis and signaling share common ancestry and evolutionary origins across Kingdoms (Marnett, 2008). Hence, uncovering the modes of actions associated with oxylipins will not only advance our understanding of the phenotypic and environmental plasticity of plants, but also assist the improvement of drug development via facilitating the rational design of more potent and safe anticancer (and anti-inflammatory) drugs. However, our current knowledge regarding oxylipin signaling is still incomplete (Funk, 2001; Mosblech et al., 2010).

Recently, molecular underpinnings have been investigated for (+)-12-oxophytodienoic acid [OPDA; (1*S*,2*S*)-3-oxo-2-(2*Z*-pentenyl)-cyclopent-4-ene-1-octanoic acid], activating an autonomous signaling that regulates a unique subset of jasmonate-responsive genes (Taki et al., 2005; Mueller et al., 2008; Liu et al., 2021). OPDA is a primary precursor of the jasmonate family of plant oxylipins, derived from trienoic-fatty acids via the octadecanoid pathway in the chloroplasts. Once accumulated, a portion of OPDA travels to the peroxisomes and undergoes β-oxidations to form (-)-jasmonic acid [JA; (1*R*,2*R*)-3-oxo-2-(2*Z*)-2-pentenyl-cyclopentaneacetic acid] (Taki-Nakano et al., 2014). In the meantime, the rest of OPDA sets out metabolic cascades via binding and stimulating its receptor, cyclophilin 20-3 (CYP20-3), to form a complex with serine acetyltransferase 1 (SAT1), which stimulates the formation of hetero-oligomeric cysteine (Cys) synthase complex (CSC) with *O*-acetylserine(thiol)lyase B. CSC formation then actuates sulfur assimilation that leads to increased levels of thiol metabolites (e.g., glutathione, GSH) and the buildup of cellular reduction potential. The enhanced redox capacity in turn coordinates the expression of a subset of OPDA-responsive genes (ORGs) in controlling basal and race-specific

(local and systemic) disease resistances, and defense responses against various abiotic stresses (Dominguez-Solis et al., 2008; Park et al., 2013).

CYP20-3 is a dual-function enzyme, exerting peptidyl-prolyl *cis-trans* isomerase (PPIase) and reductase activities, that directly interacts and metabolizes cofactor proteins such as SAT1 (see above) and 2-Cys peroxiredoxin A (2CPA) (Dominguez-Solis et al., 2008; Park et al., 2013; Laxa et al., 2007; Muthuramalingam et al., 2009; Cheong et al., 2017). 2CPA is a highly abundant plastid peroxidase, protecting and modulating photosynthetic mechanisms (Muthuramalingam et al., 2009). However, 2CPA typically forms an obligatory homodimer as the peroxidatic Cys $(C^P)_{175}$ from one monomer is connected via a disulfide bond to the resolving Cys $(C^R)_{53}$ located at another monomer. The oxidation of $C^P{}_{175}$, in consequence, arrests the catalytic activity of 2CPA. Therefore, 2CPA dimers require electron (e^-, H^+) donors such as thioredoxins (TRXs), NADPH-dependent TRX reductase C and/or CYP20-3, which reduces (activates) it to be able to metabolize the detoxification of a toxic byproduct (i.e., H_2O_2) in photosynthesis and the operation of fructose 1,6-bisphosphatase, a key enzyme in the Calvin cycle (Laxa et al., 2007; Muthuramalingam et al., 2009; Dietz et al., 2006; Caporaletti et al., 2007; Liebthal et al., 2019). Hence, deficiency of 2CPA in antisense and T-DNA insertion mutant plants manifested the increased levels of H_2O_2 and carbonylated proteins, while decreasing the quantum yield of photosystem II (PSII) and CO_2 fixation rates, which together result in growth and developmental inhibition (Baier et al., 1999; Baier et al., 2000; Pulido et al., 2010; Awad et al., 2015). In line with this scenario, OPDA-binding promotes CYP20-3 to transfer electrons (e^-, H^+) from PSI via TRXs toward 2CPA, along with SAT1, concomitantly (Dominguez-Solis et al., 2008; Park et al., 2013; Liu et al., 2020). Reduction of 2CPA thereby enhances its antioxidant capacity and fosters photosynthetic efficacy, whereas activation of SAT1 induces GSH productions and activating retrograde signaling to elevate defense gene expressions, in the end, ensuring optimal growth, reproduction and survival of plants (Park et al., 2013; Laxa et al., 2007; Pulido et al., 2010; Konig et al., 2002).

GSH is the most prevalent nonprotein thiol in plants, playing a crucial role in maintaining cellular redox homeostasis under different ecological conditions. Most importantly, it reduces reactive oxygen species (ROS) and other peroxides by providing its electron (e^-, H^+), and is subsequently oxidized to a disulfide form (GSSG). Hence, increased levels in cellular GSH and attendant reduction capacity often coincide with the generation of free radicals and oxidants, supporting a notion that GSH status is involved in transmitting oxidative stress signaling (Noctor et al., 2011). The oxidative bursts, therefore, decrease GSH:GSSG ratios which in turn stimulates the reversible formation of mixed disulfides between protein sulfhydryl groups (PSH) and GSSG (i.e., S-glutathionylation). S-glutathionylation then engenders the structural and functional modification of redox-sensitive enzymes, reformatting the electron transport chain (ETC) of cellular metabolic and signaling pathways in plant growth, immune responses and injury recovery (Grek et al., 2013). For instance, under ROS stresses, 2CPA was originally believed to be hyperoxidized and become homodecamers that lose their peroxidase activities, but instead gain chaperone activity against oxidative damages (Dietz et al., 2006). However, later studies with human PrxI and pea 2CP detailed that they are S-glutathionylated by GSSG, shifting their quaternary structures back from decamers to dimers, and subsequently inactivating their molecular chaperone activity, proposing the alternative roles of 2CPA via S-glutathionylation in response to cell signaling and oxidative stress (Park et al., 2009; Park et al., 2011; Calderón et al., 2017).

In the present study, we unveil the unique mode and activity of S-glutathionylation that conveys plant defense, OPDA, hormone signaling to modulate ROS levels and photosynthetic rates during plant defense and repairing processes against various environmental stresses. Mechanistically, under stress conditions, CYP20-3-depednent OPDA signaling induces high levels of GSH which triggers the S-glutathionylation (posttranslational activation) of 2CPA in accelerating peroxide detoxification and maintaining energy supply, whilst actuating retrograde (from plastids to nucleus) signaling that coordinates ORG expressions and plant defense activation against various exterior pressures. The mode of OPDA signaling thus reconstitutes GSH as a unique and

independent signal cue in controlling an interplay between growth and defense responses, which makes instant and appropriate adaptive decisions to maximize plant plasticity and survival ('fitness') under a range of environmental constraints.

2.3. MATERIALS AND METHODS

2.3.1. Plant Growth Condition.

Arabidopsis WT and mutants (i.e., Δ*2cp*, *pad2*, *cad2*, *cyp20-3*, and *jar1*) (Dominguez-Solis et al., 2008; Pulido et al., 2010; Cobbert et al., 1998; Parisy et al., 2006; Staswick et al., 2002) in Columbia (Col-0) background were grown in a chamber (Caron) with a 12-h light:dark cycle (80-100 $\mu E/m^2/s$) at 22 ^oC and 60% to 80% relative humidity.

2.3.2. Preparation of Recombinant Proteins.

The coding sequence of mature 2CPA, removing the N-terminus signal peptide of 66 amino acids, was cloned into pET28a (Novagen) (Liu et al., 2020) and site-specific mutations were introduced using the QuickChange II site-directed mutagenesis kit (Agilent) and mutagenic primer sets (Table 2.1), according to the manufacturer's instructions. Each recombinant WT and mutant ($C_{53}S$, $C_{175}S$ and $C_{53}S{\cdot}C_{175}S$) protein was then expressed by 0.1 M isopropyl ß-D-1-thiogalactopyranoside in *E. coli* BL21 (DE3), and purified through a nikel- (Pur^{TM} Ni-NTA, Thermo Scientific) column, as previously performed (Cheong et al., 2017; Liu et al., 2020). To remove the His-tag, purified recombinant proteins were incubated with biotinylated thrombin (U/0.5mg) in 20 mM Tris-HCl, pH 8.4, containing 150 mM NaCl and 2.5 mM $CaCl_2$ which were later removed using streptavidin agarose beads (Novagen).

Each preparation for PAGE and LC/MS assays, 2CPAs were oxidized by treating 0.1 mM H_2O_2 for 15 min or reduced by applying 5 mM tris(2-carboxyethyl)phosphine hydrochloride (TCEP-HCl) for 60 min. Excess H_2O_2 was removed using size-exclusion chromatography (Sephadex G-25 medium, GE Healthcare) prewashed with 50 mM Tris-HCl, pH 7.5, while excess TCEP-HCl

was removed by the EZ-Desalt^{TM} spin column (BioVision) pretreated with deionized water, and then 10 mg/mL catalase followed by 50 mM Tris-HCl, pH 7.5 containing 0.1 mM diethylenetriamine-pentaacetic aicd. Tris-HCl was pretreated with 10 µg/mL catalase, which was removed by passage through a Microsep^{TM} centrifugal device 10K filter (Pall Corp.). Finally, protein concentrations were measured using the Amresco Bradford assay kit with bovine serum albumin (BSA) as standard, and stored at 4 °C until use.

2.3.3. S-glutathionylation Reaction of 2CPAs.

Typically, reactions were conducted by incubating 1 or 2 µM 2CPAs with 1.0 - 2.0 mM GSH or GSSG in 50 mM Tris buffer, pH 7.5, at 25 °C for 30 min, while some reactions varied GSH or GSSG concentrations between 0.5 and 20 mM.

2.3.4. LC/MS analysis of 2CPAs.

Samples were prepared in 50 mM Tris buffer, pH 7.5, at 25 °C by treating reduced or oxidized 2CPAs with varying GSH or GSSG concentrations and/or 30 mM *N*-ehylmaleimide (NEM) for >30 min to block remaining thiols. The 2CPAs were then separated by an UltiMate 3000 UHPLC system (Thermo Scientific) equipped with a Aeris C4 column (3.6 µm, 250 x 4.6 mm; Phenomenex), through an acetonitrile gradient from 90% (v/v) solvent A (0.1% [v/v] HCOOH in water) and 10% (v/v) solvent B (0.1% [v/v] HCOOH in MeCN) to 80% solvent B over 5 min at a flow rate of 0.2 mL/min (Peskin et al., 2016). Subsequently, mass spectra for all charge states were acquired using the Orbitrap Exploris mass spectrometer (Thermo Scientific) between *m*/*z* 400 and 2000 in positive mode, averaged over the full-length of each protein peak, and deconvoluted to yield the molecular masses and relative intensities using ProMass for Xcalibur (Novatia). The masses used to identify glutathionylated species are given in Table 2.2.

2.3.5. Peroxidase Activity Assay.

Reduction of H_2O_2 by 2CPAs was quantified via the eFOX assay method, as described previously (Cheeseman, 2006). Briefly, the assay was performed at 37 °C in 50 mM Tris buffer, pH 7.5, containing 50 mM NaCl with 5 µM 2CPAs. Each reaction was initiated by the addition of 50 µM H_2O_2, then incubated for 10 min, and terminated by 2% (w/v) TCA. A volume of 500 µL eFOX reagent (250 µM $Fe(NH_4)_2(SO_4)_2$, 100 µM sorbitol, 100 µM xylenol orange, and 1% [v/v] in 20 mM H_2SO_4) was then mixed with 100 µL of the reaction solution and the reduction in H_2O_2 levels was tracked spectrophotometrically by measuring the difference in absorbance between 550 and 800 nm.

2.3.6. Total Protein Extraction.

Leaf tissues were immersed in liquid N_2 and ground to powder using a mortar and pestle. At 4 °C, ground tissues were dissolved into two volumes of 50 mM Tris buffer, pH 7.5, containing protease inhibitor cocktails (Sigma-Aldrich), agitated for 60 min, and centrifuged for 30 min at 10,000*g*. The supernatant was collected, and immediately used for Bradford assays and immunoblot analyses.

2.3.7. Total Chloroplast Protein Extraction.

Leaf tissues were blundered in 1X chloroplast isolation buffer (CIB, 0.1 M Tris buffer, pH 7.8, containing 0.33 M sorbitol, 5 mM $MgCl_2$, 10 mM NaCl and 2 mM EDTA) and filtered through 6 layers of muslin cloth. The collected aqueous was then centrifuged for 3 min at 200 g, and the supernatant was transferred to a new, pre-chilled tube and centrifuged again for 7 min at 1,000 g to obtain a green pellet. The pellet was gently resuspended with 1X CIB containing 2 mg BSA, carefully layered on the top of 40% percoll^{TM} (in 1X CIB with BSA) and 100% percoll^{TM} (GE Healthcare). After centrifugation at 1,700 g for 6 min, intact chloroplasts were sediment to the tube bottom, which was finally resuspended with 1X CIB for further use.

2.3.8. PAGE and Immunoblot Analyses.

Samples were prepared by adding NuPAGE^{TM} LDS sample buffer (Thermo Scientific) with/without β-mercaptonethanol to total proteins or 2CPAs, reduced, oxidized, S-glutathionylated, and/or alkylated with NEM, and resolved via 10% to 13% SDS/PAGE and then electroblotted onto the PVDF membrane (Millipore). The resulting blots were probed with polyclonal anti-2CPA antibody (1:7500, MyBioSource) for 2 h, or monoclonal anti-GSH antibody (1:3000, Enzo Life Science) for 2 - 16 h, and visualized by chemiluminescence (ECL kit; GE Healthcare).

2.3.9. Stress Treatments.

For the salt and rose bengal treatments, sterilized seeds were plated on MS medium supplemented with increasing concentrations (25, 50 and 100 mM) of NaCl or 3 μM of rose bengal, incubated at 4 ^{o}C for 2 days, and then placed at 22 ^{o}C under a 12-h day cycle (80-100 μE/m^2/s). For high light treatments, 2-wk-old plants, grown under a normal condition were transferred to high-intensity light (300 μE/m^2/s) under a long-day condition (16-h light/ 8-h dark) for 6 days. Photographs were taken on the seventh to fourteenth day after treatments.

2.3.10. Quantification of JA-Ile and OPDA.

The samples of (+)-7-*iso*-jasmonoyl-L-isoleucine [JA-Ile; N-(2-((1R,2R)-3-oxo-2-(2Z)-2-pentenyl-cyclopentaneacetic acid)-L-isoleucine) and (+)-12-oxo-phytodienoic acid [OPDA; (1S,2S)-3-oxo-2-(2Z- pentenyl)-cyclopent-4-ene-1-octanoic acid] were prepared from leaves, harvested at 0 and 3 h after wounding. The jasmonates were separated by a Vanquish UHPLC system (Thermo Scientific) equipped with a reversed-phased column (C18 Luna 5.0 μm, 150 × 2.1 mm; Phenomenex) by using a binary solvent system composed of water with 0.1% (v/v) HCOOH and MeOH with 0.1% (v/v) HCOOH as a mobile phase at a flow rate of 0.2 mL/min. Separations were performed stepwise: 30% (v/v) methanol for 4 min, 60% (v/v) for 6 min, linear increase to 95% for (v/v) 12.5 min. Identity of jasmonates was confirmed by ion fragmentation on an Orbitrap Exploris 120 mass spectrometer (Thermo scientific) with direct injection and operated

with a source voltage of 4.0 kV and source temperature of 300 °C. The analysis parameters were optimized by infusing 10 ng/μL of standard compound, (-)-dihydrojasmonic acid [HJA; 2-((1R,2R)-3-oxo-2-pentylcyclopentyl)acetic acid], JA-Ile and OPDA in 50% (v/v) MeOH with 0.1% (v/v) HCOOH at a flow rate of 0.2 mL/min, in multiple reaction- monitoring mode; the fragments m/z 322.3 → 130.2 (JA-Ile), 213.20 → 195.1 (HJA) and 293.4 → 275.4 (OPDA) were monitored in a positive mode and used for the quantification, respectively.

2.3.11. Photosynthesis Measurements.

The data collection for chlorophyll fluorescence-based photosynthetic traits, the total non-photochemical excitation quenching (NPQt, Tietz et al., 2017) and the quantum efficiency for photosystem II photochemistry (*Φ*II, Kuhlgert et al., 2016) was carried out hourly from 9:00 am to 3:00 pm on two leaves of five plants using the hand-held MultispeQ device (Kulgert et al., 2016) and uploaded to the PhotosynQ platform (http://www.photosynq.org) according to the manufacturer's instructions.

2.3.12. Determination of GSH and GSSG.

The level of GSH and GSSG present in leaf tissues were measured by using a GSH (GSH/GSSG/total) fluorometric assay kit (BioVision) according to the manufacturer's instructions. Briefly, leaf tissues were homogenized in ice cold 0.1 M phosphate buffer, PH 7.4, containing 5 mM EDTA, and subsequently treated with 6 N perchloric acid (PCA) to extract GSH and GSSG. PCA was then precipitated by 6 N KOH immediately before assays. For GSH detections, a fluorescence probe o-phthalaldehyde (OPA) was directly added to KOH-neutralized samples, whereas - for GSSG detections - OPA was added to the samples after pre-incubating with 1-methyl-2-vinylpuridinium triflate and GSH reductase to quench pre-existed GSH, and next convert GSSG to GSH, respectively. Finally, levels of GSHs labeled with OPA were fluorometrically measured at Ex/Em=340/420 nm using the BioTek reader (Agilent).

2.3.13. Semiquantitative and Quantitative RT-PCR.

Total leaf RNA was prepared using TRIzol reagent (Invitrogen) and the Direct-zol RNA Kit (Zymo Research) according to the manufacturer's instructions. RNA qualities were assessed by agarose gel electrophoresis and NanoDrop (A_{260}/A_{280} > 1.8 and A_{260}/A_{230} > 2.0) (Udvardi et al., 2008). RT reactions were performed using an oligo(dT) reverse primer and a qScript reverse transcriptase (Quantabio). Semi-quantitative RT-PCR was then performed using 2 μL cDNA with *Taq* 2X master mix (New England BioLabs) at an annealing temperature, 55 °C, for primer pairs (**Table 2.1**) for 30 cycles, whereas quantitative PCR was performed with the PerfeCT® SYBR® Green Fast Mix® Reaction Mixes (QuantaBio) in the CFX96 Touch™ (Bio-Rad) PCR system cycled 40 times using gene-specific primer sets (**Table 2.1**). The annealing temperature for the primer pairs was 53 °C. To determine the relative abundance of target transcripts, the sample cDNA was assessed with housekeeping genes, *POLYUBIQUITIN* (*UBC*) (Czechowski et al., 2005), and the average threshold cycle (i.e., Ct) was normalized to that of *UBC* as $2^{-\Delta Ct}$ where $-\Delta Ct = (Ct_{,gene} - Ct_{,UBC})$.

2.3.14. Statistical Analysis.

All statistical analyses were performed using R statistics software (R Foundation for Statistical Computing).

2.4. RESULTS

2.4.1. GSH Binds and Determines the Quaternary Structure of 2CPA in the Chloroplasts. To further delineate an OPDA signaling circuitry, we investigated the cellular and organismal activity of an OPDA receptor, CYP20-3, and its cofactors including 2CPA (Park et al., 2013; Cheong et al., 2017; Liu et al., 2020). 2CPA however appeared to bind a reduced form GSH, and became insensitive to the enzymatic (reductase) activity of CYP20-3, unless conditioned at high temperatures (≥36 °C) (Liu et al., 2020). Thus, we inspected if and/or how 2CPA mechanistically binds GSH using nonreducing SDS/PAGE and LC/MS separations (Figure 2.1A-C and 2.2). Both

analyses indeed corroborated that increases in GSH concentrations progressively promote total S-glutathionylation of 2CPA, and subsequently lead to its monomerization. As shown in Figure 2.3 without GSH, 2CPA was obligatorily oxidized and dimerized by itself (~47.959 kDa, Table 2.2). GSH (0.307 kDa) supplementation then steadily targeted and S-glutathionylated 2CPAs, increasing its molecular weight (MW) to ~48.390 kDa (2x 23.975_{2CPA} + 0.125_{NEM} + 0.307_{GSH}), and eventually cleaving them to monomeric species ~24.409 kDa (23.975_{2CPA} + 0.125_{NEM} + 0.307_{GSH}) in a concentration-dependent manner (Figure 2.1B and C).

The in vitro results (Figure 2.1A and 2.2) sign that the basal-level cellular concentrations of GSH in the chloroplasts (~1 mM) (Koffler et al., 2013) where 2CPA is localized are sufficient to S-glutathionylate part of 2CPAs in planta. To substantiate this hypothesis, we compared the MW of 2CPA with those of GSH-bound proteins in total Arabidopsis extracts using anti-2CPA (2CPA-α) and anti-GSH (GSH-α) antibodies (Figure 2.1D). In the nonreducing condition (-β-mer), both antibodies cross-reacted with several proteins including two major bands (lane 1 and 3) that correspond to monomeric and homodimeric 2CPAs respectively, as those were markedly attenuated in T-DNA insertion mutants of *2CPs* (Δ*2cp*, Figure 2.1E). Note that Δ*2cp* is not a complete null mutant of *2CPA*, displaying residual-level accumulations of its mRNA and protein (Figures 2.1E and 2.4) as previously described (Pulido et al., 2010). In comparison, the supplement of reductant (+β-mer) engendered the monomerization of 2CPA (Figure 2.1D, lane 2) and the de-glutathionylation of all GSH-binding proteins (lane 4), reassuring that S-glutathionylation, occurred by thiol-disulfide exchanges, defines the conformation. In further support, the depletion of GSH accumulations in *pad2* and *cad2* mutants (Cobbert et al., 1998; Parisy et al., 2006) notably decreased 2CPA S-glutathionylation (Figure 2.1F, right panel) and, as a result, hindered monomerizing 2CPA (left panel). The need of GSH-producing enzyme, γ-glutamylcysteine synthetase, in 2CPA S-glutathionylation (Figure 2.1F) clearly defines the intrinsic role of GSH in balancing the redox and structural homeostasis of 2CPA upon arriving in the chloroplasts.

2.4.2. GSH-dependent S-glutathionylation Stimulates the Enzymatic Activity of 2CPA. The LC/MS analysis identified that GSH-binding yields dimeric and monomeric 2CPA species through the single S-glutathionylation (~24.409 and ~48.390 kDa, Figure 2.1B and Table 2.2). To understand a functional context for the S-glutathionylation, we assessed if GSH targets a specific or random Cys between two C^{R}_{53} and C^{P}_{175} residues of 2CPA, by probing the binding capacity of GSH to three different Cys to Serine (Ser) single or double mutagenized 2CPA ($C_{53}S$, $C_{175}S$ and $C_{53}S{\cdot}C_{175}S$) proteins (~23.955 kDa, Figure 2.5A, B, and 2.6). The immunoblot (IB) detection revealed that GSH binds only 2CPA·$C_{175}S$ (Figure 2.5A) and releases an extra species with increased MW ~24.260 kDa ($23.955_{2CPA{\cdot}C175S}$ + 0.307_{GSH}, Figure 2.5B), elucidating that GSH selectively S-glutathionylates the C^{R}_{53}, and its occurrence with one or both C^{R}_{53} from $2CPA^{ox}$ dimers determines the quaternary structure (e.g., dimer and monomer) of S-glutathionylated $2CPA^{(GS)}$ (Figure 2.1B, C and 2.5C). On the other hand, the catalytic Cys (C^{P}_{175}) thus becomes available to receive an electron (e^{-}, H^{+}) from GSH and in turn activates the peroxidase activity of $2CPA^{GS}$, enabling to reduce and detoxify H_2O_2 (Figure 2.5D). The result concours with the conclusion that GSH act as an electron (e^{-}, H^{+}) donor to 2CPA.

2.4.3. GSSG-dependent S-glutathionylation Protects 2CPA against Oxidative Stresses. A unique mode and cellular activity of GSH-dependent 2CPA S-glutathionylation prompted us to assess if and/or how GSSG S-glutathionylates 2CPA, once examined in pea using a reduced form (pre-treated with 10mM DTT) of $Ps2CPA^{(red)}$ (Calderón et al., 2017). In running the nonreducing SDS/PAGE (Figure 2.7A), $2CPA^{red}$ monomers (visible when their free thiols were alkylated/blocked by NEM, lane 2) were mostly oxidized to dimers (lane 1) through either strong oxidants used as initiators in gel polymerization such as ammonium persulfate or molecular oxygen generated during the gel polymerization (Sun et al., 2004). In this condition, GSSG supplementations progressively prevented the artifactual oxidation of $2CPA^{red}$ in a concentration-dependent manner (lane 3 to 5) indicating that GSSG forms mixed disulfides with the PSH of $2CPA^{red}$ and in consequence occludes 2CPA dimerization. GSSG could target, unlike GSH, both

C^{R}_{53} and C^{P}_{175} of $2CPA^{red}$ (Figure 2.7B) and formed double S-glutathionylation ~24.581 kDa (23.975_{2CPA} + 2x 0.307_{GSH}, Figure 2.7C and D). S-glutathionylation of the C^{P}_{175} (catalytic Cys) then led to the deactivation of $2CPA^{red}$ peroxidase activity (Figure 2.7E vs. 2.5D), illuminating the potentially different role of GSSG vs. GSH in controlling the cellular activity of 2CPA. Note that GSSG did not S-glutathionylate $2CPA^{ox}$ (Figure 2.8). In this respect, protein S-glutathionylation by GSSG is often considered a way to protect irreversible oxidation of, while inactivating, protein thiols, and the $proteins^{GS}$ are reactivated/restored by deglutathionylating enzymes such as sulfiredoxin and glutaredoxin when oxidative stress conditions are over (Baier et al., 1999; Baier et al., 2000; Park et al., 2009; Calderón et al., 2017; Peskin et al., 2016; Dalle-Donne et al., 2007; Zhang et al., 2017). We hence surveyed the structural integrity of single (GSH-treated) and double (GSSG-treated) S-glutathionylated 2CPAs against hyperoxidation (Figure 2.7F). The IB analysis detecting level 2CPAs exhibited as anticipated that the pre-treatment of GSSG sustains 2CPA structures better than GSH against the higher concentrations (e.g., 2 mM) of H_2O_2. However, GSSG-induced S-glutathionylation of $2CPA^{red}$ was clearly less effective than GSH toward $2CPA^{ox}$ (Figure 2.7G), entailing excessive negative potentials (≥1 mM GSSG, Figure 2.7A and D) that is ≥10-fold greater than its cellular concentrations (~70-100 μM) (Koffler et al., 2013).The results together with the fact that 2CPA is obligatorily an oxidized dimer (Figure 2.6, Liebthal et al., 2019) reconstitute that GSH is, rather than GSSG, a preferential modifier of 2CPA S-glutathionylation. Indeed, increased GSH:GSSG ratios (>14:1) stimulate 2CPA S-glutathionylation, whereas decreased reduction capacity (≤14:1) showed little effect on 2CPA S-glutathionylation (Liu et al., 2020). Note that the chloroplasts maintained basal GSH:GSSG ratios of 14:1 (Koffler et al., 2013).

2.4.4 GSH-dependent S-glutathionylation Relies an OPDA Signal in Protecting Photosynthesis under Environmental Stresses. Our data suggests two distinctive modes and activities of S-glutathionylation in conditioning the cellular structure and function of 2CPA (Figure 2.9A). In line with this scenario, our earlier study revealed that CYP20-3 relays an OPDA signal to stimulate GSH biogenesis, independently of the oxidative bursts, under stresses e.g., wounding

(Figure 2.9B and 2.10, Table 2.2, Park et al., 2013). These together postulate that OPDA signaling conveys stress inputs into the output, the activation of 2CPA, that maintains photosynthetic redox homeostasis (Dietz et al., 2006; Caporaletti et al., 2007; Liebthal et al., 2019). To substantiate this hypothesis, we first IB surveyed ex vivo dynamics of 2CPA S-glutathionylation in conjunction with wound-responsive jasmonate biosynthesis. Wounding induced the accumulation of OPDA with a peak at ~1 to 3 h post wounding (hpw), subsequently JA-Ile, and ultimately the differential expression of various genes (Figure 2.11 and Table 2.3, Park et al., 2013). As anticipated, 2CPA S-glutathionylation was promoted in parallel with OPDA, but not JA-Ile, signaling which channels wound-responsive GSH synthesis (Figure 2.9B, 2.9C, S7 and Table 2.2 and 2.3). At 4 hpw, level 2CPAs were increasingly upregulated while progressively monomerized in WT and *jar1* (+OPDA/-JA-Ile signaling), whereas mostly cumulated as dimers in the *cyp20-3* (-OPDA/+JA-Ile signaling), indicating that GSH-dependent S-glutathionylation conveys OPDA signaling to drive redox reaction routes that accelerate peroxide detoxification capacity (elevated 2CPA activity) during plant stress recovery/acclimation processes.

In agreement with the in situ IB results, *cyp20-3* impaired the timely removal of wound-responsive H_2O_2 accumulations that otherwise peaked at 4 hpw and were steadily neutralized as shown in wounded WT and *jar1* (Figure 2.9D and Table 2.4). Wounded Δ*2cp*, on the other hand, accumulated significantly higher H_2O_2 amounts at 4 hpw than wounded WT and *jar1*, corroborating an essential role of 2CPA in resolving stress-responsive increases in H_2O_2, which is functionally coupled with protecting photosynthetic machinery (Liebthal et al., 2019). We hence assessed if the wound-reactive spike of H_2O_2 antagonizes photosynthetic efficiency. As expected, wounded Δ*2cp* and *cyp20-3* reduced the utility of light energy lower than wounded WT and *jar1*, as revealed by the extensive total nonphotochemical quenching($NPQ_{(T)}$, Tietz et al., 2017, Figure 2.12 and Table 2.5) and the decreased photosynthetic efficiency (photosystem II quantum yield (Φ_{II}), Kuhlgert et al., 2016, Figure 2.9E and Table 2.6). These results describe that CYP20-3-dependent GSH synthesis and its protein (e.g., 2CPA) S-glutathionylation (referred to as 'reductant

(GSH) signaling') relay an OPDA defense signal in maintaining photosynthetic processes and efficiency, shedding light on a unique regulatory hub and interplay between growth and defense processes. Indeed, the disruption of reductant signaling in *cyp20-3* also attenuated the wound-responsive upregulation of ORG expressions such as *GLUTATHIONE S-TRANSFERAE 8* (*GST8*) and *GST6* (Mueller et al., 2008) (Figure 2.9F) that activate defense responses (Gullner et al., 2018). However, wounded Δ*2cp* exhibited WT-like wound-responses of *GST8* and *GST6* expressions, indicating that GSH and its reductant signaling are an upstream regulator and metabolic pathway in the maintenance of photosynthesis and the activation of defense gene expressions.

2.4.5. A Programmed Synthesis of GSH by CYP20-3-dependent OPDA Signaling is Intrinsic in Plant Stress Defense and Acclimation. Our results explain the role of GSH in relaying CYP20-3-dependent OPDA signaling that delivers different stress cues to two distinct cellular processes, *1*) fostering 2CPA activations in photosynthesis and *2*) coordinating ORG expressions. The latter then reprograms plant cells toward defense modes against various environmental challenges (Liu et al., 2021). Thus *cyp20-3*, impeding stress-responsive GSH biogenesis (Figure 2.9B, 2.10, 2.13 and Table 2.2, Park et al., 2013), manifested hypersensitivity to various exterior stresses, including rose bengal, a light-dependent inducer of ROS, singlet oxygen ($^1O_2$, Figure 2.14A). When seeds were plated on Murashige and Skoog (MS) medium supplemented with 3 μM rose bengal, germination and growth of *cyp20-3* seedlings were significantly suppressed relative to WT, *jar1* and Δ*2cp*, validating a crucial role of OPDA-induced reductant signaling in stress and defense responses.

Abiotic stresses such as elevated salt levels and high light also damage plants by producing ROS. When subjected to these stresses, *cyp20-3* showed a response similar to that observed with rose bengal (Figure 2.14B and 2.14C). Under the increasing concentrations of excess NaCl (25 to 100 mM), the germination rate of *cyp20-3* seedlings was progressively inhibited (Figure 2.14B). Similarly, high light treatment (300 μmol photons $m^{-2}s^{-1}$) severely inhibited growth and

photosynthetic efficiency in all plants (Figure 2.14C). Once again, however, *cyp20-3* suffered the most, whereas *jar1* (-JA-Ile signaling) grew noticeably larger in the optimal condition and exhibited a slight increase in photosynthesis under high light intensity. These results together allow us to locate CYP20-3 and its GSH production at a central metabolic pathway of OPDA signaling which cross-regulates a light-dependent ETC (growth) and ORG expressions (defense) under stressed states (Figure 2.14D).

2.5. DISCUSSION

In nature, plants must grow and defend themselves to survive and reproduce. A caveat is that defense activations come at the expense of growth and vice versa (Huot et al., 2014). This phenomenon, referred to as 'growth and defense tradeoff', well circumstantiates plant responses toward the persistent and/or excess surges of environmental pressures. Plants, however, are more often situated at resisting a series of transient and modest level stresses, while concurrently completing growth to achieve maximum yields and development. Thus, recent studies have begun to elaborate an alternative model 'growth and defense coordination' wherein a balancing act between growth and defense can collectively optimize plant fitness and survival (Kliebenstein, 2016). For instance, perception of changes in light intensity leads to the spatial production of auxins that fosters phototropic growth and, at the same time, initiates jasmonate signaling that actuates defense machinery in Arabidopsis (Holliday et al., 2009; Sakai et al., 2012; Ballaré et al., 2014). Auxins however suppress JA-Ile signaling via promoting gibberellin (GA) synthesis which in turn triggers the degradation of DELLA proteins, negative regulators of GA but activators of MYC2 TF (Ballaré et al., 2014; Frigerio et al., 2006; Hou et al., 2010). MYC2 is a key TF relaying COI1/JA-Ile signaling (Pieterse et al., 2012). Hence, the light-responsive jasmonate signaling likely is conveyed by OPDA, another biologically active jasmonate, that is in fact induced by EL intensity on a time scale of hours with the concomitant accumulation of a subset of jasmonate-responsive genes (Riemann et al., 2003; Kazan et al., 2011). In this context, the disruption of OPDA signaling (*cyp20-3*) manifested both plant growth retardation under EL, and

hypersensitivity toward EL-originated oxidative stress (Figure 2.14A and 2.14C, Dominguez-Solis et al., 2008). Besides, a sorghum inbred line accumulating higher level OPDA displayed not only enhanced defense capacity to aphid attacks, but also minimal biomass loss as well as robust photosynthetic machinery. On the other hand, the aphid-tolerant line accumulated similar or attenuated levels of JA-Ile and other plant defense-associated hormones including salicylic acid (SA) and cytokinin, comparing to aphid-susceptible lines (Grover et al., 2020). The results from our and other groups indicate a crucial role of OPDA signal as a key facet of plant growth and defense coordination, which assists in making instant and appropriate adaptive decisions to maximize plant plasticity and survival ('fitness') under a range of environmental constraints.

In the present study, OPDA activates CYP20-3-dependent GSH biogenesis that deploys redox-dependent signal transmissions in i) stimulating the retrograde regulation of defense ORG expressions, while ii) enriching the S-glutathionylation (activation) of 2CPA, which optimizes photosynthetic efficacy and redox homeostasis (Figure 2.14D). In light of this, 2CPA S-glutathionylation appears to convey two distinctive metabolic, cellular redox signaling. Thus far, a number of studies have focused on the activity of GSSG-dependent $2CPA^{red}$ S-glutathionylation in oxidative stress signaling (Noctor et al., 2011; Grek et al., 2013; Park et al., 2009; Dalle-Donne et al., 2007). When GSSG levels are increased by mitigating the ROS burst under environmental stresses, GSSG targets and forms disulfide bonds with two PSHs at C^{R}_{53} and C^{P}_{175} of $2CPA^{red}$, resulting in its deactivation but protection against ROS damages (e.g., Figure 2.7D to 2.7F). Hence, GSSG-dependent $2CPA^{red}$ S-glutathionylation is proposed to relay 'oxidant signaling' in fostering organismal adaptations to new environmental changes (Park et al., 2009; D'Autréaux et al., 2007; Ahmad et al., 2008). However, the GSSG-dependent PTM often requires ~10 to 50-folds higher GSSG concentrations than its cellular levels, as well as 2CPA is found to obligatorily form an oxidized homodimer (Liebthal et al., 2019; Noctor et al., 2011; Calderón et al., 2017; Koffler et al., 2013; Gelhave et al., 2004; Bender et al., 2015), needing further validation of its physiological efficacy and relevance. Herein, we observed that GSH could be more effective than GSSG (> ~8-

folds, Figure 2.7G) capable, at its physiological concentrations, of S-glutathionylating $2CPA^{ox}$ (Figure 2.1). Interestingly, GSH confers differential structural and functional PTM, compared with GSSG (Figure 2.5 and 2.7). GSH targets only one PSH (C^{R}_{53}, non-catalytic thiol) and, in lieu, reduces catalytic thiol (C^{P}_{175}), switching on the activation of oxidized 2CPA dimer to monomer, and maintaining optimal photosynthesis.

In plants, photosynthesis, transforming sunlight and water into chemical energy that fuels growth and survival under various ecological conditions, is on the other hand a principal manufacturer of H_2O_2. In the light-dependent reactions, a water molecule is split to O_2 as a high-energy waste product at PSII. Subsequently, the reduction of O_2 at PSI generates superoxide radical (O^{-}_{2}) and releases H_2O_2, which in turn reduces photosynthetic activity to half, and stimulates the production of hydroxyl radicals (•OH) causing irreversible damage in the chloroplasts (Miyake, 2010). Hence, H_2O_2 in optimal condition is rapidly scavenged back to water by ascorbate peroxidases (called, water-water cycle; WWC), safely dissipating excess excitation energy. When exposed to stresses, however, most ascorbate peroxidase (APX) isoforms, highly sensitive to oxidative inactivation, become completely deactivated (Shikanai et al., 1998), entailing different peroxidases to complete the O_2-dependent sequential reactions. In line with this scenario, we revealed that i) an arresting the peroxidase activity of 2CPA manifests drastic increases in H_2O_2 concentrations, and attendant decreases in photosynthetic efficiency, under stresses (Figure 2.9D, 2.9E, 2.12 and Table 2.4-2.6), and ii) the 2CPA-dependent, APX-independent, stimulation of WWC is intertwined with a major plant defense apparatus actuating OPDA signaling, which in turn stimulates reductant signaling (GSH-dependent S-glutathionylation), and peroxidase activity of 2CPA (Figure 2.5D, 2.9B, 2.9C, 2.11 and Table 2.2, 2.3). These results further validate a previous hypothesis that 2CPA is a critical H_2O_2-scavenger in preventing photoinhibition occurs under environmental pressures, safeguarding and enriching a flux of linear electron flow in photosynthesis step (Konig et al., 2002).

Besides its role in photosynthesis, the OPDA/GSH pathway puts forward an alternative, retrograde directional route of reductant signaling, which sheds new insights on regulatory gaps in plant defense hormone (e.g., OPDA and SA) signaling. Under stressed conditions, OPDA and SA accumulated in the chloroplasts and/or cytosol promote GSH accumulations and build up cellular reduction capacity, which in turn coordinate defense gene expressions (Mueller et al., 2008; Park et al., 2013; D'Autréaux et al., 2007; Mou et al., 2003). In these signaling pathways, GRX480 can be considered as a multifunctional transcriptional regulator (TR) as it can be induced by both OPDA and SA. GRX480 is an electron carrier using GSH as a cofactor that binds and regulates a series of TGA TFs (Mueller et al., 2008; Ndamukong et al., 2007; Li et al., 2009). TGAs belong to a basic leucine zipper TF family that conveys various signaling pathways involving hormones, reactive electrophilic species (RES) and ROS, in supporting environmental plasticity in plants (Mueller et al., 2008; Ndamukong et al., 2007; Mhamdi et al., 2010). The latter could explain signal redundancy between CYP20-3-dependent OPDA signaling and 2CPA-mediated ETC (Figure 2.15). We in this study observed that both *cyp20-3* and Δ*2cp* impair the transcriptional induction of selective ORGs, particularly those involved in general defense responses such as *GLUTAREDOXIN 480* (*GRX480*) *HEAT SHOCK PROTEIN 70.6* (*HSP70.6*), and *HSP17.6* (Park et al., 2013; Mou et al., 2003; Finka et al., 2011). When stressed, *cyp20-3* and Δ*2cp* both cause the dysregulation of redox states, e.g., increased H_2O_2 accumulations (Figure 2.16 and Table 2.7), that subsequently actuate general stress tolerance (*HSPs*, Figure 2.15) machineries through ROS-responsive NAC TFs (Mhamdi et al., 2010; Wu et al., 2012). Alternatively, stress-responsive breakage of linolenic acid in the chloroplast membranes produces RES in parallel to OPDA, which could regulate TGA TF-dependent transcriptions, including *GRX480* and *HSP70.6* (Figure 2.13) (Mueller et al., 2008). Indeed, we were able to show in this study that oxidative ROS (e.g., GSSG) signaling shares target (e.g., 2CPA) and a starting signal (e.g., GSH) metabolites with reductant signaling that regulates general and/or signal-specific defense responses and gene expressions.

GSH is a major redox homeostatic buffer in aerobic life, reducing oxidative damages and transmitting oxidative stress signaling throughout a range of plant growth and survival processes. However, our knowledge of mechanistic details on its function remains to be fully explained (Noctor et al., 2011). In this study, we reveal a unique role of GSH as a key, autonomous signal messenger that shapes plant plasticity and optimal phenotype ("fitness"). This model sheds new light on the understudied i) mode of capacity of plants, being able to enhance stress responses without growth penalties, ii) unique interface between light and hormone signaling, which fine-tune energy (e^-, H^+) allocations between growth and defense while being challenged constantly by environmental pressures, ultimately maximizing survival and yield potential, and iii) signaling circuitry of OPDA and its crosstalk with other hormone hormones and reactive species, which activate unique and conserved (general) defense mechanisms to coordinate ultimate recovery systems. Hence, the future study on the finer, global aspects of S-glutathionylation and reductant signaling will further delineate the regulatory dynamics of balancing acts in plant growth and defense coordination.

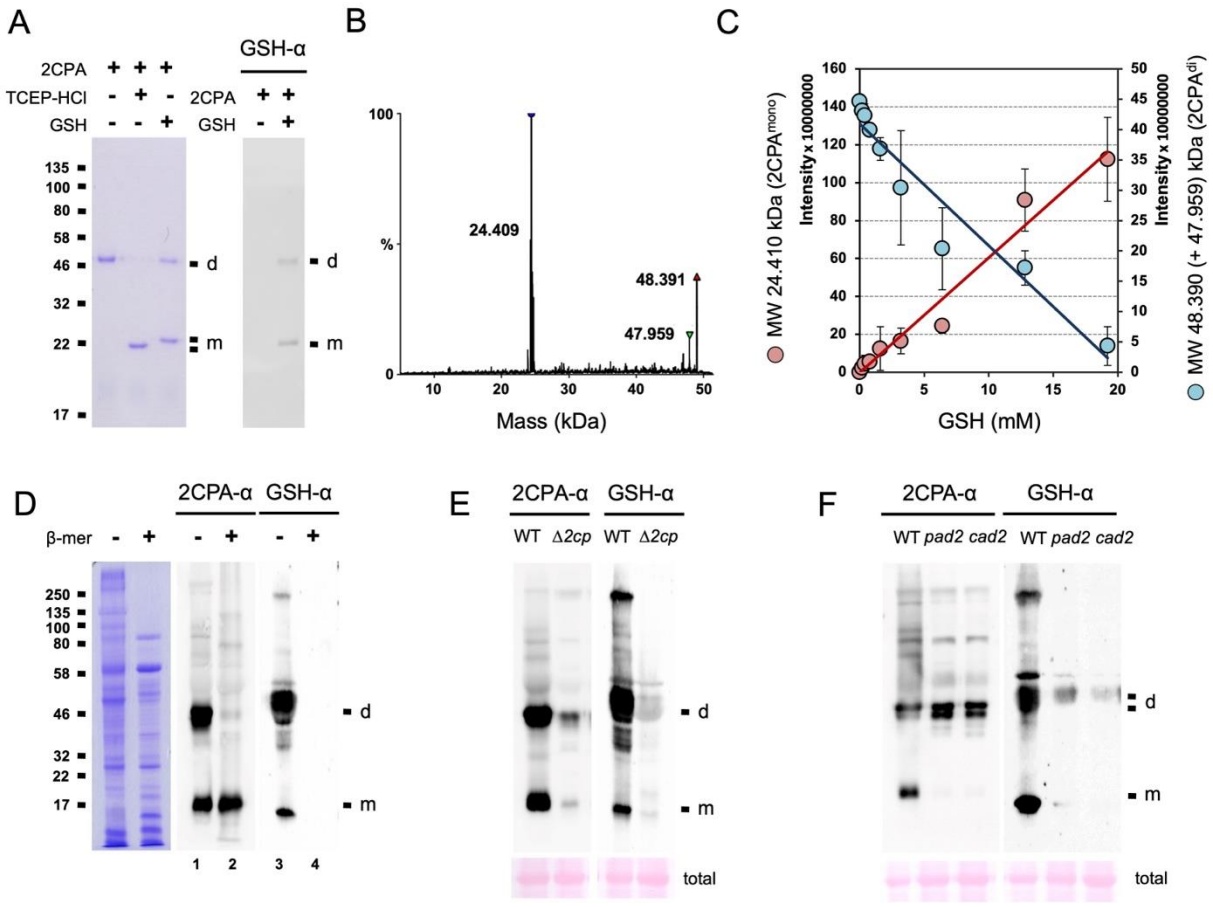

Figure 2.1. GSH-dependent S-glutathionylation Determines the Cellular Structure and Function of 2CPA. (A) Reduced GSH S-glutathionylates and monomerizes 2CPA. The 1 μM 2CPA, incubated with/without 1 mM GSH or TCEP-HCl (a reducing agent) for 30 min, were subjected to nonreducing SDS/PAGE (left panel) and immunoblot (IB, right panel) analyzed using monoclonal anti-GSH antibody (GSH-α, noted on the top). **(B,C)** LC/MS analysis of GSH-treated 2CPA. A representative spectra **(B)**, and the μM kinetics **(C)** of deconvoluted masses of 2CPA incubated with increased concentrations (0, 0.2, 0.4, 0.8, 1.6, 3.2, 6.4, 12.8 and 19.2 mM) of GSH and 15 mM NEM. Three major peaks in **(B)** indicate a monomeric $2CPA^{GS}$ (~24.409 kDa = $23.957_{2CPA} + 0.125_{NEM} + 0.307_{GSH}$), a dimeric $2CPA^{GS}$ (~48.391 kDa = 2x $23.957_{2CPA} + 0.125_{NEM} + 0.307_{GSH}$) and a dimeric 2CPA (~47.959 kDa = 2x 23.957_{2CPA}). **(D-F)** GSH-dependent S-glutathionylation determine the structure homeostasis of 2CPA in planta. **(D)** Equal amounts of

total protein extracts prepared from WT (Col-0) were subjected to nonreducing (-β-mer) and denaturing (+β-mer) SDS/PAGE (left panel), and IB analyzed by polyclonal anti-2CPA antibody (2CPA-α, middle panel) and GSH-α (right panel). **(E,F)** Equal amounts of total proteins extracted from WT (Col-0; **E,F**) and Δ*2cp* (*2cpa* and *2cpb* double mutant; **E**), or *pad2* and *cad2* (GSH-deficient mutants; **F**) were separated in nonreducing SDS/PAGE and IB analyzed by 2CPA-α (left panel) and GSH-α (right panel). PVDF membranes of total Arabidopsis extracts were stained with Ponceau S (bottom). d or $2CPA^{di}$, dimeric 2CPA. m or $2CPA^{mono}$, monomeric 2CPA. Note that all proteins used in this study were tag-free versions.

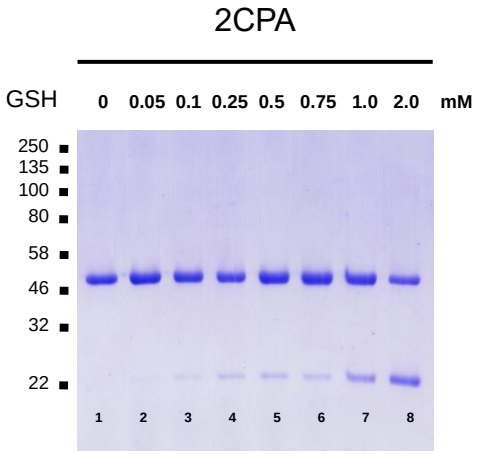

Figure 2.2. Reduced Form GSH Stimulates the Monomerization of 2CPA in a Concentration-Dependent Manner. Homodimeric, oxidized 2CPAs$^{(ox)}$ (lane 1) were subjected to nonreducing SDS/PAGE, following 30-min incubation with the increasing concentration of GHS (0 to 2 mM) at 25 ^{o}C. Gel was stained with Coomassie Brilliant Blue, and the standard molecular-weight (MW) sizes (kDa) were indicated in the left of gels.

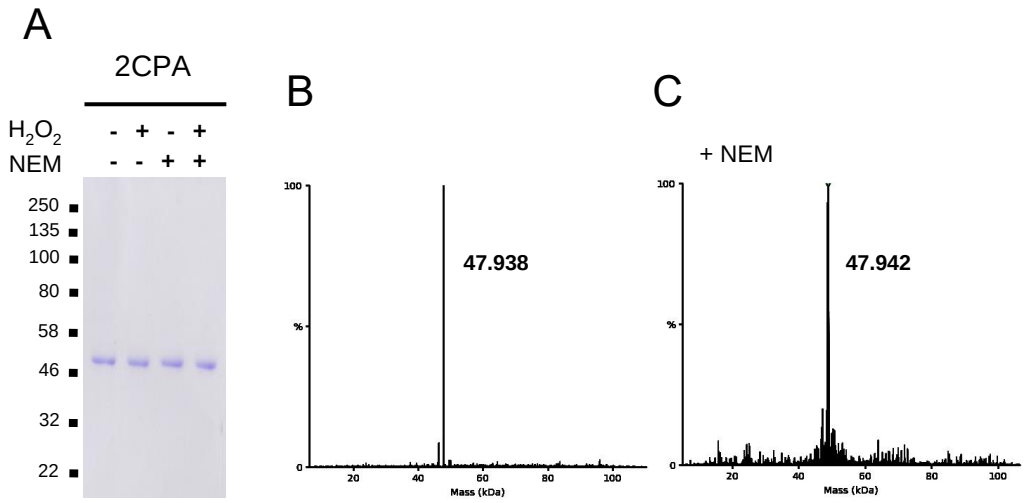

Figure 2.3. In Our Experimental Buffer (50 mM Tris-HCl, pH 7.5) Condition, 2CPA Forms an Obligatory Homodimer through Double Disulfide Bonds. (A) MWs of Ni-column purified, His-tag freed 2CPA in the presence or absence of 10 μM H_2O_2 and/or 30 mM *N*-ehylmaleimide (NEM) in nonreducing SDS/PAGE. The gel was stained with Coomassie Brilliant Blue, and the standard MW sizes (kDa) were indicated in the left of gels. **(B and C)** Typical examples of deconvoluted mass spectra of Ni-resin purified, His-tag removed 2CPA (~23.975 kDa, 5 μM) in the absence (B) and presence **(C)** of 15 mM NEM (0.125 kDa) treatment, exhibiting that ***i***) two 2CPAs assemble a dimeric structure (~47.950 kDa, Table 2.1), and ***ii***) NEM did not derivatize a dimeric 2CPA. The result elucidates that a homodimeric 2CPA forms double disulfide (S-S) bonds.

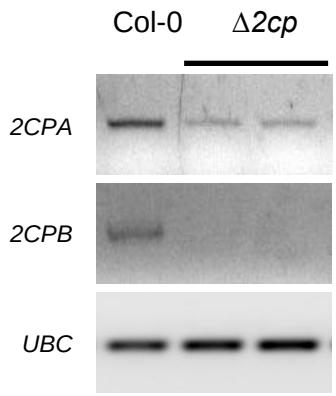

Figure 2.4. The Δ*2cp* Attenuates the Level Expression of *2CPA*. Semiquantitative RT-PCR analyses of *2CPA* and *2CPB* in WT (Col-0) and Δ*2cp* mutant plants. Total RNAs were prepared from the leaves of each plant, and transcript levels of *POLYUBIQUITIN* (*UBC*, Czechowski et al., 2005) were used as an equal loading control.

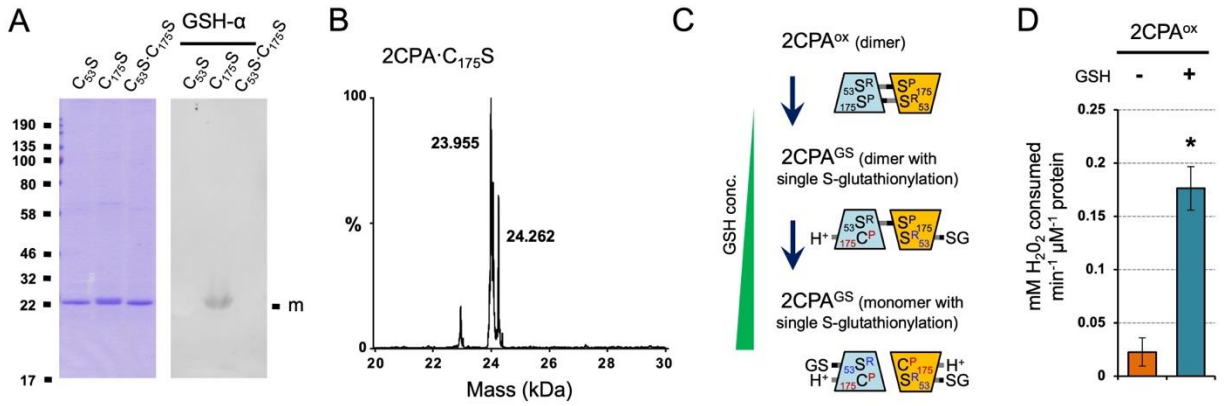

Figure 2.5. GSH Selectively S-glutathionylates the C_R^{53} of 2CPA and Activates Its Peroxidase Activity. (A, B) Reduced GSH binds only the Cys175 to Ser mutagenized 2CPA ($C_{175}S$). Three single or double Cys to Ser mutant 2CPAs ($C_{53}S$, $C_{175}S$ and $C_{53}S{\cdot}C_{175}S$, 1 μM) were incubated with 2 mM GSH for 30 min, and IB analyzed by GSH-α **(A)** and separated in LC/MS (**B** and **Figure 2.6**). Two major peaks in **(B)** indicate a monomeric $2CPA{\cdot}C_{175}S$ (~23.955 kDa) and $2CPA{\cdot}C_{175}S^{GS}$ (~24.260 kDa = $23.955_{2CPA{\cdot}C175S}$ + 0.307_{GSH}). m, monomeric 2CPA mutant. **(C)** Proposed mode of GSH-dependent S-glutathionylation of 2CPA. From the top, GSH exchanges S-S bond(s) with the C^R_{53} residue of $2CPA^{ox}$ dimer, while donating electron (H^+, e^-) to the adjacent C^P_{175} residue, which release single S-glutathionylated $2CPA^{GS}$ dimer (middle) and monomer (bottom) in a GSH concentration-dependent manner. GSH conc., GSH concentrations. **(D)** S-glutathionylation activates $2CPA^{ox}$. Peroxidase activity was measured in $2CPA^{ox}$ and $2CPA^{GS}$ by incubating with 50 μM H_2O_2 for 10 min. H_2O_2 was then quantified using the eFOX method (Cheeseman, 2006, mean ± SD; *n* = 3). The asterisk (*) indicates statistically significant differences ($P < 0.05$, the student's t-test).

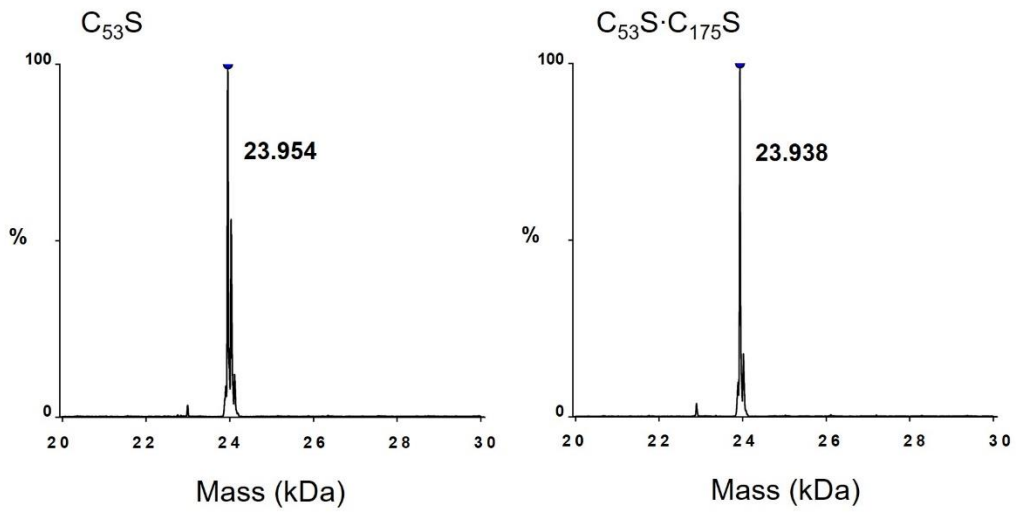

Figure 2.6. GSH Does Not S-glutathionylates $C_{53}S$ and $C_{53}S$・$C_{175}S$ Mutant 2CPAs. A single or double Cys53 to Ser mutant 2CPAs ($C_{53}S$ and $C_{53}S$・$C_{175}S$, 1 μM) were incubated with 2 mM GSH for 30 min, and analyzed by LC/MS.

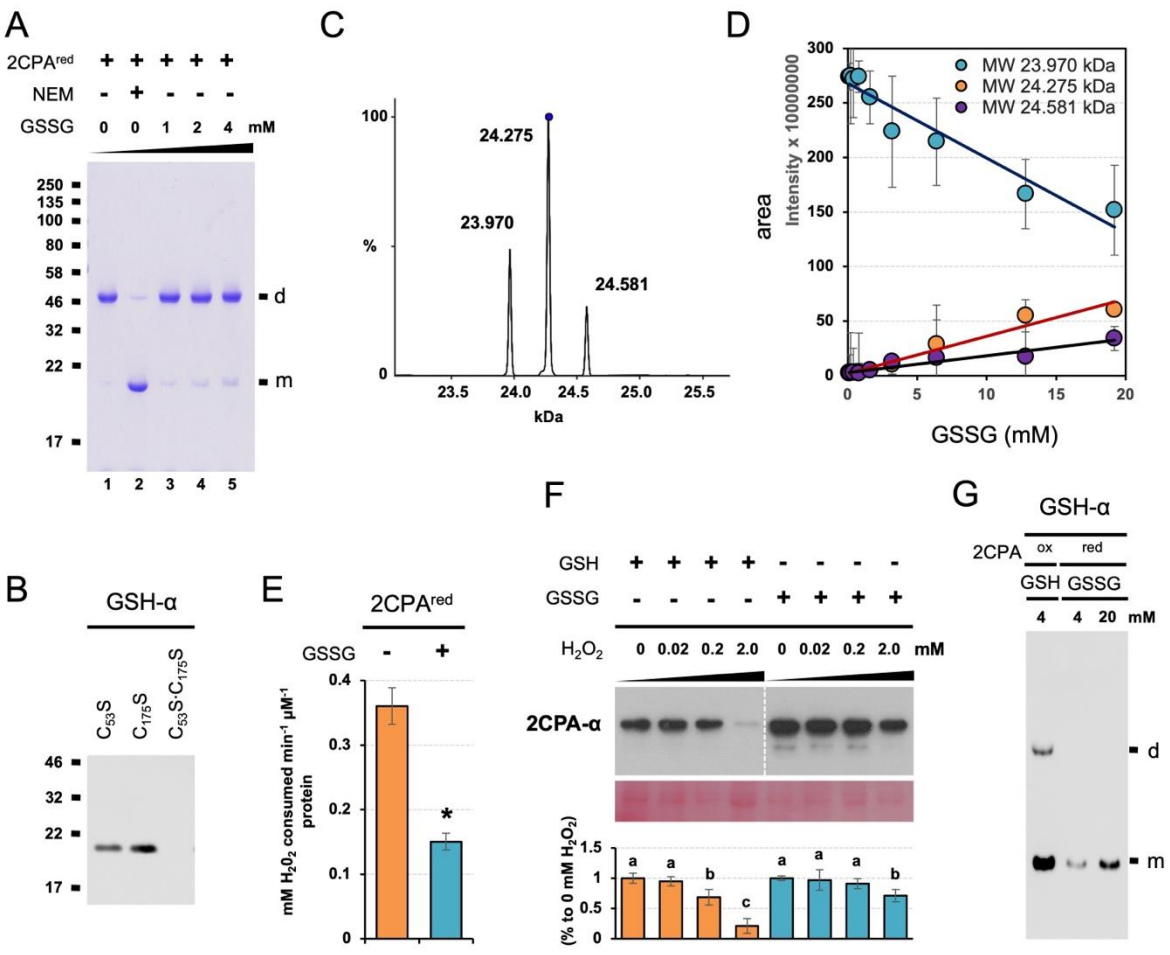

Figure 2.7. GSSG-dependent S-glutathionylation Deactivates but Protects 2CPA from Hyperoxidative Denaturation. (A) GSSG binds and prevents 2CPA^{red} from its oxidation and dimerization. The 1 µM reduced 2CPAs$^{(red)}$, incubated with/without various concentrations (0, 1, 2 and 4 mM) of GSSG or 30 mM NEM for 30 min, were subjected to nonreducing SDS/PAGE. **(B-D)** GSSG leads double S-glutathionylation at the Cys53 and Cys175 residues of 2CPA^{red}. A representative spectra **(B)**, and the kinetics **(C)** of deconvoluted masses of 2CPA^{red} incubated with increased concentration (0, 0.2, 0.4, 0.8, 1.6, 3.2, 6.4, 12.8 and 19.2 mM) of GSSG. Three major peaks in **(B)** indicate a monomeric 2CPA without (~23.970 kDa) and with single (~24.275 kDa = 23.970_{2CPA} + 0.307_{GSH}) or double (~24.581 kDa = 23.970_{2CPA} + 2x 0.307_{GSH}) S-glutathionylation. **(D)** Mutant 2CPAs ($C_{53}S$, $C_{175}S$ and $C_{53}S$•$C_{175}S$) were analyzed by IB using GSH-α, following 30

min incubation with 20 mM GSSG. **(E)** GSSG-binding inactivates $2CPA^{red}$. Peroxidase activity was measured using eFOX method (Cheeseman, 2006) in $2CPA^{red}$ and $2CPA^{GS}$ with double S-glutathionylation by incubating with H_2O_2 for 10 min (mean ± SD; $n = 3$). The asterisk (*) indicates statistically significant differences ($P < 0.05$, the student's t-test). **(F)** GSSG-mediated S-glutathionylation suppresses H_2O_2-induced deactivation of 2CPA. Equal amounts of total plastid proteins were pretreated overnight with 2 mM of GSH or 20 mM of GSSG, and dialyzed by desalt columns. The plastid $proteins^{GS}$ were then incubated with the indicated concentration of H_2O_2 for another 30 min at 37 ^oC, and subjected to denaturing SDS/PAGE and IB analyzed using 2CPA-α. The PVDF membrane of chloroplast protein extracts was stained with Ponceau S (bottom). The level IB signals of 2CPA were quantified (mean ± SD; $n = 3$) through the Image J (Schneider et al., 2012) and normalized to the expression of PSII monomer. Different letters indicate significant differences between H_2O_2 concentrations (Tukey-Kramer honestly significant difference test on all pairs; $\alpha = 0.05$). **(G)** GSH binds $2CPA^{ox}$ more strongly than GSSG toward $2PCA^{red}$. The 1 µM $2CPAs^{red}$ or $2CPAs^{ox}$, incubated with various 4 mM GSH or 4 and 20 mM of GSSG, respectively, were separated in nonreducing SDS/PAGE and IB analyzed using GSH-α. **(A, G)** d, dimeric 2CPA. m, monomeric 2CPA.

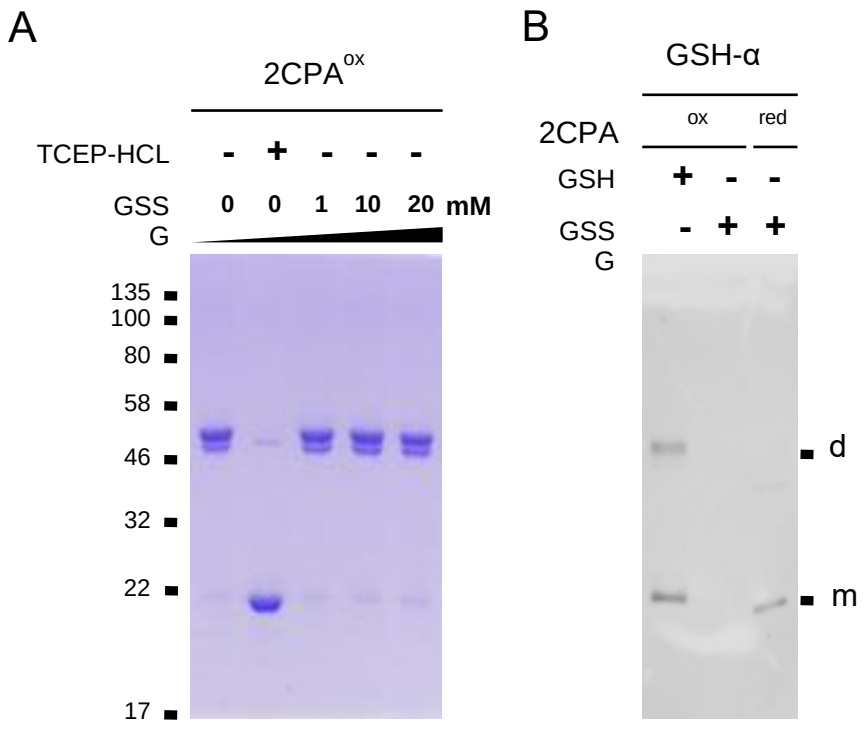

Figure 2.8. GSSG is not Able S-glutathionylate Dimeric 2CPA^{ox}. (A) The 1 µM 2CPA^{ox} incubated with/without various concentrations (0, 1, 10 and 20 mM) of GSSG, or 5 mM TCEP-HCL for 60 min following 30 mM NEM for 30 min, were subjected to nonreducing SDS/PAGE. The gels were stained with Coomassie Brilliant Blue, and the standard MW sizes (kDa) were indicated on the left of gels. **(B)** The 1 µM 2CPA^{ox} or 2CPAs^{red}, incubated with 1 mM GSH or 20 mM GSSG, subjected to nonreducing SDS/GAPGE and IB analyzed using GSH-α. d, dimeric 2CPA. m, monomeric 2CPA.

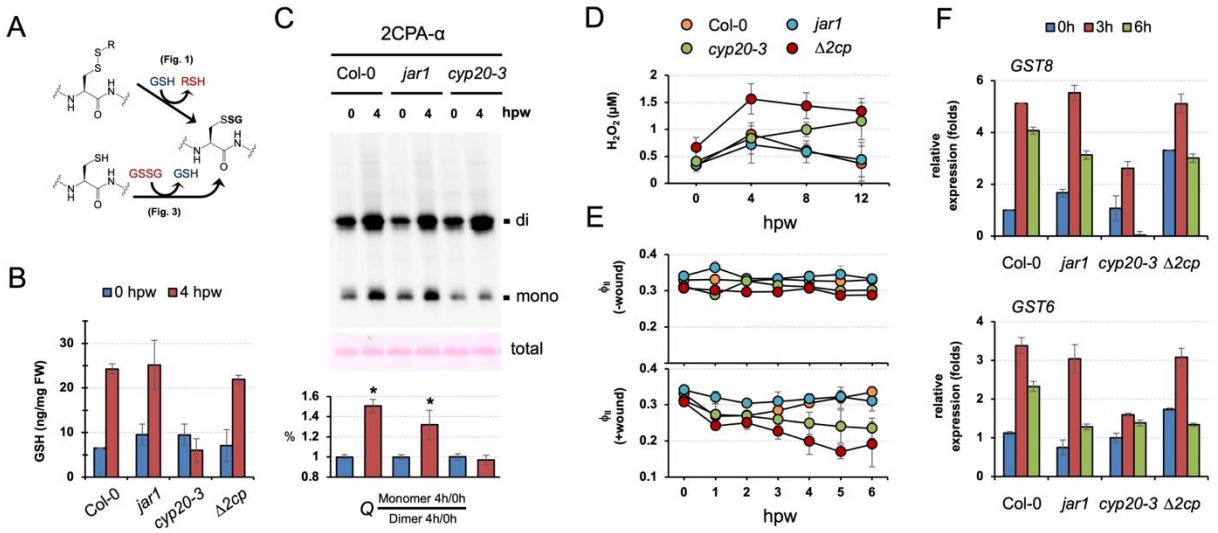

Figure 2.9. GSH-dependent 2CPA S-glutathionylation Relays CYP20-3/OPDA Signaling in the Maintenance of Photosynthesis during Wound Healing. (A) The representative schematic of GSH- or GSSG-dependent protein S-glutathionylation. **(B)** CYP20-3/OPDA signaling stimulates wound-responsive accumulations of GSH. Levels of GSH in stressed WT and mutant (*jar1*, *cyp20-3* and Δ*2cp*) plant leaves extracted at 0 and 4 hpw were measured (mean ± SD; *n* = 9) utilizing a fluorometric assay kit (BioVision), according to the manufacturer's instruction. The results of statistical analyses are summarized in Table 2.3. **(C)** The disruption of CYP20-3/OPDA signaling impairs wound-responsive S-glutathionylation and monomerization of 2CPA. In situ IB assay determines the quaternary structure of 2CPA in wounded WT (Col-0), JA-Ile synthesis mutant (*jar1*), and OPDA signaling mutant (*cyp20-3*) plants at 0 and 4 hpw. The level IB signals of monomeric 2CPAs (*Q*) were quantified (mean ± SD; *n* = 3) by the Image J (Schneider et al., 2012), and normalized to those of dimeric forms (bottom). Statistical analysis was performed with the student's t-test ($P < 0.05$). **(D and E)** CYP20-3/OPDA signaling promotes the peroxidase activity of 2CPA in protecting photosynthesis under wound healing. Time-course changes of H_2O_2 levels (**D**), and *Φ*II (**E**) values in unwounded (-wound) or wounded (+wound) WT (Col-0, orange circles) and mutant, *jar1* (blue circles), *cyp20-3* (green circles) and Δ*2cp* (red circles), plants

(means ± SD; n = 10). The results of statistical analyses by Tukey-Kramer honestly significant difference test on all pairs are summarized in Table 2.4 and 2.6. (**F**) Time-resolved qRT-PCR analysis of *GST8* and *GST6* in wounded WT (Col-0) and mutant (*jar1*, *cyp20-3* and Δ*2cp*) plants. Total RNAs were prepared from leaves at 0 (blue bars), 3 (red bars) and 6 (green bars) hpw. Values were normalized to the expression of *POLYUBIQUITIN* (mean ± SD; n = 3) (Czechowski et al., 2005).

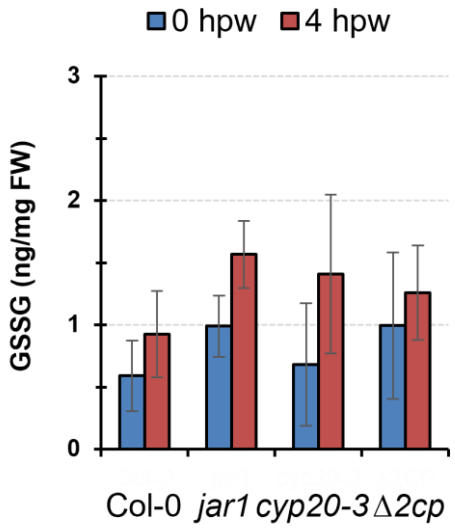

Figure 2.10. Wounding Causes Little Change in the Level Accumulations of GSSG. Levels of GSSG in wounded WT (Col-0) and mutant (*jar1*, *cyp20-3* and Δ*2cp*) plant leaves, extracted at 0 and 4 hpw (mean ± SD; 3 independent experiments, $n = 3$), were measured by the GSH/GSSG/total fluorometric assay kit (BioVision), according to the manufacturer's instruction. The results of statistical analyses are summarized in Table 2.3.

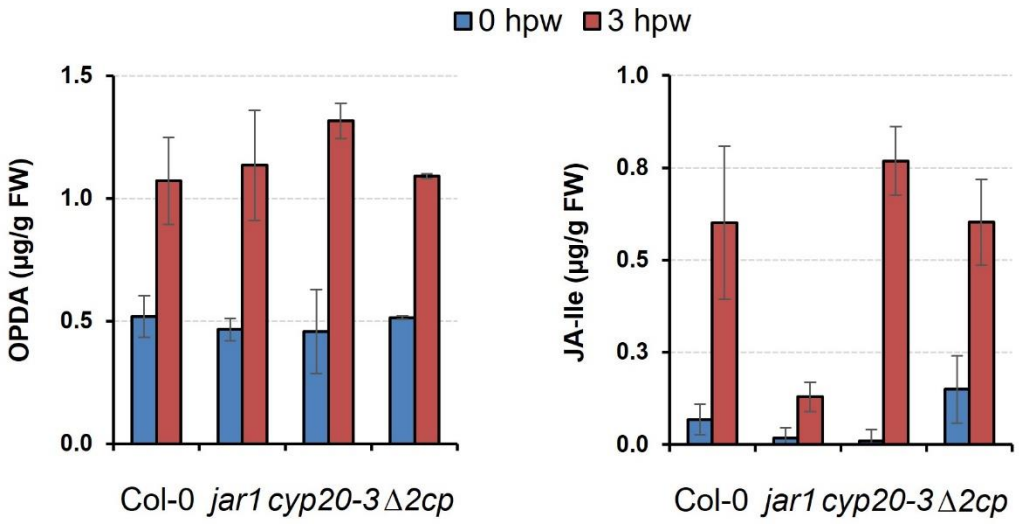

Figure 2.11. Rapid Accumulations of OPDA and JA-Ile in Wounded WT (Col-0) and Mutant (*jar1*, *cyp20-3* and Δ*2cp*) Plants. Jasmonates were extracted from leaves at 0 and 3 hpw (mean ± SD; $n = 3$). The results of statistical analyses are summarized in Table 2.4.

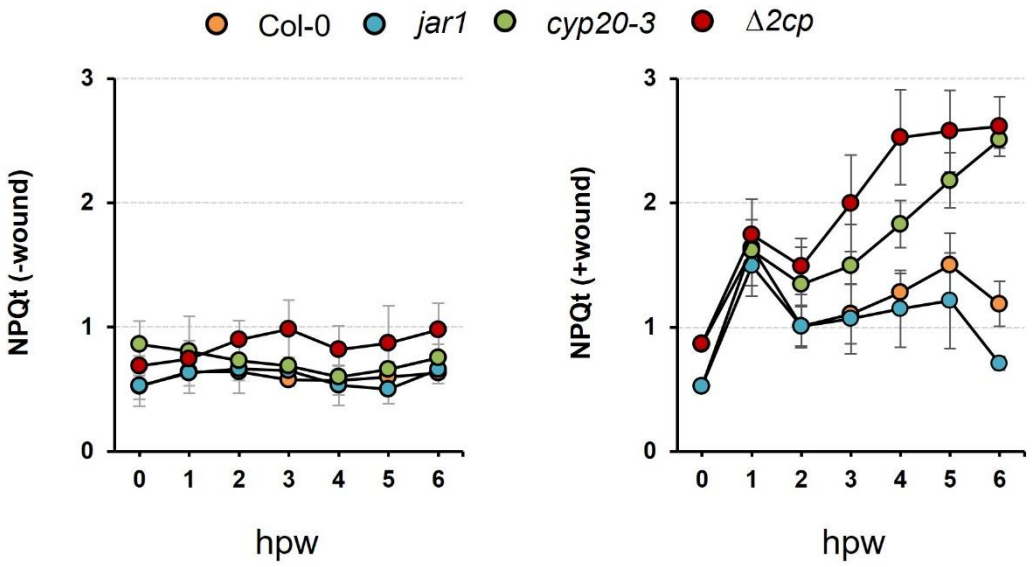

Figure 2.12. CYP20-3-dependent OPDA signaling Fosters the Protection of Photosynthetic Efficacy during Plant Defense Responses. The increased total nonphotochemical quenching (NPQt, Tietz et al., 2017) was determined in wounded WT (Col-0) and mutant (*jar1*, *cyp20-3* and Δ*2cp*) plant leaves at 0, 1, 2, 3, 4, 5 and 6 hpw (mean ± SD; $n = 10$) using the MultispeQ (Kuhlgert et al., 2016). The results of statistical analyses are summarized in Table 2.6.

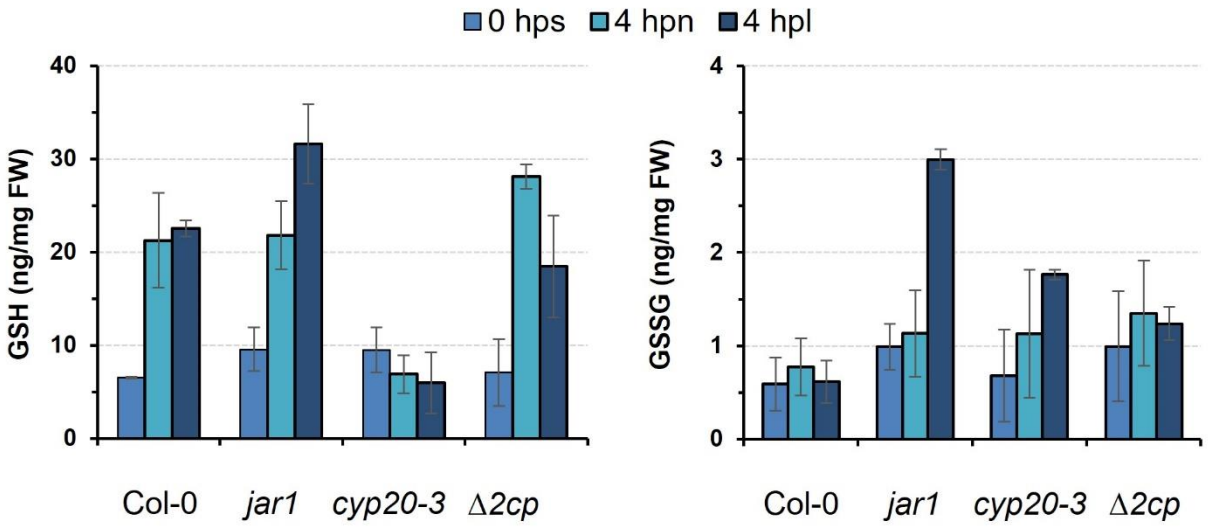

Figure 2.13. CYP20-3/OPDA Signaling Stimulates the Stress-responsive Accumulations of GSH. Levels of GSH and GSSG in stressed WT and mutant (*jar1*, *cyp20-3* and Δ*2cp*) plant leaves, extracted at 0 hps, 4 hpn and 4 hpl, were measured (mean ± SD; n = 3) by a GSH (GSH/GSSG/ total) fluorometric assay kit (BioVision), according to the manufacturer's instruction. The results of statistical analyses are summarized in Table 2.3.

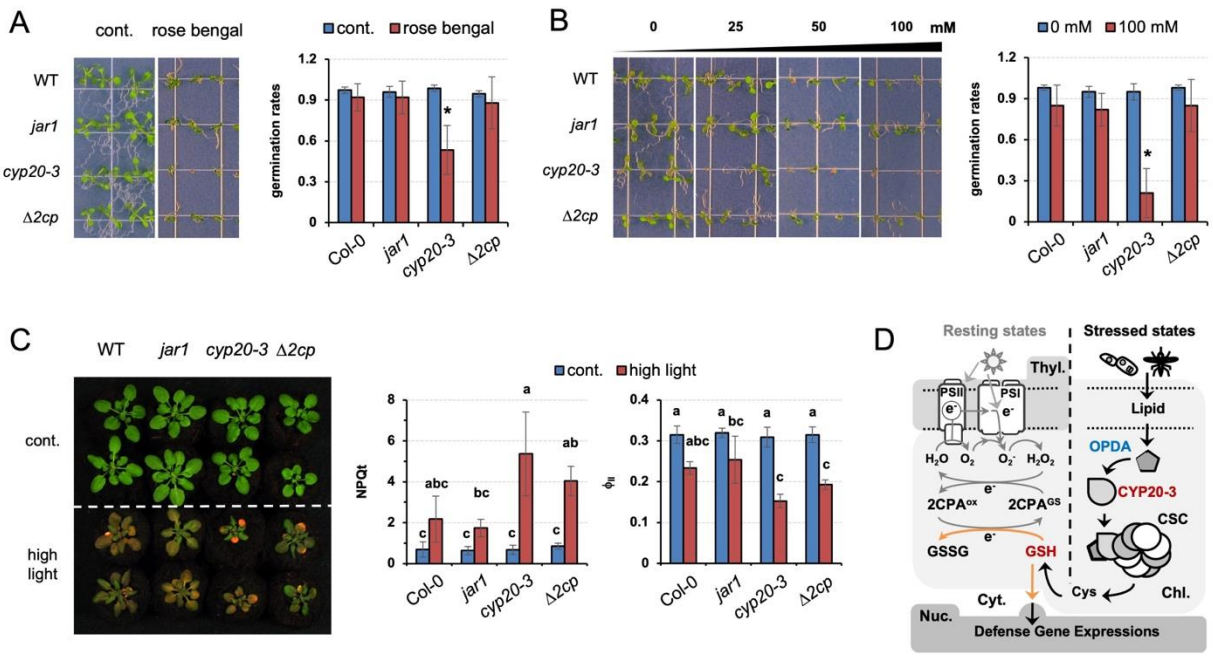

Figure 2.14. Programmed Induction of GSH by OPDA Signaling Plays a Crucial Pole in Plant Defense Responses. **(A-C)** The OPDA signaling mutant, *cyp20-3*, impairing stress-responsive GSH induction (Figure 4B), is hypersensitive to excess ROS stresses, comparing to WT (Col-0) and *jar1* and Δ*2cp* mutant plants. Seeds were plated on MS agar medium without or containing 3 μM rose bengal **(A)** or different concentrations (0, 25, 50 and 100 mM) of NaCl **(B)**, and their germination rates were counted on the 5-d after vernalization (means ± SD; *n* = 25). **(C)** The 2-wk-old plants, grown under a normal condition, were transferred to high-intensity light for 6 days, and subjected to the measurement of NPQt and *Φ*II values (means ± SD; *n* = 10). Photographs were taken on the seventh to fourteenth day after treatments. The asterisks (*) and different letters indicate statistically significant differences (Tukey-Kramer honestly significant difference test on all pairs; α = 0.05). **(D)** Proposed model of GSH-dependent reduction signaling that relays OPDA signaling to cross-regulate an interplay between photosynthesis (growth) and ORG expressions (defense) under stressed conditions. When the PSI antenna captures solar energy

(in resting states), it prompts the ETC that controls energy (sugar) conversion and consumption. By contrast, under stressed conditions, OPDA is accumulated and binds CYP20-3 to stimulate the formation of CSC (Cys synthase complex) and the generation of Cys and GSH, which in turn coordinates (*i*) the S-glutathionylation (activation) of 2CPA in peroxide detoxification, while (*ii*) triggering the retrograde regulation of defense ORG expressions. This regulatory interface between growth and defense responses shapes the optimal growth plasticity and survival potential of plants under constant environmental pressures.

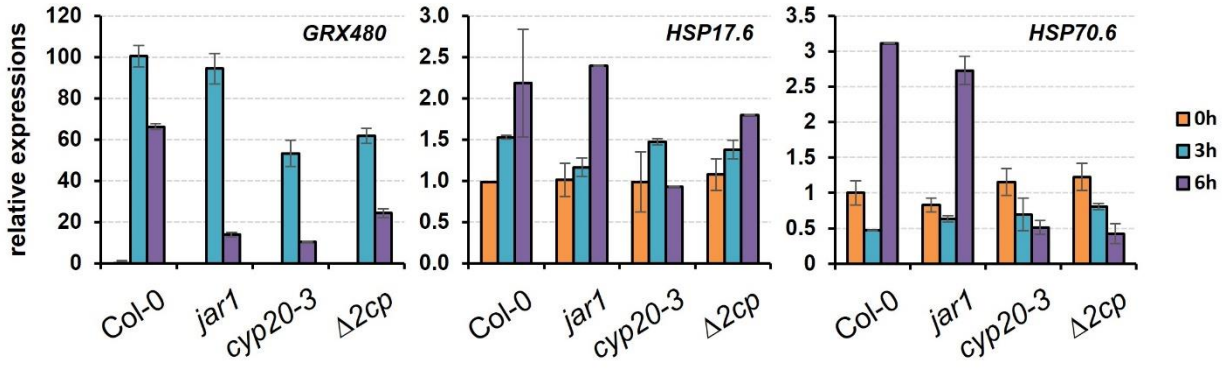

Figure 2.15. *cyp20-3* and Δ*2cp* Mutant Plants Attenuate the Level Expression of Selective ORGs. Time-resolved quantitative RT-PCR analyses in wounded WT (Col-0) and mutant (*jar1*, *cyp20-3* and Δ*2cp*) plants demonstrated that the transcriptional induction of selective ORGs, particularly those involved in general defense responses such as *GLUTAREDOXIN 480* (*GRX480*), *HEAT SHOCK PROTEIN 17.6* (*HSP17.6*) and *HSP70.6* (Mou et al., 2003; Finka et al., 2011) was impaired not only in wounded *cyp20-3*, but also wounded Δ*2cp*. Wounded Δ*2cp* however operates, unlike *cyp20-3*, intact OPDA and reductant signaling (Figure 2.9B, F) whereas both Δ*2cp* and *cyp20-3* are incapable of balancing photosynthetic H_2O_2 (Figure 2.9D and Table 2.6), potentially underpinning a cellular network that intertwines reductant and oxidative (ROS) signaling in controlling plant environmental plasticity under different ecological conditions. Total RNAs were prepared from the leaves of each plant, and transcript levels of *UBC* (Czechowski et al., 2005) were used as an equal loading control.

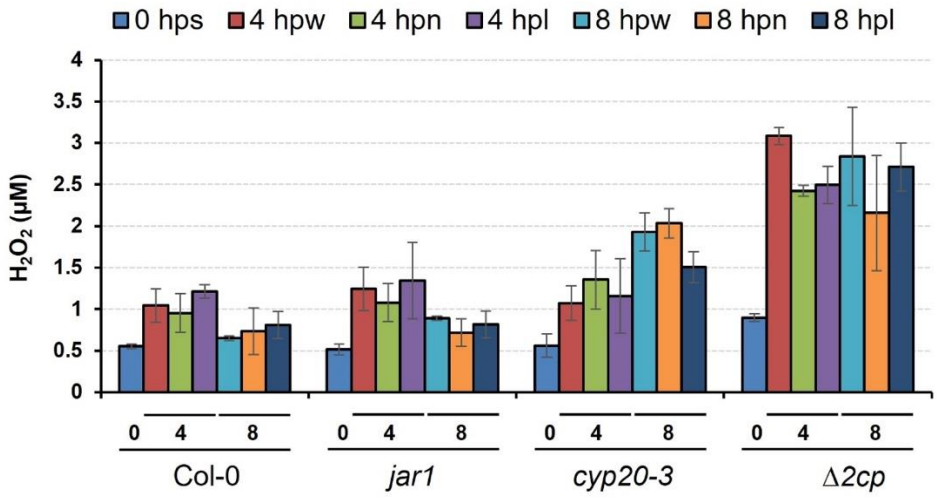

Figure 2.16. CYP20-3/OPDA Signaling Fosters the Peroxidase Activity of 2CPA during Plant Stress Responses. Cellular levels of H_2O_2 in stressed WT and mutant (*jar1*, *cyp20-3* and Δ*2cp*) plant leaves were measured (mean ± SD; $n = 9$) at 0 hps, 4 and 8 hpw, 4 and 8 hpn, and 4 and 8 hpl by the eFOX assay method, as described previously (Cheeseman et al., 2006; Liu et al., 2020). The results of statistical analyses are summarized in Table 2.8.

Table 2.1. Oligonucleotides used in this study.

Name	Direction	Sequence, 5′ to 3′	purpose
2CPA·C_{53}S·F[†]	Forward	TTGGACTTTACTTTCGTCAGCCCAACAGAGATTACTG	Mutagenesis[††]
2CPA·C_{53}S·R[†]	Reverse	CAGTAATCTCTGTTGGGCTGACGAAAGTAAAGTCCAA	Mutagenesis[††]
2CPA·C_{175}S·F	Forward	CCCGGATGAAGTCAGCCCAGCAGGATG	Mutagenesis[††]
2CPA·C_{175}S·R	Reverse	CATCCTGCTGGGCTGACTTCATCCGGG	Mutagenesis[††]
2CPA·Fw	Forward	AACTACTCTCATCTCTTCTCC	RT-PCR
2CPA·Rev	Reverse	AGGGAAGAGCGTCGAGCAAAT	RT-PCR
2CPB·Fw	Forward	TTCTTCCACCACCCTACT	RT-PCR
2CPB·Rev	Reverse	GGAACCGAGACTGGAGAAC	RT-PCR
CYP18D11·Fw	Forward	TCTCAACATG^GGTTTGTGAA	qRT-PCR[^]
CYP18D11·Rev	Reverse	AAGTATC^ATAACAAGTATGA	qRT-PCR[^]
HSP17.6·Fw	Forward	CTTGCCTGGATTAAGAAGG	qRT-PCR
HSP17.6·Rev	Reverse	CATCGCAGCCTTAACCTGAT	qRT-PCR
HSP70·Fw	Forward	GGAAAGTTCGAGCTCAGTGG	qRT-PCR
HSP70·Rev	Reverse	ACCTTCCCTTGTCGTTTGTG	qRT-PCR
GST6·Fw	Forward	TGCCCTCAACCCCTTCGGTC	qRT-PCR
GST6·Rev	Reverse	GGTTGCCTTGACTTTCTTGC	qRT-PCR
GST8·Fw	Forward	TGACAAGAAGCTG^TATGATGC	qRT-PCR[^]
GST8·Rev	Reverse	ACATAGCCAAAGTCATCGCC	qRT-PCR
GRX480·Fw	Forward	TGATTGTGATTGGACGGAGA	qRT-PCR
GRX480·Rev	Reverse	TAAACCGCCGGTAACTTCAC	qRT-PCR
UBC·Fw	Forward	CTGCGACTCAG^GGAATCTTCTAA	qRT-PCR[^]
UBC·Rev	Reverse	TTGTGCCATTGAATTGAACCC	qRT-PCR

[†] Primers, 2CPA·C_{53}S·F and 2CPA·C_{53}S·R, were used to generate the 2CPAC_{53}S·C_{175}S plasmid using the 2CPAC_{175}S plasmid as the template.

[††] Mutated nucleotide bases are grey highlighted.

[^] Position of an exon-exon junction.

Table 2.2. Theoretical masses used to identify the oxidized and glutathionylated forms of 2CPA.

Species	Molecular mass[a] (*kDa*)
Reduced monomer	24.225
Monomer with single glutathionylation	24.407
Monomer with double glutathionylation	24.589
Dimer	47.950
Dimer with single glutathionylation	48.382
Dimer with double glutathionylation	48.564

[a] Based on complete alkylation of all cysteines, namely Cys-53 (C_R) and Cys-175 (C_P) in the reduced WT protein with NEM (+ 125 Da). Molecular mass of non-alkylated reduced monomer of 2CPA is 23,975 Da.

Table 2.3. Statistical analysis (Tukey-Kramer test) on the level of GSH and GSSG in stressed WT (Col-0) and mutant (*jar1*, *cyp20-3* and Δ*2cp*) plant leaves at 0 hpw/s (hr-poststress), 4 hpw (hr-postwounding), 4 hpn (hr-post-NaCl treat) and 4 hpl (hr-post-excess light treat) (mean ± SD; 3 independent experiments, $n = 3$) in Figure 2.9B, 2.10 and 2.15.

genotypes	hps	letter (GSH)	letter (GSSG)
Col-0	0 hps	cde	a
	4 hpw	ab	a
	4 hpn	ab	a
	4 hpl	ab	a
jar1	0 hps	cd	a
	4 hpw	ab	ab
	4 hpn	ab	ab
	4 hpl	a	ab
cyp20-3	0 hps	cd	a
	4 hpw	cde	a
	4 hpn	cde	a
	4 hpl	cde	ab
Δ2cp	0 hps	d	a
	4 hpw	ab	a
	4 hpn	a	ab
	4 hpl	ab	a

Table 2.4. Statistical analysis (Tukey-Kramer test) on the level of OPDA and JA-Ile in wounded WT (Col-0) and mutant (*jar1*, *cyp20-3* and Δ*2cp*) plant leaves at 0 and 3 hpw (mean ± SD; 3 independent experiments, $n = 3$) in Figure 2.11.

genotypes	hps	letter (OPDA)	letter (JA-Ile)
WT (Col-0)	0 hpw	a	a
	3 hpw	b	b
jar1	0 hpw	a	a
	3 hpw	b	a
cyp20-3	0 hpw	a	a
	3 hpw	b	b
Δ2cp	0 hpw	a	a
	3 hpw	b	b

Table 2.5. Statistical analysis (Tukey-Kramer test) on the level of H_2O_2 in wounded WT (Col-0) and mutant (*jar1*, *cyp20-3* and Δ*2cp*) plant leaves at 0, 4, 8 and 12 hpw (mean ± SD; 3 independent experiments, $n = 3$) in Figure 2.9D.

hpw	genotypes	letter	genotypes	letter
0 hpw	WT (Col-0)	ab	*cyp20-3*	ab
4 hpw		ab		ab
8 hpw		ab		bc
12 hpw		ab		c
0 hpw	*jar1*	ab	*Δ2cp*	b
4 hpw		ab		c
8 hpw		ab		c
12 hpw		ab		c

Table 2.6. Statistical analysis (Tukey-Kramer test) on the photosynthetic efficacy (total nonphotochemical quenching [NPQt]) of unwounded (-) and wounded (+) WT (Col-0) and mutant (*jar1*, *cyp20-3* and Δ*2cp*) plant leaves at 0, 1, 2, 3, 4, 5 and 6 hpw (mean ± SD; 3 independent experiments, $n = 9$) in Figure 2.12.

hpw	genotypes	letter (-wound)	letter (+wound)	genotypes	letter (-wound)	letter (+wound)
0 hpw	Col-0	ab	ij	*cyp20-3*	bcd	efghi
1 hpw		abcd	ab		bcd	bcdefgh
2 hpw		abcd	ab		abcd	abcde
3 hpw		ab	abcdefg		abcd	abcd
4 hpw		ab	bcdefgh		abc	abcd
5 hpw		ab	cdefgh		abcd	abc
6 hpw		abcd	defghi		abcd	a
0 hpw	*jar1*	a	j	*Δ2cp*	abcd	ghij
1 hpw		abcd	ghij		abcd	abcd
2 hpw		abcd	ghij		bcd	abcdef
3 hpw		abcd	ghij		d	abcd
4 hpw		abcd	ghij		abcd	a
5 hpw		abcd	hij		abcd	a
6 hpw		abcd	fghi		cd	a

Table 2.7. Statistical analysis (Tukey-Kramer test) on the photosynthetic efficacy (PSII quantum yield [Φ_{II}]) of unwounded (-) and wounded (+) WT (Col-0) and mutant (*jar1*, *cyp20-3* and Δ*2cp*) plant leaves at 0, 1, 2, 3, 4, 5 and 6 hpw (mean ± SD; 3 independent experiments, n = 9) in Figure 2.9E.

hpw	genotypes	letter (-wound)	letter (+wound)	genotypes	letter (-wound)	letter (+wound)
0 hpw	Col-0)	a	ef	*cyp20-3*	a	ef
1 hpw		a	abcdef		a	cdef
2 hpw		a	abcdef		a	abcdef
3 hpw		a	bcef		a	abcdef
4 hpw		a	cdef		a	abcdef
5 hpw		a	def		a	abcde
6 hpw		a	cdef		a	abcd
0 hpw	*jar1*	b	a	*Δ2cp*	a	f
1 hpw		a	ef		a	cdef
2 hpw		a	bcdef		a	cdef
3 hpw		a	abcdef		a	cdef
4 hpw		a	bcdef		a	abc
5 hpw		a	ef		a	a
6 hpw		a	f		a	ab

Table 2.8. Statistical analysis (Tukey-Kramer test) on the level of H_2O_2 in stressed WT (Col-0) and mutant (*jar1*, *cyp20-3* and Δ*2cp*) plant leaves at 0 hps, 4 and 8 hpw, 4 and 8 hpn and 4 and 8 hpl (mean ± SD; 3 independent experiments, $n = 9$) in Figure 2.16.

genotypes	hps	letter (4 hps)	letter (8 hps)
Col-0	0 hps	st	
	hpw	klmno	opq
	hpn	lmnopq	mnop
	hpl	ijklmn	lmno
jar1	0 hps	t	
	hpw	hijklm	klmno
	hpn	jklmno	nopq
	hpl	ghijk	lmno
cyp20-3	0 hps	st	
	hpw	klmno	def
	hpn	ghijk	cdef
	hpl	efghi	fghij
Δ2cp	0 hps	mnopqr	
	hpw	a	ab
	hpn	abcd	bcde
	hpl	abcd	abc

CHAPTER 3: CYP20-3 CONVEYS 12-OXO-PHYTODIENOIC ACID SIGNALING IN ALLOCATING PHOTOSYNTHETIC ENERGY TO DEFENSE ACTIVATION

3.1. INTRODUCTION

For centuries naturalists and scientists have observed plants responding to wound injury and healing themselves. Gottlieb Haberlandt in his 1922 review describes the presence of 'wound hormones' (Haberlandt, 1922). Then systemic studies by James English Jr. in the late 1930's identified the first wound hormone, 12-oxo-trans-10-dodecanoic acid, that enhances cell proliferation at the wound site: it was then given the trivial name 'traumatin' (English et al., 1939a, b). Traumatin is an oxygenated product of unsaturated fatty acids (FAs) now referred to as a type of oxylipin (Zimmerman and Condron, 1979). Today, it is widely known that oxylipins together with their wounding responses play essential roles in various aspects of plant development and survival (Mosblech et al., 2009). However, our knowledge of the architecture of oxylipin-associated healing responses and its signaling circuits remains quite unclear.

Lately, molecular underpinnings have been investigated for (+)-12-oxo-phytodienoic acid (OPDA, [1*S*,2*S*]-3-oxo-2-[2*Z*-pentenyl]-cyclopent-4-ene-1-octanoic acid), a primary precursor of jasmonate family plant oxylipins that includes (-)-jasmonic acid (JA, [1*R*,2*R*]-3-oxo-2-[2*Z*]-2-pentenyl-cyclopentaneacetic acid) and its precursors as well as derivatives. Jasmonates are produced from trienoic FAs (TFA) through the octadecanoid pathway in chloroplasts. Lipase-dependent oxidation of TFA releases OPDA that travels to the peroxisomes where undergoes β-oxidations to form JA. JA is then exported to cytosol, and further metabolized to various derivatives such as (+)-7-iso-jasmonyl-L-isoleucine (JA-Ile) and JA-methyl ester. OPDA herein also can trigger autonomous signaling pathways that regulate unique subsets of jasmonate-responsive genes, activating and fine-tuning plant defense responses, as well as growth processes (Liu and Park, 2021). Its intrinsic activity was first described by the pathoanalyses of mutant

Arabidopsis (*opr3*) arresting the conversion of OPDA to JA (Stintzi et al., 2001). Wild type (WT)-like resistance of *opr3,* in contrast to decreased resistance in mutant plants disrupting TFA biosynthesis (*fad3*/*7*/*8*) and the octadecanoid pathway (*dde2*), against fungal and insect infections underlined the crucial roles of OPDA signaling in plant defense responses in the absence of JA and JA-Ile (Stintzi et al., 2001; Zhang and Turner, 2008; Stotz et al., 2011). Following studies with several mutant plants suppressing or impairing JA production (e.g., *siOPR3*, *OPR3-RNAi*, *cts-2*/*opr3* and *acx1*) further substantiated that OPDA signaling is crucial in basal defense responses against a variety of pathogenic fungi and insects, as well as seed germination, embryogenesis and balancing abscisic acid signaling (Dave et al., 2011; Goetz et al., 2012; Bosch et al., 2014; Guo et al., 2014; Scalschi et al., 2015).

Earlier search of jasmonate receptors uncovered that a small plastid protein cyclophilin 20-3 (CYP20-3) can physically interact with OPDA, and its mutant Arabidopsis (*cyp20-3*) attenuates the expression of OPDA-responsive genes (ORGs, Park et al., 2013). CYP20-3 is a dual functional enzyme, chaperoning protein folding (peptidyl-prolyl isomerase, PPlase) or transferring electrons (H^+, e^-) to peroxide substrates (reductase, Barbosa dos Santo and Park, 2019). Under stresses, OPDA binds and stimulates CYP20-3 to form a complex with serine acetyltransferase1 (SAT1), which triggers the formation of a hetero-oligomeric cysteine (Cys) synthase complex (CSC) with *O*-acetylserine(thiol)lyase B (OASTL-B). CSC formation then leads to the production of Cys and subsequently glutathione (GSH) and thiol metabolites (sulfur assimilation), which builds up cellular reduction potentials. The enhanced redox capacity in turn enriches the S-glutathionylation (activation) of 2-Cys peroxiredoxin A (2CPA, a recycler of water-water cycle) that optimizes photosynthetic efficacy and redox homeostasis, while promoting the retrograde expression of ORGs in controlling basal and race-specific (local and systemic) resistances, and defense responses against various ecological constraints (Park et al., 2013; Liu et al., 2020; Wang et al., 2020; Chang et al., 2023; Adhikari and Park, 2023).

On the other hand, CYP20-3 is positioned as a redox sensor of the light-dependent redox reactions (also known as an electron transport chain, ETC) of photosystem I (PSI) that plays major roles in the conversion of solar energy into biologically useful chemical energies, necessary to produce overall biomass (Cheong et al., 2017). When the PSI antenna captures solar energy, it excites electrons (H^+, e^-) that reduce thioredoxins (TRXs), small disulfide oxidoreductases, via ferredoxin (Fd) and Fd-TRX reductase. In Arabidopsis, the chloroplasts contain ~10 TRX isoforms, categorized into five types (F, M, X, Y and Z), that metabolize key enzymes in the Calvin cycle such as fructose bisphosphatase (FBPase), glyceraldehyde-3-phosphate dehydrogenase, sedoheptulose bisphosphatase and phosphoribulokinase, which balance energy conversions and consumptions in photosynthesis. (Meyer et al., 2009; Serrato et al., 2013; Nikkanen and Rintamäki, 2014). Recent studies however have unveiled that TRXs can also target other, Calvin cycle-unrelated, proteins, for instance CYP20-3 (Motohashi et al., 2001; Park et al., 2013). In the presence of OPDA, CYP20-3 appeared to bind both TRXF2 and SAT1 (Cheong et al., 2017), thereby, proposing CYP20-3 as a redox regulatory carrier, transferring electron (H^+, e^-) from PSI to the sulfur assimilation, buildup reduction potential in the chloroplasts.

In this study, we investigated the role and activity of TRX-f2 and CYP20-3-depedent OPDA (CYP20-3/OPDA) signaling, and further delineate the mechanistic mode of actions of CYP20-3 in OPDA signaling circuitry. Using a series of biochemical and genetic approaches, we demonstrated that OPDA signaling stimulate sequential interactions between TRX-f2, CYP20-3 and SAT1, cross-activating reduction signaling that conveys the ETC route allocating photosynthetic energy to defense mechanisms. OPDA binding inhibits the PPIase activity of CYP20-3, which in subsequent accentuates its reductase activity that in turn adjusts the tertiary structure of SAT1 that triggers CSC formation, highlighting the unique roles of CYP20-3 in controlling the interplay between plant light and hormone signaling to fine-tune energy inputs into outputs that shape plant growth and defense responses (‘fitness’) toward various environmental stress cues.

3.2. MATERIALS AND METHODS

3.2.1. Plant Growth Conditions

Arabidopsis WT and mutants (i.e., Δ*trxf*, *cyp20-3*, and *jar1*) in Columbia (Col-0) background were grown in a chamber (Caron) with a 12-h light:dark cycle (80-100 μE/m^2/s) at 22 ^{o}C and 60% to 80% relative humidity.

3.2.2. Preparation of Recombinant Proteins

Coding sequences for full-length proteins were cloned into pGEX-4T-1 (GE Healthcare), pET28a or pET21c (Novagen) to obtain GST:CYP20-3, HIS/T7:SAT1 and OASTL-B:HIS, respectively (Park et al., 2013). On the other hand, the coding sequence of mature CYP20-3, removing the N-terminus signal peptide of 77 amino acids, was cloned into pCR®T7/NT-TOPO® (Invitrogen, Laxa et al., 2007) and point mutations were introduced using the QuickChange II site-directed mutagenesis kit (Agilent) and mutagenic primer sets (Table 3.1), according to the manufacturer's instructions. Each recombinant protein was then expressed by 0.1 M isopropyl ß-D-1-thiogalactopyranoside in *E. coli* BL21 (DE3) and purified through a nickel-column (Pur™ Ni-NTA, Thermo Scientific), as previously described (Cheong et al., 2017). Finally, protein concentrations were measured using the Amresco Bradford assay kit with bovine serum albumin (BSA) as standard, and stored at 4 °C until use.

3.2.3. PAGE and Immunoblot (IB) Analyses

Samples were prepared by adding NuPAGE™ LDS sample buffer (Thermo Scientific) with/without β-mercaptoethanol to total extract or recombinant proteins, and resolved via 10% to 13% SDS/PAGE and then electroblotted onto the PVDF membrane (Millipore). The resulting blots were probed with monoclonal HIS-α (1:7500) for 2 h, or polyclonal CYP20-3-α (1:5000, Park et al., 2013), SAT1-α (1:3000, Na and Salt, 2011) or OASTL-B-α (1:3000, Heeg et al., 2008) for 2 - 16 h, and visualized by chemiluminescence (ECL kit; GE Healthcare).

3.2.4. In Vitro Pull-Down Assay

Individually purified proteins (1:1:1 molar ratio) were immobilized with/without ligands on affinity beads for 1 h at room temperature. GSH beads (Sigma) were used to immobilize GST:CYP20-3, whereas T7 antibody beads (Novagen) were used to immobilize T7:SAT1. After washing and elution with GSH or citric acid, proteins were resolved by SDS/PAGE and probed with a monoclonal HIS-α (Invitrogen).

3.2.5 Total Protein Extractions

Leaf tissues of Arabidopsis were immersed in liquid N_2 and ground to powder using a mortar and pestle. Ground tissues were dissolved into two volumes of 50 mM Tris buffer, pH 7.5, containing protease inhibitor cocktails (Sigma-Aldrich), agitated for 60 min, and centrifuged for 30 min at 10,000*g*. The supernatant was collected, and immediately used for IB or co-IP analyses. Note that all extraction steps were carried out at 4°C.

3.2.6. Ex Vivo Coimmunoprecipitation (co-IP) Assay

The generation of CYP20-3-α-immobilized beads, and subsequent co-IP assays were carried out by using a Direct Magnetic Co-IP Kit (Pierce) in accordance with the manufacturer's instructions. Equal amounts of eluates were fractionated by SDS/PAGE and visualized by silver staining (Pierce) and Western blot by using SAT1-α (Na and Salt, 2011).

3.2.7. PPIase Activity Assay

PPIase activity of CYP20-3 was determined by measuring the catalytic rate of the prolyl *cis*→*trans* interconversion of cis Succinyl-Ala-Leu-Pro-Phe-*para*-nitroanilide as previously described (Fisher et al., 1989). Briefly, the assay was performed at 10 °C in 35 mM HEPES (pH 7.9), 0.015% (v/v) Triton X-100, 60 μM *cis*-peptide (dissolved in 60% [v/v] DMSO), and 250 μg/mL α-chymotrypsin, with WT or mutant CYP20-3s. The reaction mixture was incubated at 10 °C until the absorbance baseline stabilized at 390 nm, and the reaction was initiated by the addition of α-

chymotrypsin; absorbance was read every second. For the dependence of PPIase activity on OPDA, CYP20-3 was preincubated at 10 °C in the presence of varying concentrations of OPDA (0.01, 0.1 and 1.0 μM), and the remaining PPIase activity was determined.

3.2.8. Stress Treatments

For the salt and rose bengal treatments, sterilized seeds were plated on MS medium supplemented with increasing concentrations (25, 50 and 100 mM) of NaCl or 3 μM of rose bengal, incubated at 4 ^{o}C for 2 days, and then placed at 22 ^{o}C under a 12-h day cycle (80-100 μE/m^2/s).

3.2.9. Semiquantitative and Quantitative RT-PCR

Total leaf RNA was prepared using TRIzol reagent (Invitrogen) and the Direct-zol RNA Kit (Zymo Research) according to the manufacturer's instructions. RNA qualities were assessed by agarose gel electrophoresis and NanoDrop (A_{260}/A_{280} > 1.8 and A_{260}/A_{230} > 2.0, Udvardi et al., 2008). RT reactions were performed using an oligo(dT) reverse primer and a qScript reverse transcriptase (Quantabio). Semi-quantitative RT-PCR was then performed using 2 μL cDNA with *Taq* 2X master mix (New England BioLabs) at an annealing temperature, 55 °C, for primer pairs (Table S6) for 30 cycles, whereas quantitative PCR was performed with the PerfeCT® SYBR® Green Fast Mix® Reaction Mixes (QuantaBio) in the CFX96 Touch™ (Bio-Rad) PCR system cycled 40 times using gene-specific primer sets (Table 3.1). The annealing temperature for the primer pairs was 53 ^{o}C. To determine the relative abundance of target transcripts, the sample cDNA was assessed with housekeeping genes, *POLYUBIQUITIN* (*UBC*, Czechowski et al., 2005) and the average threshold cycle (i.e., Ct) was normalized to that of *UBC* as $2^{-\Delta Ct}$ where $-\Delta Ct = (Ct_{,gene} - Ct_{,UBC})$.

3.3. RESULTS

3.3.1. OPDA Conveys Photosynthetic Electron Flows to CYP20-3. To further delineate an OPDA signaling circuitry, we investigated the functional and mechanistic interplay of CYP20-3,

an OPDA receptor, with its cofactor proteins including TRXF2 (Cheong et al., 2017) using ex vivo coimmunoprecipitation (co-IP) assays in combination with wound-responsive OPDA biosynthesis. Wounding induced the accumulation of OPDA with a peak at ~3 h postwounding (hpw), subsequently JA-Ile, and ultimately the differential expression of various genes (Stintzi et al., 2001; Taki et al., 2005; Mueller et al., 2008). As expected, the TRXF2 and CYP20-3 (T-C) interaction was promoted and/or stabilized in parallel with jasmonate accumulations (Fig. 3.1A). CYP20-3-coimmunoprecipitated TRXF2 increased at 3 hpw. Since TRXF2 acts as an electron carrier in the photosynthetic ETC (Meyer et al., 2009), we then asked if a reduced state $TRXF2^{(red)}$ could donate electron(s) to CYP20-3. $TRXf2^{red}$ alone however was inefficient to metabolize CYP20-3 (Fig. 3.1B, lane 3), whilst OPDA supplements (≥2.5 μM) stimulated $TRXF2^{red}$ to bind (Cheong et al., 2017, Fig. 3.1A) and reduce CYP20-3, delaying its migration in nonreducing SDS/PAGE (Fig. 3.1B, lanes 5, 6). In contrast, oxidized $TRXF2^{(ox)}$ was unable to reduce CYP20-3 despite of the presence of ample OPDA levels (5 μM, Fig. 3.2A).

Our results suggest that the T-C pathway conveys redox signaling (e^- transport) in channeling light input into outputs that drive OPDA signaling (e.g., ORG expressions) under stress conditions. To substantiate this hypothesis, we traced the time-dependent redox state of CYP20-3 in wounded WT (Col-0) and mutant, disrupted *TRXF1*/*F2* (Δ*trxf*, Pérez-Ruiz et al., 2017), the octadecanoid pathway (*dde2*, Von Malek et al., 2002) and JA-Ile derivatization (*jar1*, Staswick et al., 2002), plants (Figs. 3.1C, 3.2B). Immunoblot (IB) analysis using anti-CYP20-3 antibody (CYP20-3-α) indeed showed that CYP20-3 is transiently reduced at 3 hpw in wounded WT and *jar1*, but not in wounded Δ*trxf* and *dde2*, plants, indicating that OPDA promotes the T-C interaction and that TRXF2 serves as a reductant, perhaps an activator, of CYP20-3. In line with this scenario, Δ*trxf* exhibited *cyp20-3*-like attenuation of wound-responsive ORG, *CYP81D11* and *GRX480* (Mueller et al., 2008; Park et al., 2013), expressions (Fig. 3.1D), as well as *cyp20-3*-like hypersensitivity to exogenous stresses such as rose bengal, a light-dependent inducer of ROS, singlet oxygen ($^1O_2$, Fig. 3.1E), and elevated salt levels that also damage plants by producing ROS (Fig. 3.1F). When

seeds were plated on Murashige and Skoog (MS) medium supplemented with 3 µM rose bengal or the increasing concentrations of excess NaCl (25-100 mM), germination and growth of Δ*trxf* and *cyp20-3* seedlings were significantly suppressed relative to WT and *jar1* (+OPDA, -JA-Ile), validating an intrinsic role of TRXF2 in OPDA signaling, reprograming plant cells toward defense modes against various environmental challenges.

3.3.2. CYP20-3 Conveys Stress-Responsive CSC Formations. Beside TRXF2, OPDA-binding also promotes CYP20-3 to bind SAT1, which in turn prompts the CSC formation with OAS-TL B (Park et al., 2013). In total extracts prepared from the resting state of WT plants, SAT1-α IB-detected a band with a molecular weight (MW) of ~200 kDa (Fig. 3.3A) corresponding a size of SAT1 (~34 kDa) hexamers (i.e., dimeric trimers, Hell and Wirtz, 2011), while OASB-α IB-reacted with a band MW of ~60 kDa (Fig. 3.3B) equivalent to OAS-TL B (~30 kDa) dimers (Hell and Wirtz, 2011). When wounded, on the other hand, both SAT1-α and OASB-α IB revealed an extra MW band of ~180 kDa in WT plants (lane 2 in Figs. 3.3C, D) which mirrors a predicted size of CSC, proposedly formed with an OAS-TL B dimer and a singular SAT1 trimer bound to CYP20-3 (~20 kDa, Kumaran et al., 2009; Park et al., 2013). The ~180 kDa band however was undetectable in wounded *cyp20-3* (lane 3 in Figs. 3.3C, D), reassuring a critical role of CYP20-3/OPDA signaling in stress (e.g., wounding)-responsive CSC formations. In this context, CYP20-3-α IB exposed five major MW bands including its monomeric structure (~20 kDa) at 4 hpw in wounded WT plants (Fig. 3.3E). Since CYP20-3 is not able to directly bind OAS-TL B (Park et al., 2013), four additional bands indicate the quaternary complex of CYP20-3 with TRXF2 (~40 kDa), SAT1 trimers (~120 kDa), CSC (~180 kDa) and SAT1 hexamers (~220 kDa), respectively. Together, these IB studies reconstitute that CYP20-3 relays an OPDA signal in binding both TRXF2 and SAT1, and that CYP20-3 perhaps split SAT1 (dimeric trimers) in half to signal the recruitment of an OAS-TL B dimer.

3.3.3. OPDA Stimulates TRXF2 to Reduce and Activate CYP20-3 for the CSC Formation. Our data proposes that CYP20-3 works as a reductase in promoting the OPDA-responsive CSC formation. To corroborate this hypothesis, we first assessed if OPDA and/or $TRXF2^{red}$ assist a sequential interaction of CYP20-3, SAT1 and OASTL-B (C-S-O). As anticipated, $TRXF2^{red}$ elevated OPDA-dependent CSC formations, further optimizing the assembly of C-S complex, which in turn recruited more OASTL-B (Fig. 3.4A). The attendant activity of TRXF2 implies that the gain of electrons activates CYP20-3. In agreement, both $CYP20\text{-}3^{red}$ and $CYP20\text{-}3^{ox}$ bind SAT1 in equal levels, though $CYP20\text{-}3^{red}$ only was able to lead SAT1 to bind OASTL-B (Fig. 3.4B).

To further define the activity of CYP20-3 in OPDA signaling, we designed the structure-function analysis. Towards that, our enzyme assays first confirmed the active amino acid (aa) residues of reductase at Cys (C)129 (Fig. 3.5A) and PPlase at arginine (R)69 and phenylalanine (F)74 (Fig. 3.5B) in CYP20-3 (Laxa et al., 2007; Motohashi et al., 2001; 2003). In parallel, we in silico built the reliable modeling of CYP20-3, based on the structure of CYPB (PDB Id; 1CYN), in complexes with OPDA using XtralView (McRee, 1999) and Crystallography & Nuclear Magnetic Resonance (Brünger *et al*., 1998), and identified a salt-bridge at R69 and a hydrogen bond at histidine (H)140 with the carboxyl group of OPDA (Fig. 3.4C), underscoring that R69 participates in both OPDA-binding and PPIase activity. In line with this scenario, isothermal titration calorimetry analyses and/or surface plasmon resonance showed that the site-directed mutagenesis of R69 to alanine (A, R69A) and H140 to glutamine (Q, H140Q) hinders the binding affinity of CYP20-3 to OPDA (Figs. 3.4D, E, 3.5C), though only R69A, but not H140Q, mutant CYP20-3 impairs PPlase activity (Fig. 3.5B). Thus, OPDA-binding inhibits the PPlase activity of CYP20-3 in a concentration-dependent manner (Fig. 3.4F), which perhaps conditions to accentuate the reductase activity of CYP20-3. Indeed, the mutagenized variant of CYP20-3 lacking reductase (C129S) or OPDA-binding (R96A and H140Q) activity was incapable of conveying the OPDA-dependent formation of CSC (Fig. 3.4G). On the contrary, a *Δ*PPlase mutant CYP20-3 (F74L) could relay OPDA

signaling to the CSC formation, together indicating that OPDA signaling channels the ETC flow from TRX-f2 through CYP20-3 to SAT1, and the reducing cascades switches on the S-O interaction.

3.4. DISCUSSION

Light is the principal energy source for plant growth and survival. In the chloroplasts, photoreceptors capture and transform light into chemical energies for the photosynthetic carbon fixations and biomass productions, as well as create a chain of redox reactions (or ETC) which coordinates growth and defense responses (plant fitness), programing optimal phenotypes under different ecological conditions (Ballaré, 2014; Kliebenstein, 2016). Here, environmental stressors appear as a major determinant as plants must continue growing and, at the same time, need to defend themselves from the various forms of abiotic and biotic stresses. Defense (adaptive) responses toward the environmental stressors are, however, often constrained by resource availability. Diversion of resources to defense could limit growth processes, whereas their allocation to growth could reduce investment in defense responses. Therefore, plants must strike a precise balance in their responses to a myriad of environmental stress cues (Kazan and Manners, 2011; Ballaré, 2014).

Lately, emerging evidence has illuminated a unique activity of plant hormone signaling in converting light inputs into outputs that shape plant fitness. For instance, in Arabidopsis, the photoperception controls the spatial production of auxins that engenders phototropic growth and, at the same time, initiates OPDA accumulations to actuate the defense machinery (Riemann et al., 2003; Holliday *et al*., 2009; Kazan and Manners, 2011). Likewise, a sorghum inbred line accumulating higher level OPDA displayed not only enhanced defense capacity to insect infestations, but also minimal biomass loss as well as robust photosynthetic machinery. On the other hand, the insect-tolerant line accumulated the similar or attenuated levels of JA-Ile and other plant defense-associated hormones including salicylic acid and cytokinin, comparing to insect-

susceptible lines (Grover et al., 2020), together indicating an intrinsic role of OPDA signal as a key facet of plant growth and defense coordination. Recently, we revealed that OPDA triggers CYP20-3-dependent sulfur assimilations, increasing cellular levels of GSH which operates the S-glutathionylation (posttranslational activation) of 2-Cys peroxiredoxin A (2CPA), thereby enhancing its antioxidant capacity and fostering photosynthetic efficacy (energy supply), whilst actuating retrograde (from plastids to nucleus) signaling that coordinates ORG expressions, in the end, ensuring plant defense activation against various exterior pressures (Adhikari and Park, 2023).

In line with this scenario, the present study has located CYP20-3 at a regulatory hub where crisscrosses light and OPDA signaling. Light signaling conveys ETC via TRX-redox reaction systems (resting states), wherein CYP20-3 relays OPDA signaling to channel ETC routes and efficiency (stressed states). When induced under stressed conditions, OPDA binds CYP20-3 and stimulates its binding and electron (e^-, H^+) transfers from TRXF2 to SAT1 (PSI^{e-} → Fd/FTR → TRXF2 → CYP20-3 → SAT1/OASTL-B → GSH). This pathway illuminates a unique interface between light and hormone (OPDA) signaling, which i) conveys resource (e^-) allocations from its factory (PSI^{e-}) to defense signaling cascades ii) in making instant and appropriate adaptive decisions while being challenged constantly by environmental stressors.

Jasmonate signaling involves complex networks; addictively or synergistically intertwined within themselves, and cross-talking with other hormones and reactive electrophilic species (RES, Taki et al., 2005; Farmer and Davoine, 2007). In line with this scenario, OPDA triggers autonomous pathways that regulate unique subsets of jasmonate-responsive genes, coordinated with and without the canonical JA pathway (Taki et al., 2005, Mueller et al., 2008). OPDA signaling then reprograms plant cells toward defense modes against various forms of abiotic and biotic stresses, including pathogen infection, salinity, and excess oxidants. A mutant Arabidopsis disrupted in OPDA signaling (*cyp20-3*) manifested enhanced susceptibility to necrotrophic microbes (e.g., *Alternaria brassicicola*) as well as hypersensitivity to the excess level of exterior salt and ROS.

However, a mutant inhibited in JA-Ile derivatization (*jar1*) displayed WT-like disease resistance and defense responses (Figs. 1E, F, Park et al., 2013; Adhikari and Park, 2023), demonstrating an autonomous, yet additive or synergistic, role of OPDA in jasmonate signaling for complete, broad-spectrum protection and adaptation processes in plants.

Besides, OPDA works together with salicylic acid (SA) and other redox metabolites, coordinating the expression of general stress tolerant genes including *CYTOCHROME P450*, *GLUTAHIONE S-TRANSFERASE* and *HEAT SHOCK PROTEIN* (Mou et al., 2003; D'Autréaux and Toledano, 2007; Mueller et al., 2008; Park et al., 2013; Liu et al., 2020; Adhikari and Park, 2023). Under stressed conditions, OPDA and SA accumulated in the chloroplasts and/or cytosol promote GSH accumulations and build up cellular reduction capacity, which in turn orchestrate defense gene expressions. In these signaling pathways, GLUTAREDOXIN (GRX)480 is considered as a multifunctional transcriptional regulator (TR) as it can be induced by both OPDA and SA. GRX480 is an electron carrier using GSH as a cofactor that binds and regulates a series of TGA TFs, a basic leucine zipper TF family (Ndamukong et al., 2007; Mueller et al., 2008; Li et al., 2009). Alternatively, stress-responsive breakage of linolenic acid in the chloroplast membranes produces RES and/or ROS in parallel to OPDA, which could regulate TGA TF-dependent transcriptions, including *GRX480* and *HSP70.6* (Mueller et al., 2008) or
through NAC TFs (Mhamdi et al., 2010; Wu et al., 2012).

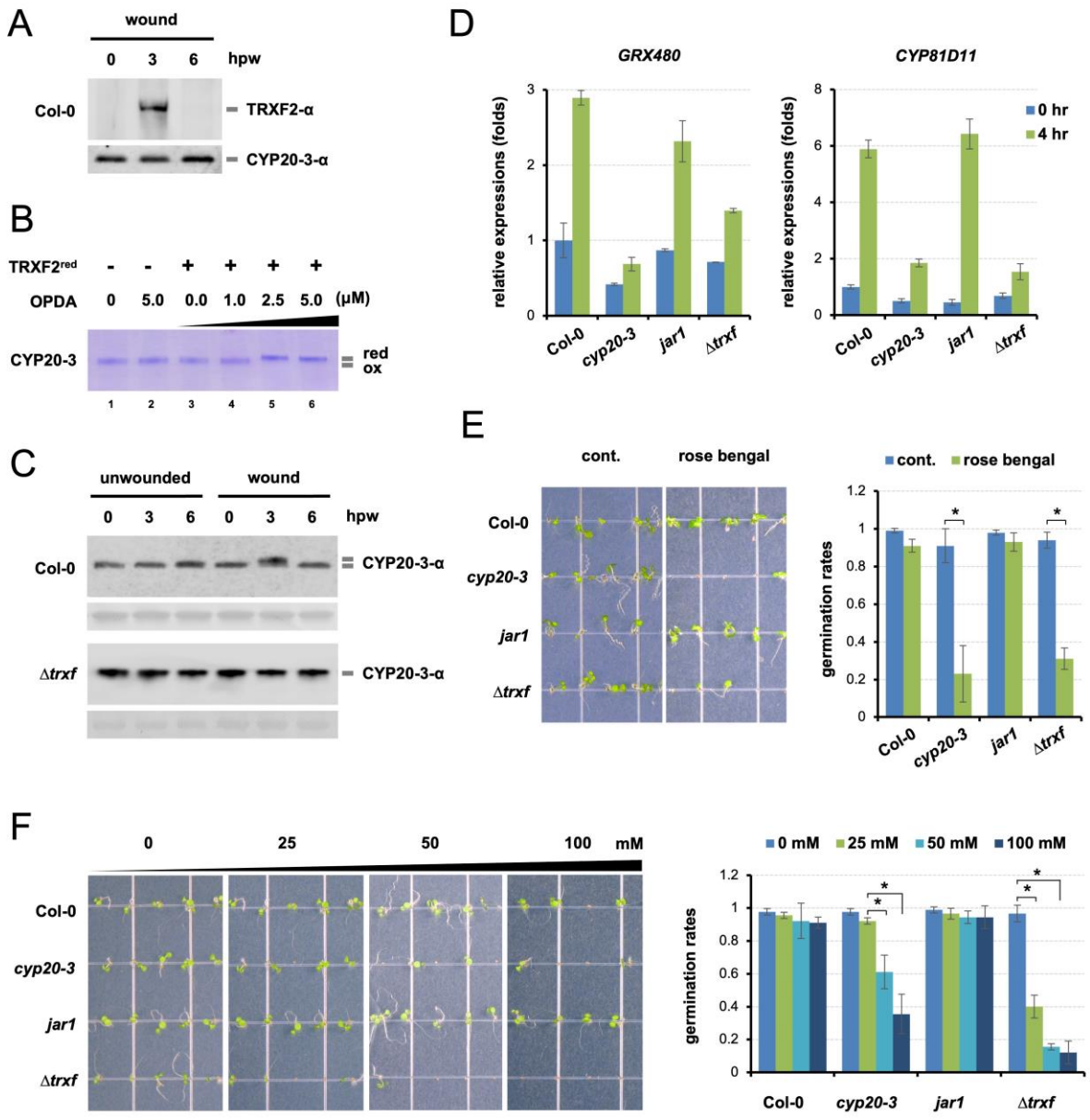

Figure 3.1. OPDA Fosters TRXF2 to Reduce CYP20-3, Activating Defense Responses. (A) Time-dependent co-IP assays probing the TRXF2 and CYP20-3 interaction in wounded WT (Col-0) plants. Total extracts of leaf tissues prepared at 0, 3 and 6 hpw were subjected to co-IP using CYP20-3-α-coupled resin. (Lower) IB assay indicating amount of bait proteins (CYP20-3) used in each IP assay. Parallel IB of proteins from co-IP with CYP20-3 were detected with TRXF2-α (Upper). **(B)** Mobility shift analysis of CYP20-3 (1 μM) upon the incubation with 1 μM TRXF2^{red}

and/or various concentrations of OPDA for 30 min. Samples were separated on nonreducing SDS/PAGE and stained with Coomassie Brilliant R250. **(C)** Time-resolved IB assays determining the redox state of CYP20-3 in wounded WT (Col-0) and Δ*trxf* plants. Equal amounts of total protein extracts were subjected to nonreducing SDS/PAGE and IB analyzed by CYP20-3-α. PVDF membranes of total extracts were stained with Ponceau S (Bottom). **(D)** qRT-PCR analysis of ORG, *GRX480* and *CYP81D11*, expressions in wounded WT (Col-0) and mutant (*cyp20-3*, *jar1* and Δ*trxf*) plants. Total RNAs were prepared from leaves at 0 and 4 hpw. Values were normalized to the expression of *POLYUBIQUITIN* (Czechowski et al., 2005, mean ± SD; n = 3). **(E,F)** Germination rates of WT (Col-0) and mutant (*cyp20-3, jar1* and Δ*trxf*) plants was counted on MS agar media without or containing 3 μM rose bengal **(E)** or different concentrations (0, 25, 50 and 100 mM) of NaCl **(F)** on the 5-d after vernalization (means ± SD; n = 25). The asterisks (*) indicate statistically significant differences (Tukey-Kramer honestly significant difference test on all pairs; α = 0.05).

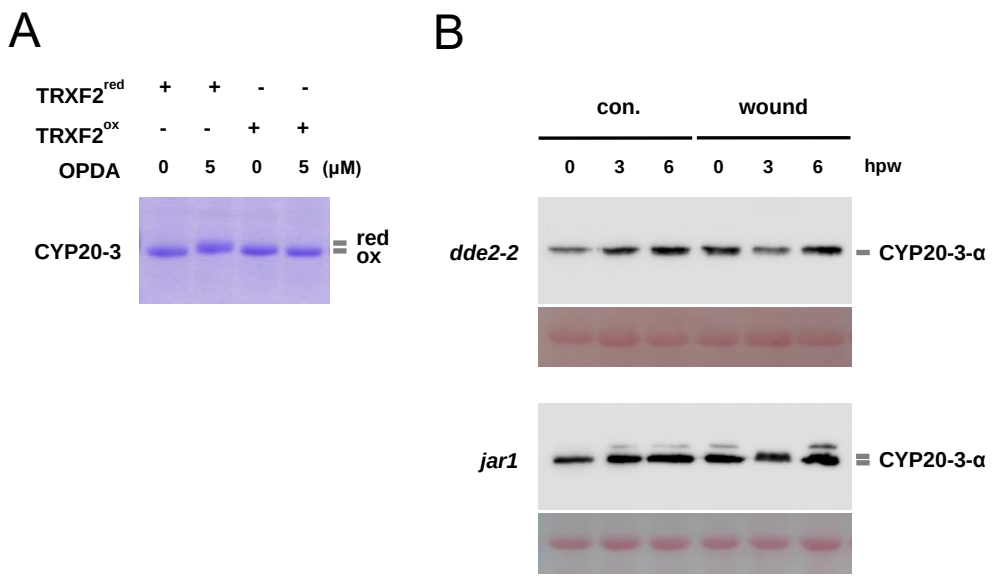

Figure 3.2. Conditional Reduction of CYP20-3 by TRXF2 and OPDA. (A) Mobility shift analysis of CYP20-3 (1 µM), following the incubation with 1 µM TRXF2red, TRXF2ox and/or 5 µM OPDA for 30 min. Samples were separated on nonreducing SDS/PAGE and subsequently stained with Coomassie Brilliant R250 **(B)** Time-resolved in situ IB assays determining the redox state of CYP20-3 in wounded dde2 and jar1 plants. Equal amounts of total protein extracts were subjected to nonreducing SDS/PAGE and IB analyzed by CYP20-3-α. PVDF membranes of total extracts were stained with Ponceau S (Bottom).

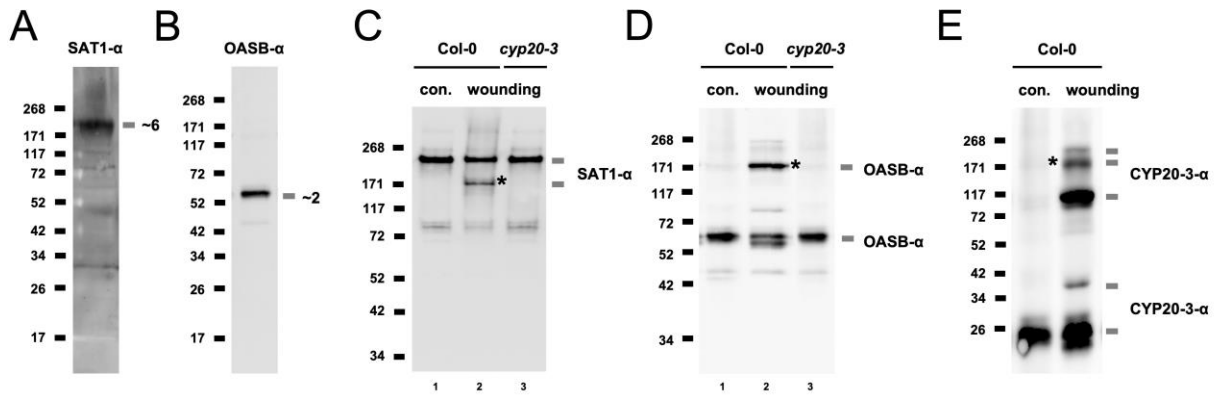

Figure 3.3. Wound-Responsive OPDA Signaling Stimulates the CSC Formation. In situ IB analyses determining the quaternary structure of SAT1 **(A)**, OAS-TL B **(B)** and CSC **(C-E)**. Total protein extracts prepared from WT (Col-0) and *cyp20-3* plants at 0 and/or 3 hpw were subjected to nonreducing SDS/PAGE and IB analyzed by SAT1-α **(A,C)**, OASB-α **(B,D)** and CYP20-3-α **(E)**. **(C-E)** The asterisks (*) indicate a band corresponding CSC.

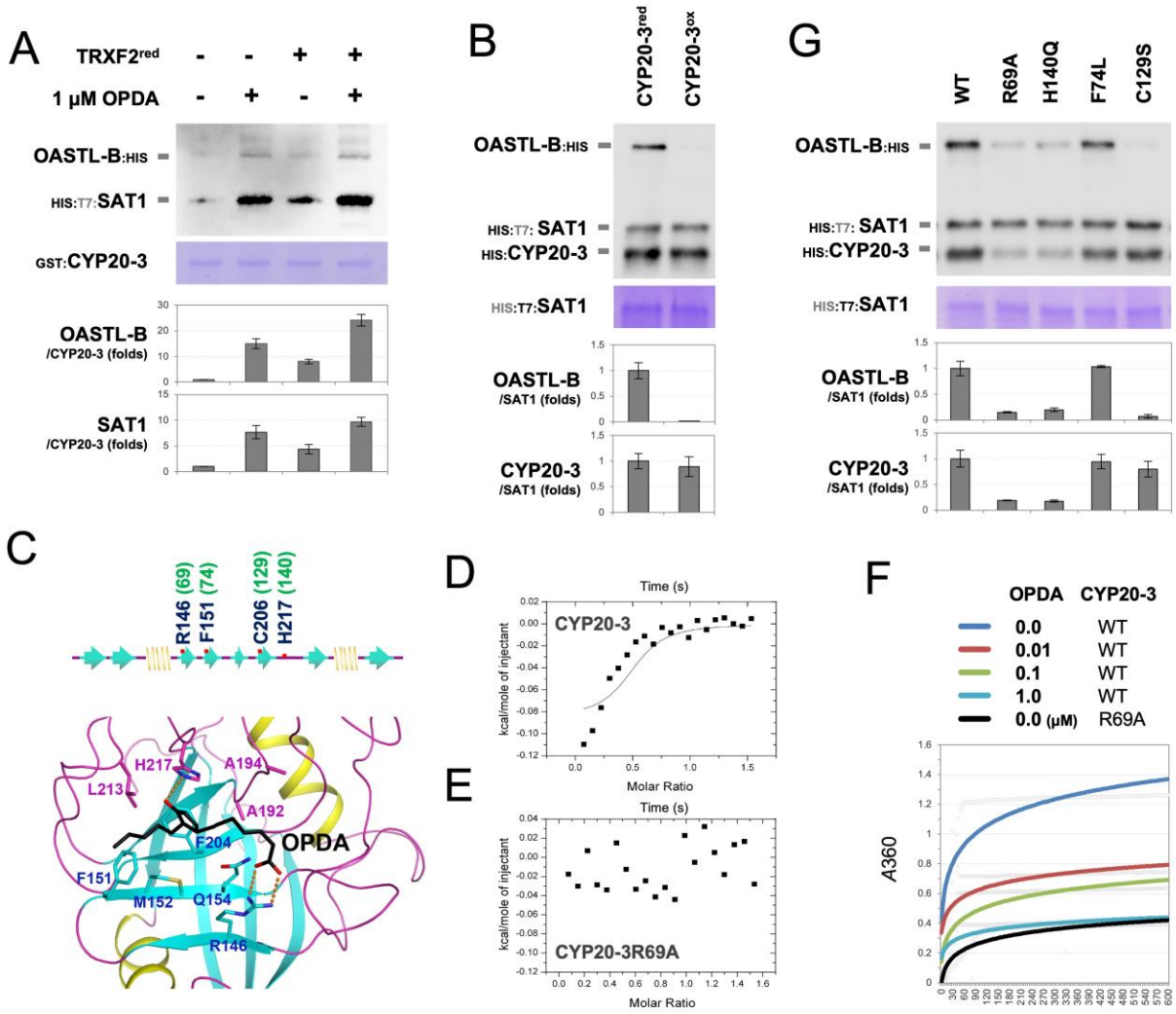

Figure 3.4. CYP20-3 Acts as a Reductase in Stimulating the CSC formation. (A,B) In vitro pull-down assays determining the physical association SAT1 and OASTL-B in the presence/absence of CYP20-3, TRXF2^{red} and/or OPDA **(A)**, and by CYP20-3^{red} or CYP20-3^{ox} **(B)**. GST:CYP20-3 fusion protein **(A)** or T7-tagged SAT1 **(B)** was used as a bait to pull down HIS:SAT1, HIS:CYP20-3 and/or OASTL-B:HIS proteins. (Lower) Coomassie Brilliant R250-stained gels indicating amount of bait proteins used in each pull-down assay. Parallel IB of proteins that copurified with the baits were probed with HIS-α (Upper). **(C)** Predicted model of CYP20-3 bound to OPDA. **(D,E)** Thermodynamics of CYP20-3 **(D)** and CYP20-3R69A **(E)** treated with 10 μM OPDA. **(F)** Effect of OPDA on the PPIase activity of CYP20-3. CYP20-3 were preincubated

with varying concentrations of OPDA (0.01, 0.1 and 1.0 μM) at 10 °C. **(A,B,G)** The level IB signals of co-purified proteins were quantified (mean ± SD; *n* = 3) by the Image J (Schneider et al., 2012), and normalized to those of bait proteins (bottom).

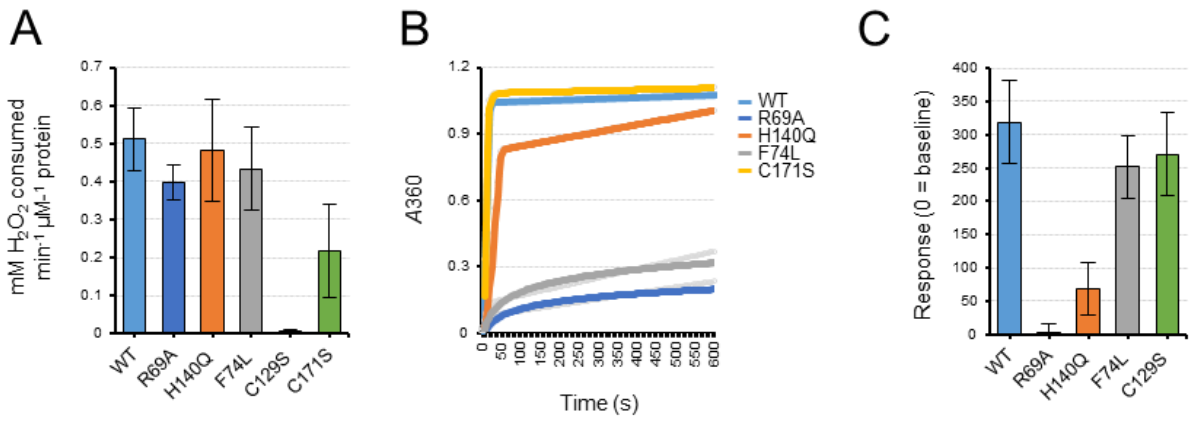

Figure 3.5. Biochemical Characterization of Mutant CYP20-3s. (A) Cys129 is a critical aa residue for the reductase activity of CYP20-3. Reductions of H_2O_2 by 5 µM WT and mutant CYP20-3s were quantified via the eFOX assay method, as described previously (Cheeseman, 2006; Adhikari and Park, 2023). The reaction of eFOX reagent (250 µM $Fe(NH_4)_2(SO_4)_2$, 100 µM sorbitol, 100 µM xylenol orange, and 1% [v/v] in 20 mM H_2SO_4) with H_2O_2 was tracked spectrophotometrically by measuring the difference in absorbance between 550 and 800 nm. **(B)** Arg69 and Phe74 are active aa residues for the PPlase activity of CYP20-3. **(C)** Arg69 and His140 are critical aa residues for the binding activity of CYP20-3. Optical biosensor analyses were performed with BIAcore T100 as described previously (Park et al., 2013). For protein immobilization, an amine coupling kit (BIAcore) was used for CM5 chips (BIAcore) following manufacturer's instructions. The protein–ligand interactions were monitored by injecting various concentrations of OPDA over the reference and/or protein-immobilized flow cells, with periodic buffer blank injections for double referencing (25 °C, flow rate of 20 µL/ min, BIAcore). Binding responses in the sensorgrams were corrected for reference cell responses or blank injections.

Table 3.1. Oligonucleotides used in this study.

Name	Dir†	Sequence, 5′ to 3′	purpose
CYP20-3·R_{69}A·F	F	GGTACAAGGGTTCCTCTTTCCATGCTATTATTAAGGATTTCATGATCC	Mut††
CYP20-3·R_{69}A·R	R	GGATCATGAAATCCTTAATAATAGCATGGAAAGAGGAACCCTTGTACC	Mut††
CYP20-3·F_{74}L·F	F	CCTCTTTCCATCGTATTATTAAGGATTTAATGATCCAAGGAGGT	Mut††
CYP20-3·F_{74}L·R	R	ACCTCCTTGGATCATTAAATCCTTAATAATACGATGGAAAGAGG	Mut††
CYP20-3·C_{129}S·F	F	CTAATACTAATGGAAGCCAGTTTTTCATTAGTACCGTCAAGACTTC	Mut††
CYP20-3·C_{129}S·R	R	GAAGTCTTGACGGTACTAATGAAAAACTGGCTTCCATTAGTATTAG	Mut††
CYP20-3·H_{140}Q·F	F	CTTCATGGTTAGATAACAAGCAGGTCGTGTTTGGACAAGTAATTG	Mut††
CYP20-3·H_{140}Q·R	R	CAATTACTTGTCCAAACACGACCTGCTTGTTATCTAACCATGAAG	Mut††
CYP20-3·C_{171}S·F	F	GATGTTCCCAAGAAAGGTAGTAGAATCTATGCCTGCG	Mut††
CYP20-3·C_{171}S·R	R	CGCAGGCATAGATTCTACTACCTTTCTTGGGAACATC	Mut††
2CPA·Fw	F	AACTACTCTCATCTCTTCTCC	RT-PCR
2CPA·Rev	R	AGGGAAGAGCGTCGAGCAAAT	RT-PCR
2CPB·Fw	F	TTCTTCCACCACCCTACT	RT-PCR
2CPB·Rev	R	GGAACCGAGACTGGAGAAC	RT-PCR
CYP18D11·Fw	F	TCTCAACATG^GGTTTGTGAA	qRT-PCR^
CYP18D11·Rev	R	AAGTATC^ATAACAAGTATGA	qRT-PCR^
HSP17.6·Fw	F	CTTGCCTGGATTAAGAAGG	qRT-PCR
HSP17.6·Rev	R	CATCGCAGCCTTAACCTGAT	qRT-PCR
HSP70·Fw	F	GGAAAGTTCGAGCTCAGTGG	qRT-PCR
HSP70·Rev	R	ACCTTCCCTTGTCGTTTGTG	qRT-PCR
GST6·Fw	F	TGCCCTCAACCCCTTCGGTC	qRT-PCR
GST6·Rev	R	GGTTGCCTTGACTTTCTTGC	qRT-PCR
GST8·Fw	F	TGACAAGAAGCTG^TATGATGC	qRT-PCR^
GST8·Rev	R	ACATAGCCAAAGTCATCGCC	qRT-PCR
GRX480·Fw	F	TGATTGTGATTGGACGGAGA	qRT-PCR
GRX480·Rev	R	TAAACCGCCGGTAACTTCAC	qRT-PCR
UBC·Fw	F	CTGCGACTCAG^GGAATCTTCTAA	qRT-PCR^
UBC·Rev	R	TTGTGCCATTGAATTGAACCC	qRT-PCR

† Dir, Direction. F, Forward. R, Reverse.

†† Mutated nucleotide bases are grey highlighted.

^ Position of an exon-exon junction.

CHAPTER 4: REFERENCES

Acosta, I.F., Farmer, E.E. (2010). "Jasmonates," *In* Arabidopsis Book, eds. C.R. Somerville, E.M. Meyerowitz (American Society of Plant Biologists, Rockville) 8, e0129.

Ahmad, P., Sarwat, M., Sharma, S. (2008). Reactive oxygen species, antioxidants and signaling in plants. J. Plant Biol. 51: 167-173.

Andersson, M.X., Hamberg, M., Kourtchenko, O., Brunnström, A., McPhail, K.L., Gerwick, W.H., Göbel, C., Feussner, I., Ellerström, M. (2006). Oxylipin profiling of the hypersensitive response in *Arabidopsis thaliana*: formation of a novel oxo-phytodienoic acid-containing glactolipid, arabidopsides E. J. Biol. Chem. 281: 31528-31537.

Arc, E., Sechet, J., Corbineau, F., Rajjou, L., Marion-Poll, A. (2013). ABA crosstalk with ethylene and nitric oxide in seed dormancy and germination. Front. Plant Sci. 4: 63.

Awad, J., Stotz, H.U., Fekete, A., Krischke, M., Engert, C., Havaux, M., Berger, S., and Baier, M., Dietz, K.J. (1999). Protective function of chloroplast 2-cysteine peroxiredoxin in photosynthesis, evidence from transgenic Arabidopsis. Plant Physiol. 119: 1407-1414.

Baier, M., Noctor, G., Foyer, C.H., Dietz, K.J. (2000). Antisense suppression of 2-cysteine peroxiredoxin in Arabidopsis specifically enhances the activities and expression of enzymes associated with ascorbate metabolism but glutathione metabolism. Plant Physiol. 124: 823-832

Balfagón, D., Sengupta, S., Gómez-Cadenas, A., Fritschi, F.B., Azad, R.K., Mittler, R., Zandalinas, S.I. (2019). Jasmonic acid is required for plant acclimation to a combination of high light and heat stress. Plant Physiol. 18: 1668-1682.

Ballaré, C.L. (2014) Light regulation of plant defense. Annu Rev Plant Biol. 65, 335-363.

Barbosa dos Santos, I., Park, S.W. (2019) Versatility of cyclophilins in plant growth and survival: A case study in *Arabidopsis*. Biomolecules 9: 20.

Barros-Galvão, T., Dave, A., Cole, A., Harvey, D., Langer, S., Larson, T.R., Vaistij, F.E., Graham, I.A. (2019). *cis*-12-Oxo phytodienoic acid represses Arabidopsis seed germination in shade conditions. J. Exp. Bot. 70: 5919-5927.

Bosch, M., Wright, L. P., Gershenzon, J., Wasternack, C., Hause, B., Schaller, A., Stintzi, A. (2014). Jasmonic acid and its precursor 12-oxophytodienoci acid control different aspects of constitutive and induced herbivore defenses in tomato. Plant Physiol. 116: 396-410.

Böttcher, C., Pollmann, S. (2009). Plant oxylipins: Plant responses to 12-oxo-phytodienoic acid are governed by its specific structural and functional properties. FEBS J. 17: 4693-4703.

Brünger, A.T., Adams, P.D., Clore, G.M., DeLano, W.L., Gros, P., Grosse-Kunstleve, R.W., Jiang, J.S., Kuszewski, J., Nilges, Pannu N.S. et al. (1998). Crystallography & NMR system: A new software suite for macromolecular structure determination. Acta Crystallogr. D. Biol. Crystallogr. 54(Pt 5): 905-921.

Buseman, C.M., Tamura, P., Sparks, A.A., Gaughman, E.J., Maatta, S., Zhao, J., Roth, M.R., Esch, S. W., Shah, J., Williams, T.D., Welti, R. (2006). Wounding stimulates the accumulation of glycerolipids containing oxophytodienoic acid and dinor-oxophytodienoic acid in Arabidopsis leaves. Plant Physiol. 142: 28-39.

Calderón, A., Lázaro-Payo, A., Iglesias-Baena, I., Camejo, D., Lázaro, J.J., Sevilla, F., and Jiménez, A. (2017). Glutathionylation of pea chloroplast 2-Cys Prx and mitochondrial Prx IIF affects their structure and reroxidase activity and sulfiredoxin deglutathionylates only the 2-Cys Prx. Front. Plant Sci. 8: 118.

Caporaletti, D., D'Alessio, A.C., Rodriguez-Suarez, R.J., Senn, A.M., Duek, P.D., Wolosiuk, R.A. (2007). Non-reductive modulation of chloroplast fructose-1,6-bisphos-phatase by 2-Cys peroxiredoxin. Biochem. Biophys. Res. Commun. 355, 722-727.

Chang, Y., Shi, M., Sun, Y., Cheng, H., Ou, X., Zhao, Y., Zhang, X., Day, B., Miao, C., Jiang, K. (2023). Light-induced stomatal opening in Arabidopsis is negatively regulated by chloroplast-originated OPDA signaling. Curr. Biol. 33: 1071-1081.

Cheeseman, J.M. (2006). Hydrogen peroxide concentrations in leaves under natural conditions. J. Exp. Bot. 57: 2435-2444.

Cheong, H., Barbosa dos Santos, I., Liu, W., Gosse, H.N., Park, S.W. (2017) Cyclophilin 20-3 is positioned as a regulatory hub between light-dependent redox and 12-*oxo*-phytodienoic acid signaling. Plant Signal. Behav. 12: e1362520.

Cheng, G., Chen, M.S., Zhu, L. (2018). 12-oxo-phytodienoic acid enhances wheat resistance to Hessian Fly (Diptera: Cecidomyiidae) under heat stress. J. Econ. Entomol. 111: 917-922.\

Chini, A., Fomseca, S., Fernández, G., Adie, B., Chico, J.M., Lorenzo, O., García-Casado, G., López-Vidriero, I., Lozano, F.M., Ponce, M.R., Micol, J.L., Solano, R. (2007). The JAZ family of repressors is the missing link in jasmonate signaling. Nature 448**:** 666-671.

Chini, A., Monte, I., Zamarreño, A.M., Hamberg, M., Lassueur, S., Reymond, P., Weiss, S., Stintzi, A., Schaller, A., Porsel, A., García-Mina, J.M., Solano, R. (2018). An OPR3-independent pathway uses 4,5-didehydrojasmonate for jasmonate synthesis. Nat. Chem. Biol. 14,: 171-178.

Chitnis, P.R. (2001). Photosystem I: function and physiology. Annu. Rev. Plant Physiol. Mol. Biol. 52: 593-626.

Chung, H.S., Koo, A.J.K., Gao, X., Jayanty, S., Thines, B., Jones, A.D., Howe, G.A. (2008). Regulation and function of *Arabidopsis JAMONATE ZIM*-domain genes in response to wounding and herbivory. Plant Physiol. 146: 952-964.

Cobbert, C.S., May, M.J., Howden, R., Rolls, B. (1998). The glutathione-deficient, cadmium-sensitive mutant, *cad2-1*, of *Arabidopsis thaliana* is deficient in *γ*-glutamylcysteine synthetase. Plant J. 16: 73-78

Dalle-Donne, I., Rossi, R., Giustarini, D., Colombo, R., Milzani, A. (2007). S-glutathionylation in protein redox regulation. Free Radical. Biol. Med. 43: 883-898.

Dang, H.T., Lee, H.J., Yoo, E.S., Hong, J., Bao, B., Choi, J.S., Jung, J.H. (2008). New jasmonate analogues as potential anti-inflammatory agents. Bioorg. Med. Chem. 16, 10228-10235.

D'Autréaux, B., Toledano, M.B. (2007). ROS as signaling molecules: mechanisms that generate specificity in ROS homeostasis. Mol. Cell. Biol. 8: 813-824.

Dave, A., Hernández, M.L., He, Z., Andriotix, V.M.E., Vaistij, F.E., Larson, T.R., Graham, I.A. (2011). 12-oxo-phytodienoic acid accumulation during seed development represses seed germination in *Arabidopsis*. Plant Cell 23: 583-599.

Dave, A., Graham, I.A. (2012). Oxylipin signaling: A distinct role for the jasmonic acid precursor *cis*-(+)-12-oxo-phytodienoic acid (*cis*-OPDA). Front. Plant Sci. 3: 42.

Dave, A., Vaistij, F.E., Gilday, A.D., Penfield, S.D., Graham, I.A. (2016). Regulation of *Arabidopsis thaliana* seed dormancy and germination by 12-oxo-phytodienoci acid. J. Exp. Bot. 67 : 2277-2284.

Davoine, C., Douki, T., Iacazio, G., Montillet, J.L., Triantaphylidès, C. (2005). Conjugation of keto fatty acids to glutathione in plant tissues. Characterization and quantification by HPLC-tandem mass spectrometry. Anal. Chem. 77 : 7366-7372.

Davoine, D., Falletti, O., Douki, T., Iacazio, G., Ennar, N., Montillet, J.L., Triantaphylidès, C. (2006). Adducts of oxylipin electrophiles to gluatathione reflect a 13 specificity of the downstream lipoxygenase pathway in the tobacco hypersensitive response. Plant Physiol. 140: 1484-01493.

De Storme, N., Geelen, D. (2014). Callose homeostasis at plasmodesmata: molecular regulators and developmental relevance. Front. Plant Sci. 5: 138.

Devoto, A., Ellis, C., Magusin, A., Chang, H.S., Chilcott, C., Xhu, T., Turner, J.G. (2005). Expression profiling reveals COI1 to be a key regulator of genes involved in wound- and methyl jasmonate-induced secondary metabolism, defence, and hormone interactions. Plant Mol. Biol. 58: 497-513.

Dietz, D.J., Jacob, S., Oelze, M.L., Laxa, M., Tognetti, V., de Miranda, S.M., Baier, M., Finkemeier, I. (2006). The function of peroxiredoxins in plant organelle redox metabolism. J. Exp. Bot. 57: 1697-1709.

Dominguez-Solis, J.R., He, Z., Lima, A., Ting, J., Buchanan, B.B., Luan, S. (2008). A cyclophilin links redox and light signals to cysteine biosynthesis and stress responses in chloroplasts. Proc. Natl. Acad. Sci. USA 105: 16386-16391.

Dos Santos, I.B., Park, S.W. (2019). Versatility of cyclophilins in plant growth and survival: a case study in *Arabidopsis*. Biomolecules 9: 20.

English, J., Bonner, J., and Haagen-Smit, A.J. (1939a) Structure and synthesis of a plant wound hormone. Science 90: 329.

English, J., Booner, J., and Haagen-Smit, A.J. (1939b) The wound hormones of plants: II. The isolation of crystalline active substance. Proc. Natl. Acad. Sci. USA. 25: 323-329.

Finka, A., Mattoo, R.U., Goloubinoff, P. (2011). Meta-analysis of heat- and chemically upregulated chaperone genes in plant and human cells. Cell Stress Chaperones 16: 15-31.

Fischer, G., Wittmann-Liebold, B., Lang, K., Kiefhaber, T., Schmid, F.X. (1989) Cyclophilin and peptidyl-prolyl cis-trans isomerase are probably identical proteins. Nature 337: 476-478.

Flescher, E. (2005). Jasmonates–a new family of anti-cancer agents. Anticancer Drugs 16: 911-916.

Flescher. E (2007). Jasmonates in cancer therapy. Cancer Lett. 245: 1-10.

Frigerio, M., Alabad, D., Pérez-Gómez, J., García-Cárcel, L., Phillips, A.L., Hedden, P., and Blázquez, M.A. (2006). Transcriptional regulation of gibberellin metabolism genes by auxin signaling in Arabidopsis. Plant Physiol. 142: 553-563.

Funk, C.D. (2001). Prostaglandins and leukotrienes: Advances in Eicosanoid Biology. Science 294: 1871–1875.

Gelhave, E., Rouhier, N., Gérard, J., Jolivet, Y., Gualberto, J., Navrot, N., Ohlsson, P.I., Wingsle, G., Masakazu, H., Knaff, D.B. et al. (2004). A specific form of thioredoxin *h* occurs in plant mitochondria and regulates the alternative oxidase. Proc. Natl. Acad. Sci. USA 101: 14545-14550.

Genva, M., Deleu, M., Andersson, M.X., Lins, L., Fauconnier, M.L. (2019). "Evaluation of interactions between Arabidopsides and plant plasma membrane lipids," *In* Scientific Congresses and Symposiums. https://orbi.uliege.be/bitstream/2268/222461/1/Bruxelles%20congress.pdf.

Goetz, S., Hellwege, A., Stenzel, I., Kutter, C., Hauptmann, V., Forner, S., McCaig, B., Hause, G., Mierxch, O., Wasternack, C., Hause, B. (2012) Role of cis-12-oxo-phytodienoic acid in tomato embryo development. Plant Physiol. 4: 1715-1727.

Grover, S., Versani, S., Kolomietx, M.V., Louis, J. (2020). Maize defense elicitor, 12-oxo-phytodienoic acid, prolongs aphid salivation. Commun. Integr. Biol. 13: 63-66.

Gullner, G., Komives, T., Király L., and Schröder, P. (2018) Glutathione S-transferase enzymes in plant-pathogen interaction. Front. Plant Sci. 9: 1836.

Guo, H.M., Li, H.C., Zhou, S.H., Xue, H.W., Miao, X.X. (2014). *Cis*-12-oxo- phytodienoic acid stimulates rice defense response to a piercing-sucking insect. Mol. Plant 7: 1683-1692.

Haberlandt, G. (1922) Über Zellteilungshormone und ihre Beziehungen zur Wundheilung, Befruchtung, Parthenogenesis und Adventiv-Embryonie. Biol. Zentralbl. 42: 145-172.

Hazman, M., Hause, B., Eiche, E., Nick, P., Riemann, M. (2015). Increased tolerance to salt stress in OPDA-deficient rice *ALLENE OXDE CYCLASE* mutants is linked to an increase ROS-scavenging activity. J. Exp. Bot. 66: 3339-3352.

He, J., Duan Y., Hua, D., Fan, G., Wang, L., Liu, Y., Chen, Z., Han, L., Qu, L.J., Gong, Z. (2012). DEXH box RNA helicase-mediated mitochondrial reactive oxygen species production in Arabidopsis mediates crosstalk between abscisic acid and auxin signaling. Plant Cell 24: 1815-1833.

Heeg, C., Kruse, C., Jost, R., Gutensohn, M., Ruppert, T., Wirtz, M., Hell, R. (2008). Analysis of the *Arabidopsis O*-acethylserine(thiol)lyase gene family demonstrates compartment-specific differences in the regulation of cysteine synthesis. Plant Cell 10: 168-185.

Hell, R., Wirtz, M. (2011). Molecular biology, biochemistry and cellular physiology of cysteine metabolism in *Arabidopsis thaliana*. The Arabidopsis Book 9: e0154.

Hisamatsu, Y., Goto, N., Hasegawa, K., Shigemori, H. (2003). Arabidopsides A and B, two new oxylipins from *Arabidopsis thaliana*. Tetrahedron Lett. 44: 5553-5556.

Hisamatsu, Y., Goto, N., Sekiguchi, M., Hasegawa, K., Shigemori, H. (2005). Oxylipins arabidopsides C and D from *Arabidopsis thaliana*. J. Nat. Prod. 68: 600-603.

Hofhuis, H., Laskowski, M., Du, Y., Prasad, K., Grigg, S., Pinon, V., Scheres, B. (2013). Phyllotaxis and rhizotaxis in Arabidopsis are modified by three PLETHORA transcription factors. Curr. Biol. 23: 965-962.

Holliday, K.J., Martínez-García, J., Josse, E.M. (2009). Integration of light and auxin signaling. Cold Spring Harb. Perspect. Biol. 1: a001586.

Hossain, M.A., Li, A.G., Hoque, T.S., Burritt, D.J., Fujita, M., Munnè-Bosch, S. (2018). Heat or cold priming-induced cross-tolerance to abiotic stresses in plants: key regulators and possible mechanisms. Protoplasma 255: 399-412.

Hou, X., Lee, L.Y.C., Xia, K., Yan, Y., Yu, H. (2010). DELLAs modulate jasmonate signaling via competitive binding to JAZs. Dev. Cell 19: 884-894.

Huot, B., Yao, J., Montgomery, B.L., He, S.Y. (2014). Growth-defense tradeoffs in plants: A balancing act to optimize fitness. Mol. Plant 7, 1267-1287.

Jensen, P.E., Bassi, R., Boekema, E.J., Dekker, J.P., Jansson, S., Leister, D., Robinson, C., Scheller, H.V. (2007). Structure, function and regulation of plant photosystem I. Biochim. Biophys. Acta. 1767: 335-352.

Jiao, Y., Sun, L., Song, Y., Wang, L., Liu, L., Zhang, L., Liu, B., Li, N., Miao, C., Hao, F. (2013). AtrbohD and atrbohF positively regulate abscisic acid-inhibited primary root growth by affecting Ca^{2+} signaling and auxin response of roots in Arabidopsis. J. Exp. Bot. 64: 4183-4192.

Kazan, K., Manners, J.M. (2011). The interplay between light and jasmonate signaling during defence and development. J. Exp. Bot. 62: 4087-4100.

Kliebenstein, D.J. (2016). False idolatry of the mythical growth versus immunity tradeoff in molecular systems plant pathology. Physiol. Mol. Plant Pathol. 95: 55-59.

Ko, J.H., Yang, S.H., Han, K.H. (2006). Upregulation of an Arabidopsis RING-H2 gene, *XERICO*, confers drought tolerance through increased abscisic acid biosynthesis. Plant J. 47: 343-355.

Konig, J., Baier, M., Horling, F., Kahmann, U., Harris, G., Schurmann, P. (2002). The plant-specific function of 2-Cys peroxiredoxin-mediated detoxification of peroxides in the redox-hierarchy of photosynthetic electron flux. Proc. Natl. Acad. Sci. U.S.A. 99: 5738-5743.

Kourtchenko, O., Andersson, M.X., Hamberg, M., Brunnström, A., Göbel, C., McPhail, K.L., Gerwick, W.H., Geussner, I., Ellerström, M. (2007). Oxo-phytodienoic acid-containing galactolipids in Arabidopsis: jasmonate signaling dependence. Plant Physiol. 145: 1658-1669.

Kuhlgert, S., Austic, G., Zegarac, R., Osei-Bonsu, I., Hoh, D., Chilvers, M.I., Roth, M.G., Bi, K., TerAvest, D., Weebadde, P. et al. (2016). MultispeQ beta: a tool for large-scale plant phenotyping connected to the open photosynQ network. R. Soc. Open Sci. 3: 160592.

Laxa, M., Konig, J., Dietz, K.J., Kandlbinder, A. (2007). Role of the cysteine residues in *Arabidopsis thaliana* cyclophilin CYP20-3 in peptidylprolyl *cis-trans* isomerase and redox-related function. Biochem. J. 401: 287-297.

Li, S., Lauri, A.,Ziemann, M., Busch, A., Bhavev, M., Zachgo, S. (2009). Nuclear activity of ROXY1, a glutaredoxin interacting with TGA factors, is required for petal development in *Arabidopsis thaliana*. Plant Cell 21: 429-441.

Liebthal, M., Maynard, M., Dietz, K.J. (2019). Peroxiredoxins and redox signaling in plants. Antioxid. Redox Signal. 28: 609-624.

Liu, W., Barbosa dos Santos, I., Moye, A., Park, S.W. (2020). CYP20-3 deglutathionylates 2-CysPRX A and suppresses peroxide detoxification during heat stress. Life Sci. Alliance 3: e202000775.

Liu, W., Park, S.W. (2021). 12-*oxo*-phytodienoci acid: a fuse and/or switch of plant growth and defense response? Front. in Plant Sci. 12: 724079.

Luna, E., Pastor, V., Robert, J., Flors, V., Mauch-Mani, B., Ton, J. (2010). Callose deposition: a multifaceted plant defense response. Mol. Plant Microbe. Interact. 24: 183-193.

Luo, X., Chen, Z., Gao, J., Gong, Z. (2014). Abscisic acid inhibits root growth in Arabidopsis through ethylene biosynthesis. Plant J. 79: 44-58.

Marnett, L.J. (2008). Divergence from the superfamily. Nature 455: 300-301.

Maynard, D., Gröger, H., Dierks, T., Dietz, K.J. (2018). The function of the oxylipin, 12-oxo-phytodienoic acid in cell signaling, stress acclimation, and development. J. Exp. Bot. 69: 5341-5354.

McRee, D.E. (1999). XtalView/Xfit-A versatile program for manipulating atomic coordinates and electron density. J Struct. Biol. 125: 156-165.

Meyer, Y., Buchanan, B.B., Vignols, F., Reichheld, J.P. (2009). Thioredoxins and glutaredoxins: unifying elements in redox biology. Annu. Rev. Genet. 43: 335–367.

Mhamdi, A., Hager, J., Chaouch, S., Queval, G., Han, Y., Taconnat, L., Saindrenan, P., Gouia, H., Issakidis-Bourguet, E., Renou, J.-P. et al. (2010). *Arabidopsis* GLUTATHIONE REDUCTASE1 plays a crucial role in leaf responses to intracellular hydrogen peroxide and in ensuring appropriate gene expression through both salicylic acid and jasmonic acid signaling pathways. Plant Physiol. 153: 1144-1160.

Miyake, C. (2010). Alternative electron flows (water-water cycle and cyclic electron flow around PSI) in photosynthesis: molecular mechanisms and physiological functions. Plant Cell Physiol. 51: 1951-1963.

Mou, Z., Fan, W., Dong, X. (2003). Inducers of plant systemic acquired resistance regulate NPR1 function through redox changes. Cell 113: 935-944.

Mosblech, A., Feussner, I., Heilmann, I. (2009). Oxylipins: structurally diverse metabolites from fatty acid oxidation. Plant Physiol. Biochem. 47: 511-517.

Mosblech, A., Feussner, I., Heilmann, I. (2010). "Oxylipin signaling and plant growth," *In* Lipid Signaling in Plants, ed. T. Munnik (Springer-Verlag, Berlin, Heidelberg), 277-291.

Monte, I., Kneeshaw, S., Franco-Xorrilla, J.M., Chini, A., Zamarreño, A.M., García-Mina, J.M., Solano, R. (2020). An ancient COI1-independent function for reactive electrophilic oxylipins in thermotolerance. Curr. Biol. 30: 962-971.

Motohashi, K., Kondoh, A., Stumpp, M.T., Hisabori, T. (2001). Comprehensive survey of proteins targeted by chloroplast thioredoxin. Proc. Natl. Acad. Sci. USA. 98: 11224-11229.

Motohashi, K., Koyama, F., Nakanishi, Y., Ueoka-Nakanishi, H., Hisabori, T. (2003). Chloroplast cyclophilin is a target protein of thioredoxin. J. Biol. Chem. 278: 31848-31852.

Mueller, S., Hilbert, B., Dueckershoff, K., Roitsch, T., Krischke, M., Mueller, M.J., Berger, S. (2008). General detoxification and stress responses are mediated by oxidized lipids through TGA transcription factors in *Arabidopsis*. Plant Cell 20: 768-785.

Mueller, M.J. (2015). 2-cysteine peroxiredoxins and thylakoid ascorbate peroxidase create and water-water cycle that is essential to protect the photosynthetic apparatus under high light stress conditions. Plant Physiol. 167: 1592-1603.

Muench, M., Hsin, C.H., Ferber, E., Berger, S., Muller, M.J. (2016). Reactive electrophilic oxylipins triggers a heat stress-like response through HSFA1 transcription factors. J. Exp. Bot. 67: 6139-6148.

Muthuramalingam, M., Seidel, T., Laxa, M., Nunes de Miranda, S.M., Gärtnner, F., Ströher, E., Kandlbinder, A., Dietz, K.J. (2009). Multiple redox and non-redox interactions define 2-Cys peroxiredoxin as a regulatory hub in the chloroplasts. Mo. Plant 2: 1273-1288.

Na, G., Salt, D.E. (2011). Differential regulation of serine acetyltransferase is involved in nickel hyperaccumulation in *Thlaspi goesingense*. J. Biol. Chem. 286: 40423-40432.

Ndamukong, I., Abdallat, A.A., Thurow, C., Fode, B., Zander, M., Weigel, R., Gatz, C. (2007). SA-inducible *Arabidopsis* glutaredoxin interacts with TGA factors and suppresses JA-responsive PDF1.2 transcription. Plant J. 50: 128-139.

Nikkanen, L., Rintamäki, E. (2014). Thioredoxin-dependent regulatory networks in chloroplasts under fluctuating light conditions. Phil. Trans. R. Soc. B. 369: 20130224.

Noctor, G., Queval, G., Mhamdi, A., Chaouch, S., Foyer, C.H. (2011). "Glutathione," *In* Arabidopsis Book, eds. C.R. Somerville, E.M. Meyerowitz, (American Society of Plant Biologists, Rockville) 9, e0142.

Ohkama-Ohtsu, N., Sasaki-Sekimoto, Y., Oikawa, A., Jikumaru, Y., Shinoda, S., Inoue, E., Kamide, Y., Yokoyama, T., Hirai, M.Y., Shirasu, K., Kamiya, Y., Oliver, D.J., Saito, K. (2011). 12-oxo-phytodienoic acid-glutathione conjugate is transported into the vacuole in Arabidopsis. Plant Cell Physiol. 52: 205-209.

Ortiz-Masia, D., Perez-Amdor, M.A., Carbonell, J., Marcote, M.J. (2007). Diverse stress signals activate the C1 subgroup MAP Kinases of *Arabidopsis*. FEBS Lett. 58: 1834-1840.

Parisy, V., Poinssot, B., Owsianowski, L., Buchala, A., Glazebrook, J., Mauch, F. (2006). Identification of *PAD2* as a γ-glutamylcysteine synthetase highlights the importance of glutathione in disease resistance of Arabiodopsis. Plant J. 49: 159-172.

Park, J.W., Mieyal, J.J., Rhee, S.G., Chock, P.B. (2009). Deglutathionylation of 2-Cys peroxiredoxin is specifically catalyzed by sulfiredoxin. J. Biol. Chem. 284: 23364-23374.

Park, J.W., Piszczek, G., Rhee, S.G., Chock, P.B. (2011). Glutathionylation of peroxiredoxin I induces decamer to dimers dissociation with concomitant loss of chaperone activity. Biochemistry 50: 3204-3210.

Park, S.W., Li, W., Viehhauser, A., He, B., Kim, S., Nilsson, A.K., Andersson, M.X., Kittle, J.D., Ambavaram, M.M., Luan, S. et al. (2013). Cyclophilin 20-3 relays a 12-*oxo*-phytodienoic acid signal during stress responsive regulation of cellular redox homeostasis. Proc. Natl. Acad. Sci. USA 110: 9559-9564.

Peltier, J.B., Cai, Y., Sun, Q., Zabrouskov, V., Giacomelli, L., Rudella, A., Ytterberg, A.J., Rutschow, H., van Wijk, K.J. (2006). The oligomeric stromal proteome of *Arabidopsis thaliana* chloroplasts. Mol. Cell Proteomics 5: 114-133.

Pérez-Ruiz, J.M., Naranjo, B., Ojeda, V., Guinea, M., Cejudo, F.J. (2017). NTRC-dependent redox balance of 2-Cys peroxiredoxins is needed for optimal function of the photosynthetic apparatus. Proc. Natl. Acad. Sci. USA 114: 12069-12074.

Peskin, A.V., Pace, P.E., Behring, J.B., Paton, L.N., Soethoudt, M., Bachschmid, M.M., Winterbourn, C.C. (2016). Glutathionylation of the active site cysteines of peroxiredoxin 2 and recycling by glutaredoxin. J Biol. Chem. 291: 3053-3062.

Pieterse, C.M.J., Van der Does, D., Zamioudis, C., Leon-Reyes, A., Van Wees, S.C.M. (2012). Hormonal modulation of plant immunity. Annu. Rev. Cell Dev. Biol. 28: 489-521.

Piskurewicz, U., Jikumaru, Y., Kinoshita, N., Nambara, E., Kamiya, Y., Lopez-Molina, L. (2008). The gibberellic acid signaling repressor RGL2 inhibits *Arabidopsis* seed germination by stimulating abscisic acid synthesis and ABI5 activity. Plant Cell 20: 2729-2745.

Pulido, P., Spinola, M.C., Korchsteiger, K., Guinea, M., Pascual, M.B., Sahrawy, D., Sandalio, L.M., Dietz, K.J., González, M., \Dejudo, F.J. (2010). Functional analysis of the pathways for 2-Cys peroxiredoxin reduction in *Arabidopsis thaliana* chloroplasts. J. Exp. Bot. 61: 4043-4054.

Ribot, C., Zimmerili, C., Farmer, E.E., Reymond, P., Poirier, Y. (2008). Induction of the Arabidopsis *PHO1;H10* gene by 12-oxo-phytodienoic acid but not jasmonic acid via a CORONATINE INSENSITIVE1-dependent pathway. Plant Physiol. 147 : 696-706.

Riemann, M., Müller, A., Korte, A., Furuya, M., Wiler, E.W., Nick, P. (2003). Impaired induction of the jasmonate pathway in the rice mutant hebiba. Plant Physiol. 133: 1820-1830.

Romano, P.G.N., Horton, P., Gray, J.E. (2004). The *Arabidopsis* cyclophilin gene family. Plant Physiol. 134: 1268-1282.

Russell, L., Larner, V., Kurup, S., Bougourd, S., Holdsworth, M. (2000). The *Arabidopsis COMATOSE* locus regulates germination potential. Development 127: 3759-3767.

Sakai, T., Haga, K. (2012). Molecular genetic analysis of phototropism in Arabidopsis. Plant Cell Physiol. 53: 1517-1534.

Savchenko, T., Dehesh, K. (2014). Drought stress modulates oxylipin signature by eliciting 12-OPDA as a potent regulator of stomatal sperture. Plant Signal. Behav. 9 : e28304.

Scalschi, L., Sanmartin, M., Camañes, G., Troncho, P., Sánchez-Serrano, J.J., García-Agustín, P., Vicedo, B. (2014). Silencing of *OPR3* in tomato reveals the role of OPDA in callose deposition during the activation of defense responses against *Botrytis cinerea*. Plant J. 81 : 304-315.

Schneider, C.A., Rasband, W.S., Eliceiri, K.W. (2012). NIH Image to ImageJ: 25 years of image analysis. Nat. Methods 9: 651-655.

Shikanai, T., Takeda, T., Yamauchi, H., Sano, S., Tomizawa, K.I., Yokota, A., Shigeoka, S. (1998). Inhibition of ascorbate peroxidase under oxidative stress in tobacco having bacterial catalse in chloroplasts. FEBS Lett. 428: 47-51.

Serrato, A.J., Fernández-Trijueque, J., Barajas-López, J., Chueca, A., Sahrawy, M. (2013). Plastid thioredoxins: a ”one-for-all” redox-signaling system in plants. Front. Plant Sci. 4: 463.

Sirichandra, C., Gu, D., Hu, H.C., Davanture, M., Lee, S., Djaoui, M., Valot, B., Zivy, M., Leung, J., Merlot, S., Kwak, J.M. (2009). Phosphorylation of the Arabidopsis AtrbohF NADPH oxidase by OST1 protein kinase. FEBS Lett. 583 : 2982-2986.

Skubacz, A., Daszkowska-Golec, A., Szarejko, I. (2016). The role and regulation of ABI5 (ABA-insensitive 5) in plant development, abiotic stress responses and phytohormone crosstalk. Front. Plant Sci. 7 : 1884.

Staswick, P.E., Tiryako, I., Rowe, M.L. (2002). Jasmonate response locus *JAR1* and several related Arabidopsis genes encode enzymes of the firefly luciferase superfamily that show activity on jasmonic, salicylic, and lidole-3-acetic acids in an assay for adenylation. Plant Cell 14: 1405-1415.

Staswick, P.E. (2008). JAZing up jasmonate signaling. Trends Plant. Sci. 13: 66-71.

Staswick, P.E. (2009). The tryptophan conjugates of jasmonic and idole-3-acetic acids are endogenous auxin inhibitors. Plant Physiol. 150: 1310-1321.

Stintzi, A., Weber, H., Reymond, P., Browse, J., Farmer, E.E. (2001). Plant defense in the absence of jasmonic acid: The role of cyclopentenones. Proc. Natl. Acad. Sci. USA 97: 10625-10630.

Stotz, H.U., Jikumaru, Y., Shimada, Y., Sasaki, E., Stingl, N., Mueller, M.J., Kamiya, Y. (2011). Jasmonate-dependent and COI1-independent defense responses against *Sclerotinia sclerotiorum* in *Arabidopsis thaliana*: Auxin is part of COI1-independent defense signaling. Plant Cell Physiol. 52: 1941-1951.

Stotz, H.U., Mueller, S., Zoeller, M., Mueller, M.J., Berger, S. (2013). TGA transcription factors and jasmonate-independent COI1 signalling regulate specific plant responses to reactive oxylipins. J. Exp. Bot. 64 : 963-975.

Sun, G., and Anderson, V.E. (2004). Prevention of artifactual protein oxidation generated during sodium dodecyl sulfate-gel electrophoresis. Electrophoresis 25: 959-965.

Sun, L.R., Wang, Y.B., He, S.B., Hao, F.S. (2018). Mechanisms for abscisic acid inhibition of primary root growth. Plant Signal. Behav. 13 : 9.

Taki, N., Sasaki-Sekimoto, Y., Obayashi, T., Kikuta, A., Kobayashi, K., Ainai, T., Yagi, K., Sakurai, N., Suzuki, H., Mauda, T., et al. (2005). 12-oxo-phytodienoic acid triggers expression of a distinct set of genes and plays a role in wound-induced gene expression in *Arabidopis*. Plant Physiol. 139: 1268-1283.

Taki-Nakano, N., Ohzeki, H., Kotera, J., Ohta, H. (2014). Cytoprotective effects of 12-oxo-phytodienoci acid, a plant-derived oxylipin jasmonate, on oxidative stress-induced toxicity in human neuroblastoma SH-SYSY cells. Biochem. Biophys. Acta. 1840: 3413-3422.

Theodoulou, F.L., Job, K., Slocombe, S.P., Footitt, S., Holdsworth, M., Baker, A., Larson, T.S., Graham, I.A. (2005). Jasmonic acid levels are reduced in COMATOSE ATP-binding cassette transporter mutants. Implications for transport of jasmonate precursors into peroxisomes. Plant Physiol. 137: 835-840.

Thines, B., Katsir, L., Melotto, M., Niu, Y., Mandaokar, A., Liu, G., Nomura, K., He, S.Y., Howe, G.A., Browse, J. (2007). JAZ repressor proteins are targets of the SCF^{COI1} complex during jasmonate signalling. Nature 448 : 661-665.

Tietz, S., Hall, C.C., Cruz, J.A., Kramer, D.M. (2017). $NPQ_{(T)}$: a chlorophylfluorescence parameter for rapid estimation and imaging of non-photochemical quenching of excitons in photosystem-II-associated antenna complexes. Plant Cell Environ. 40: 1243-1255.

Udvardi, M.K., Czechowski, T., Scheible, W.R. (2008). Eleven golden rules of quantitative RT-PCR. Plant Cell 20: 1736–1737.

Vaistij, F.E., Barros-Galvão, T., Cole, A.F., Gilday, A., He, Z., Li, Y., Harvey, D., Larson, T.R., Graham, I.A. (2018). *MOTHER-OF-FT-AND-TFL1* represses seed germination under far-red light by modulating phytohormone responses in *Arabidopsis thaliana*. Proc. Natl. Acad. Sci. USA 115: 8442-8447.

Varsani, S., Grover, S., Zhou, S., Koch, K.G., Huang, P.C., Kolomiets, M.V., Williams, W.P., Heng-Moss, T., Sarath, G., Luthe, D.S., Jander, G., Louis, J. (2019). 12-oxo-phytodienoic acid acts as a regulator of maize defense against corn leaf aphid. Plant Physiol. 179: 1402-1415.

Veronese, P., Nakagami, H., Bluhm, B., Abuqamar, S., Chen, X., Salmeron, J., Dietrich, R.A., Hirt, H., Mengiste, T. (2006). The membrane-anchored *BOTRYTIS-INDUCED KINASE1* plays distinct roles in Arabidopsis resistance to necrotrophic and biotrophic pathogens. Plant Cell 18: 257-273.

Vissenberg, K., Claeijs, N., Balcerowicz, D., Schoenaers, S. (2020). Hormonal regulation of root hair growth and responses to the environment in Arabidopsis. J. Exp. Bot. 71 : 2412-2427.

Von Malek, B., Van Der Graaff, E., Schneitz, K., Keller, B. (2002). The *Arabidopsis* male-sterile mutant *dde2-2* is defective in the *ALLENE OXIDE SYNTHASE* gene encoding one of the key enzymes of the jasmonic acid biosynthesis pathway. Planta 216: 187-192.

Wang, H., Qi, Q., Schorr, P., Cutler, A.J., Crosby, W.L., Fowke, L.C. (2008). ICK1, a cyclin-dependent protein kinase inhibitor from Arabidopsis interacts with both Cdc2a and CycD3, and its expression is induced by abscisic acid. Plant J. 15, 501-510.

Wang, K D., Borrego, E.J., Kenerley, C.M., Kolemiets, M.V. (2020). Oxylipins other than jasmonic acid are xylem-resident signals regulating systemic resistance induced by *Trichoderma virens* in maize. Plant Cell 32: 166–185.

Wang, K.L., Li, H., Ecker, J.R. (2002). Ethylene biosynthesis and signaling networks. Plant Cell 14(Suppl.) : S131-S151.

Wang, L., Hua, D., He, J., Duan, Y., Chen, Z., Hong, X., Gong, Z. (2011). Auxin response factor2 (ARF2) and its regulated homeodomain gene HB33 mediate abscisic acid response in Arabidopsis. PLoS Genet. 7: e1002172.

Wu, A., Allu, A.D., Garapati, P., Siddiqui, H., Dortay, H., Zanor, M.-I., Asensi-Fabado, M.A., Munné-Bosch, S., Antonio, C., Tohge, T. et al. (2012). JUNGBRUNNEN1, a reactive oxygen species-responsive NAC transcription factor, regulates longevity in *Arabidopsis*. Plant Cell 24: 482-506.

Xu, J., Gao, G.L., Du, J.J., Guo, Y., Yang, C.W. (2010). Cell cycle modulation in response to the primary root of Arabidopsis. Pak. J. Bot. 42 : 2703-2710.

Yao, T., Jin, D., Liu, Q., Gong, Z. (2013). Abscisic acid suppresses the highly occurred somatic homologous recombination in Arabidopsis rfc1 mutant. J. Genet. Genomics 40: 465-471.

Yin, H., Zhang, X., Liu, J., Wang, Y., He, J., Yang, T., Hong, X., Wang, Q., Gong, Z. (2009). Epigenetic regulation, somatic homologous recombination, and abscisic acid signaling are influenced by DNA polymerase epsilon mutation in Arabidopsis. Plant Cell 21: 386-402.

Zhang, X., Liu, P., Zhang, C., Chiewchenogchol, D., Zhao, F., Yu, H., Li, J., Kambara, H., Luo, K. Y., Venkataraman, A., et al. (2017). Positive regulation of interleukin-1β bioactivity by physiological ROS-mediated cysteine S-glutathionylation. Cell Rep. 20: 224-235.

Zhang, Y., Turner, J.G. (2008). Wound-induced endogenous jasmonates stunt plant growth by inhibiting mitosis. PLoS One 3: e3699.

Zhou, M., Memelink, J. (2016). Jasmonate-responsive transcription factors regulating plant secondary metabolism. Biotechnol. Adv. 34: 441-449.

Zimmerman, D.C., Condron, C.A. (1979). Identification of traumatin, a wound hormone, as 12-oxo-trans-10-dedecenoic acid. Plant Physiol. 63: 536-541.